The Effect of Wind Turbines on Subsynchronous Resonance

Ahmed Ewais
School of Engineering
Cardiff University

A thesis submitted for the degree of
Doctor of Philosophy
2014

Contents

Abstract

Name of University:	Cardiff University
Candidate's Name:	Ahmed Ewais
Degree Title:	Doctor of Philosophy
Thesis Title:	The Effect of Wind Turbines on Subsynchronous Resonance
Date:	June 2014

With the rapid growth of the penetration of wind power into the power system, fixed series compensation is considered as an economic solution to increase power transfer capability. This will render the power system vulnerable to Sub-Synchronous Resonance (SSR).

This thesis conducts research on the effect of wind turbines represented by Fixed Speed Induction Generator-Based Wind Turbines (FSIG-WTs) and Fully Rated Converter-Based Wind Turbines (FRC-WTs) on damping SSR. Firstly, SSR is investigated through mathematically modelling IEEE First Benchmark Model (FBM) using MATLAB package. Modal analysis is used to study SSR over a wide range of series compensation percentages.

Secondly, the effect of incorporating FSIG-WTs into FBM on SSR is studied over a wide range of series compensation percentage and different power size of FSIG-WTs. Furthermore, the ability of the grid-side converters of the FRC-WTs connected with the FBM to damp SSR occurrence in the steam turbine shafts is evaluated using two different types of control.

An optimal controller based on a Linear Quadratic regulator (LQR) has been designed as an auxiliary controller of the grid-side converter of FRC-WTs. A full-order observer was designed to estimate the unmeasured state variables to enable a

full-state feedback. Finally, eigenvalue sensitivity was studied to choose the most suitable feedback signal for an SSR damping controller. Lead/Lag compensation controller based on the residue method is designed as an auxiliary controller within the grid-side converters of FRC-WTs. Eigenvalue analysis and time domain simulations over widely varying levels of series compensation have been carried out. The simulation studies were carried out in MATLAB and PSCAD.

Connecting FSIG-WTs to the FBM increases the range of series compensation level at which SSR can occur. Therefore, it was shown that FSIG-WTs have an adverse effect on the SSR occurring at the multi-mass synchronous generator. If the system is visible, LQR as an auxiliary damping controller within the grid-side converters of FRC-WTs is an effective controller to damp SSR over a wide range of series compensation percentages. Based on eigenvalue sensitivity technique, synchronous generator speed deviation is the most suitable feedback signal for damping SSR occurrence in the steam turbine shafts.

Declaration

This work has not previously been accepted in substance for any degree and is not concurrently submitted in candidature for any degree.

Signed ..... (candidate) Date .....

This thesis is being submitted in partial fulfilment of the requirements for the degree of PhD.

Signed ..... (candidate) Date .....

This thesis is the result of my own independent work/investigation, except where otherwise stated. Other sources are acknowledged by explicit references.

Signed ..... (candidate) Date .....

I hereby give consent for my thesis, if accepted, to be available for photocopying and for interlibrary loan, and for the title and summary to be made available to outside organisations.

Signed ..... (candidate) Date .....

I hereby give consent for my thesis, if accepted, to be available for photocopying and for interlibrary loans after expiry of a bar on access previously approved by the Graduate Development Committee.

Signed ..... (candidate) Date .....

To my beloved Dad

I dedicate this study

List of Publication

(1) **A. Ewais,** C. Ugalde-Loo, J. Liang, J. Ekanayake, N. Jenkins, "The Influence of the Fixed Speed Induction Generator-Based Wind Turbines on Subsynchronous Resonance," University Power Engineering Conference (*UPEC 2011*), Soest, Germany, Sept. 2011.

(2) **A. Ewais,** C. J. Liang, J. Ekanayake, N. Jenkins, "Influence of the Fully Rated Converter-Based Wind Turbines on SSR," IEEE PES Innovative Smart Grid Technologies (ISGT-ASIA 2012), Tianjin, China, May 21-24, 2012.

(3) **A. Ewais,** J. Liang, N. Jenkins, "The Impact of the Fixed Speed Induction Generator-Based Wind Turbines on Power system stability," will be submitted to CSEE Journal of Power and Energy Systems.

Acknowledgments

All thanks are to Allah, my God to whom I devote this work. "*Say: truly, my prayer and my rites, my life and my death, are all for Allah, the cherisher of the worlds*" (the Holy Quran 6:162).

I am grateful to my supervisors, Prof Nick Jenkins and Dr Jun Liang whose assistance in the preparation and completion of this study has been invaluable. My sincerest thanks are due to them for their support and valuable academic advice at all stages of the research.

Special thanks also to Dr Janaka Ekanayake for his very helpful, encouragement and direction on research projects. I would also like to thank Dr Daniel Rogers and Dr Carlos Ugalde-Loo for their guidance and support during the weekly meetings.

I also would like to thank the members of the Power Electronics and HVDC group for supporting and providing me with a great deal of additional insights during the weekly meetings specially Weixing, Lee, Jonathan and Tibin. Special thanks go to all PhD researchers and my colleagues for their help and fruitful discussions. Special thanks go also to Catherina, Aderyn, Chris, Jeanette and Chiara for their help.

I am grateful to my country Egypt and the Egyptian Cultural and Educational bureau in London for sponsoring me. I am also indebted to the Faculty of Energy Engineering, Aswan University. In particular, I also would like to thank to Prof Gaber El-Saady and Prof Ashraf Hemida for their supporting and encouragement.

My appreciation and gratitude are directed to my mother for her encouragement, continuous care and patience. The same equally goes to my brother, *Abdl-Rohman*, my sisters, *Shier*, *Suzan*, *Salwa* and their families. The same equally goes to my brothers in law, Ashraf, Ahmed and Mahmoud.

Last but not least, I would like to thanks my deep loving wife, *Hagar* and my sons, *Mustafa* and *Mazen* for their endless help, encouragement and patience.

Nomenclature

Abbreviations and Acronyms

AC	Alternating Current
DC	Direct Current
CSC	Current Source Converter
FACTS	Flexible AC Transmission System
FBM	First Benchmark Model
FC	Fixed Capacitor
FRC	Fully Rated Converter
HVDC	High Voltage Direct Current
IGE	Induction Generator Effect
LQR	Linear Quadratic Regulator
OECD	Organisation for Economic Co-operation and Development
PSS	Power Systems Simulator
PWM	Pulse Width Modulation
SC	Series Compensation over the transmission line
SSR	Sub Synchronous Resonance
SUB	Sub Synchronous Mode
TCSC	Thyristor Controlled Series Capacitor
TI	Torsional Interaction
TM	Torsional Mode
VSC	Voltage Source Converter

Symbols

P	The active power transferred between two terminal of the series compensated transmission line
x_L	The total inductance of the transmission line
x_C	The reactance of the series capacitor
δ	The angular difference between end voltages of the line
f_0	The system or synchronous frequency in Hz
ω_0	The system or synchronous frequency in rad/s
f_r	The subsynchronous frequency in Hz
ω_r	The subsynchronous frequency in rad/s
f_{er}	The complementary of the subsynchronous frequency
s	The slip
f_m	The torsional oscillation frequency in Hz
f_{em}	The complementary of the torsional frequency
Δ	The prefix denotes a small deviation about the initial operating point
λ	The eigenvalues of the linearized system
I	The identity matrix
K	The stiffness of the shaft section in p.u. torque/rad
θ_i	The twist angle of mass i in rad/s
ω_i	The speed of mass i in p.u.
M_i	The inertia constant of mass i in seconds
D	The damping coefficient of each mass in p.u. torque/p.u. speed
ω_b	The base speed ($2\pi f_o$ rad/s)
δ	The electrical angle in electrical radians (load angle in rad/s)
"."	The differential operator
a	The speed relay position
g	The governor opening
K_g	The governor gain

T_{SR}, T_{SM}	The two time constants of the governor
T_{CH}	The constants due to the steam flow in the chamber in the front of the pressure turbine
T_{RH}	The constants due to the steam flow in the reheater between the high and intermediate pressure turbines
T_{CO}	The constants due to the steam flow in the crossover connection between the intermediate and low pressure turbines
a, b, c	Stator windings
e_a, e_b, e_c	Stator three phase winding voltages
i_a, i_b, i_c	Stator three phase winding currents
v_f, E_{FD}	Field winding, Field voltage
i_D	d-axis damping winding
i_Q, i_S	q-axis damping windings
v_t	The terminal voltage of the synchronous generator
v_{td} , v_{tq}	The d-q components of synchronous generator terminal voltage
E_g, V_b	The generator terminal voltage behind the transient reactance and infinite bus voltage
V_{bd}, V_{bq}	The d-q components of the infinite bus
e_{cd}, e_{cq}	The d-q components of the voltage across the series capacitance
K_A, T_A	The voltage regulator gain and its time constant
T_E	The exciter time constant
$\varphi_{ds}, \varphi_{qs},$	The stator fluxes
$\varphi_{dr}, \varphi_{qr}$	The rotor fluxes
H	The overall inertia constant of FSIG-WT
T_m	The mechanical torque in p.u.
T_e	The electromagnetic torque in p.u.
i_{ds}, i_{qs}	The d-q components of the current in the stator windings of FSIG
i_{dr}, i_{qr}	The d-q components of the current in the rotor windings of FSIG
x_{sc}	The shunt capacitor at the induction generator terminal

i_{Ld} , i_{Lq}	The d-q components of the short transmission line current
R_{s2}, x_{s2}	The resistance and reactance of the line AC in p.u.
i_{dTL}, i_{qTL}	The d-q components of the current in the series compensated transmission line
V_{od}, V_{oq}	The *d-q* components of the voltage at the infinite bus (V_o)
i_{sd}, i_{sq}	The *d-q* components of output current of the FRC-WTs
k, m, ψ	The ratio between AC and DC voltage, the modulation ratio defined by PWM and the phase angle which is defined by PWM
v_{bd}, v_{bq}	The terminal voltage of grid side converter
R_{s2}, x_{s2}	The equivalent resistance and inductance of the transmission line (Line II)
i_{dc}, i_{cs}, i_{bb}	The current in the DC capacitor, current outputs from the current source and the current inputs to the grid side converter-based wind turbine
P_{ge}, P_{gr}	The active power of the generator-side converter and the grid-side converter
k_Q, T_C	The gain and the time constant of the reactive power regulator
k_{dc}, T_C	The gain and the time constant of the DC voltage regulator
Q	The symmetric positive semi-definite weighting matrix on the states
R	The symmetric positive definite weighting matrix on the control input
k	The feedback gain matrix
J	The performance index
P	The solution of algebraic Riccati equation
$\hat{x}$	The estimated state variables
L	The observer gain matrix
$\mathcal{R}_{kji}$	The residue associated with the k^{th} mode, the i^{th} input and the j^{th} output
w_k, v_k	The left and right eigenvectors associated to the eigenvalue λ_k

List of Figures

List of Tables

Chapter 1-

Introduction

1.1 Background

Due to worldwide environmental concern, reducing the emissions of Green-House Gas (GHG) has become one of the most important targets agreed under the Kyoto protocol [1]. Furthermore, 20-20-20 Target Plan has been promoted by European Union to reduce 20% greenhouse gas emissions, to reach 20% energy efficiency improvement, and to increase the penetration of renewable sources to 20% of its energy consumption from by 2020 [2].

Over the coming decades, the global population and their energy requirements increase. Regarding Figure 1.1, the Non-Organization for Economic Co- Operation and Development countries (Non-OECD) such as China, Russia and Brazil consume more energy than OECD countries such as the UK and USA [3]. The increase in energy demand comes at a time in which the reservoir of the world's fossil fuel has decreased. The percentage that fossil fuels share the global energy will decrease from 81% in 2010 to around 75% in 2035 [4].

To overcome all these constraints, world turns to utilize renewable resources such as wind and sun to achieve a large part of the total generation by 2020. Renewable generation is suggested to increase over the coming decades. The committee for the climate change sets an energy target of 15% renewable generation by 2020 [5].

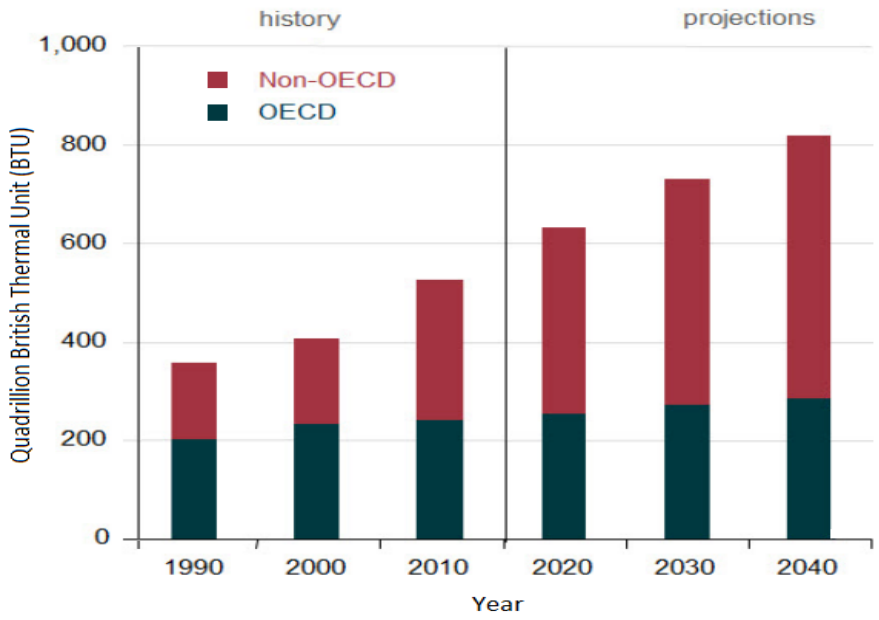

Fig. 1.1 World Energy Consumption 1990-2040 [3]

1.2 Wind Farms

Wind power is considered as the fast growing sector among the renewable sources [6-9]. According to [3], wind power has become an important electricity source for many countries such as Denmark, Portugal, Spain, China, Germany and USA. Figures 1.2 shows the wind power share of the total electricity consumption at the top countries used wind turbines. Figure 1.2 shows the cumulative installed capacity of the wind power the top countries used wind turbines in 2012 and 2013. China was leading the wind market with a total capacity of 91.32 GW and increasing 16.0GW from 2012 to 2013. The total wind power capacity installed in Denmark was almost fixed in 2012 and 2013 [3]. Figure 1.3 shows the penetration levels of the power derived from the wind sources for the top countries used wind turbines in 2013, e. g., Denmark is provided by 27% of its power demand from the wind power [9].

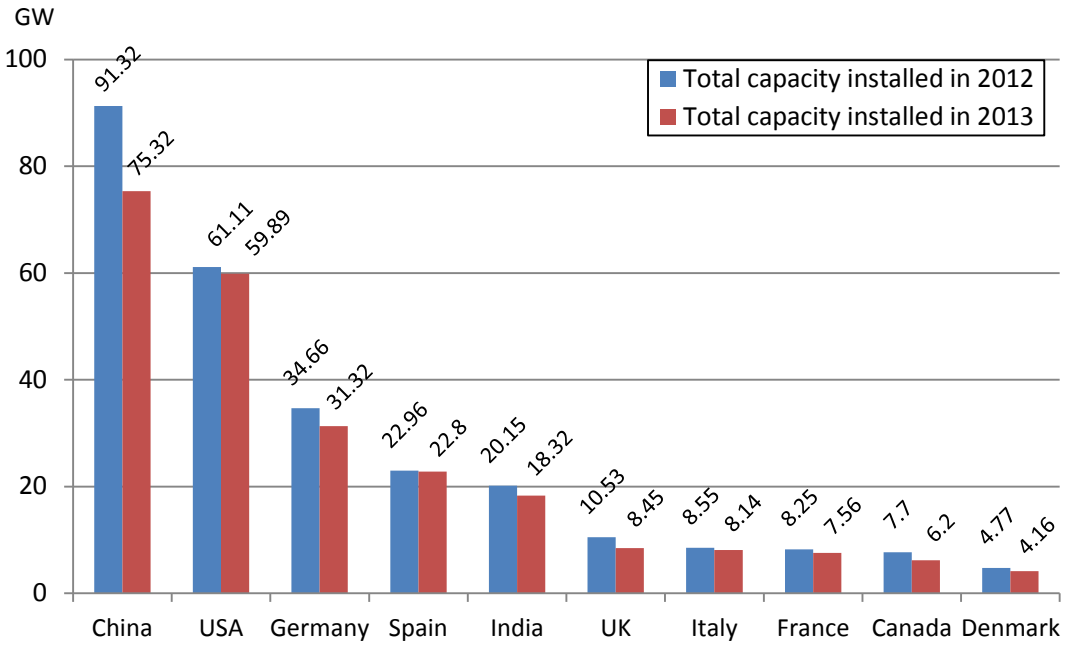

Fig. 1.2 Major wind power producers

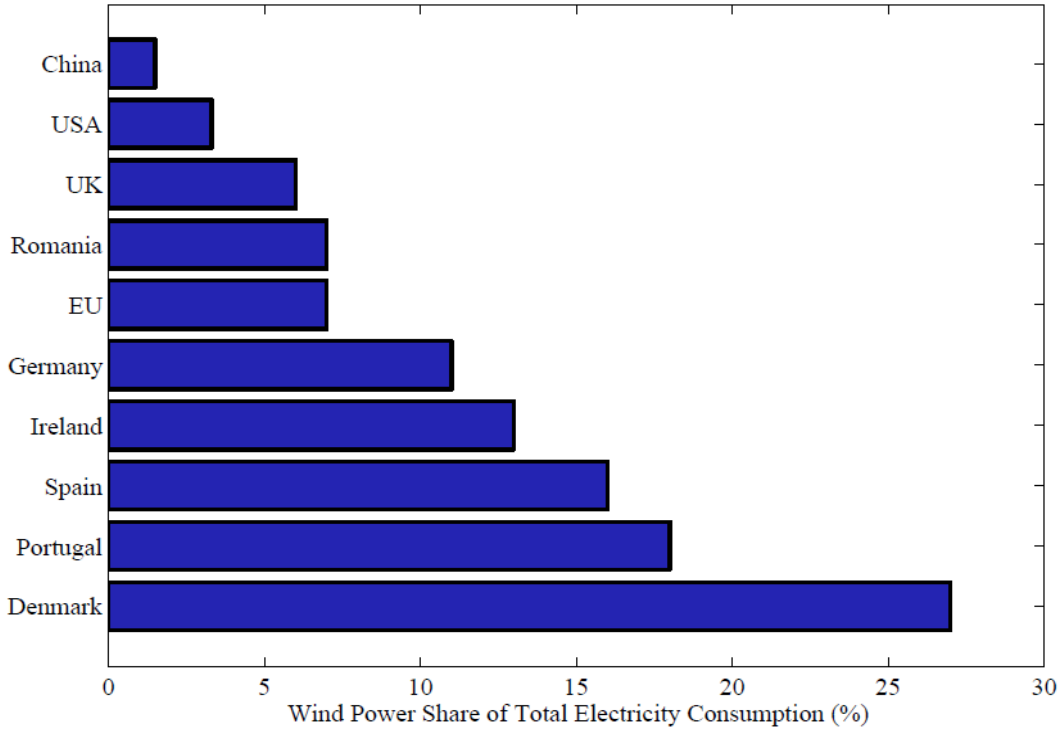

Fig. 1.3 Wind power share of the total electricity consumption

The majority of the new installed wind turbines are variable speed type using either Fully Rated Converter (FRC) or Doubly Fed Induction Generator (DFIG) [10-11]. Around 15% of the operating wind turbines in the Europe and 20% of the existing wind turbine in the world are still Fixed Speed Induction Generator (FSIG) type connected directly to the grid [12-15]. Regarding [10, 15], FSIG-WTs provide a positive contribution to the network damping due to their asynchronous nature. Since the slip curve of the induction generator within the FSIG-WT acts as an effective damping.

1.3 Series Compensation

As a consequence of the increased wind power penetration levels into the electric networks, the maximizing power transfer capability is the main target for transmission system operators. Series capacitor is considered as an economic method to increase the power transfer capability [16-21]. Series compensation is defined as insertion of reactive power elements into transmission lines and provides the following benefits [22-24]:

- Reduces line voltage drops
- Limits load-dependent voltage drops
- Influences load flow in parallel transmission lines
- Increases transfer capability
- Reduces transmission angle
- Increases system stability

Series Compensation (SC) has been installed over the transmission line in commercial since the early 1960s [20]. Due to these advantages of the series compensation, some countries, such as UK decided to install fixed series capacitors over the existing transmission lines to meet the huge amount of power generated from the wind [25]. Series compensation increases the power transfer capability in

the transmission line by reducing the overall reactance of the existing transmission line. Power transfer across the transmission system is calculated as [17-18], [26-28]:

$$P = \frac{E_1 \times E_2}{x_L - x_C} \times \sin(\delta) \quad (1.1)$$

where P is active power transfer between the terminals of the series compensated transmission line, $E_1$and E_2 are the voltages at either ends of the transmission line, x_L is the total inductance of the transmission line, x_C is the reactance of the series capacitor, and δ is the angular difference between end voltages of the line.

Series compensation increases angular and voltage stability in addition to increasing the active power transmission over the transmission line as shown in Figure 1.4 [17], [21]. As the angular difference between end voltages of the line (δ) decreases with increasing the series compensation level which in turns increases the dynamic stability of the transmission system.

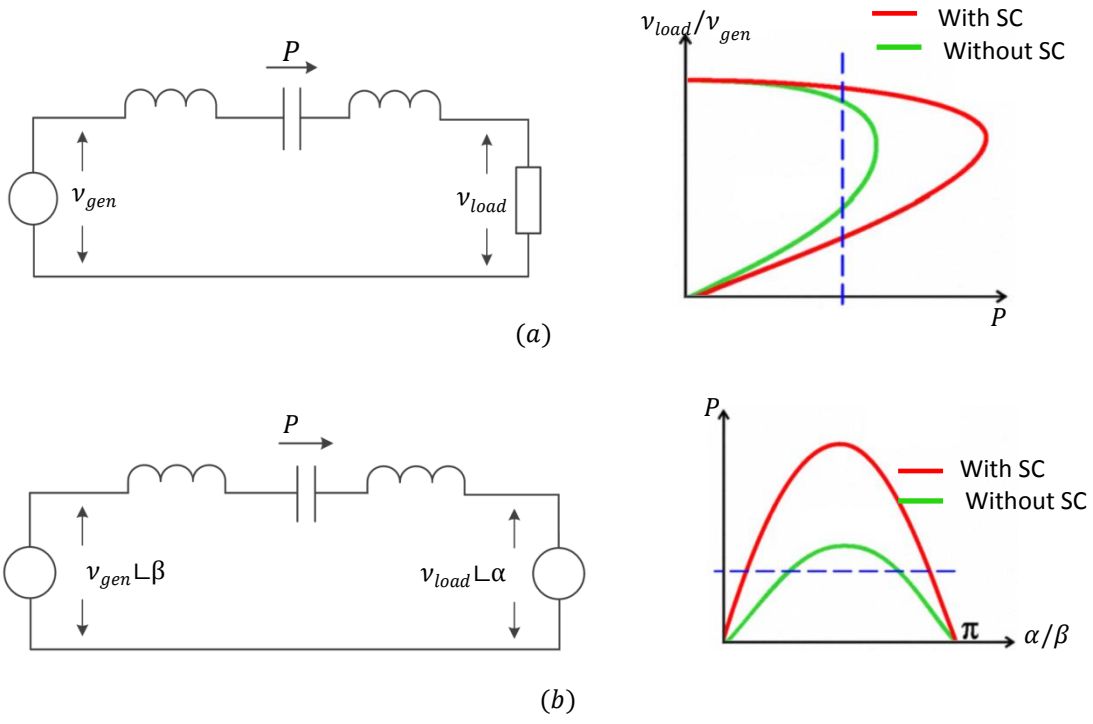

Fig. 1.4 The impact of series compensation on (a) voltage stability and (b) angular stability [17]

There are various solutions that have already been proven in numerous applications for series compensations such as: the Fixed Series Capacitor (FSC), the Thyristor–Controlled Series Capacitor (TCSC) and the Thyristor - Protected Series Capacitor (TPSC) [22-23].

1.3.1 Fixed Series Compensation (FSC)

The simplest and most cost-effective type of series compensation is provided by Fixed Series Capacitors (FSCs) [22-23]. FSC installations are protected against over-voltages using MOVs and self/forced triggered gaps. The benefits of FSC are:

- Increase in transmission capacity and
- Reduction in transmission angle

1.3.2 Thyristor–Controlled Series Capacitor (TCSC)

Reactive power compensation by means of TCSCs can be adapted not only to brand-new installations but also be implemented in a wide range of existing systems. Figure 1.7 shows a single line diagram of a TCSC [29]. The TCSC provides, in addition to the conveniences of a conventional Fixed Series Compensation, some further benefits as:

- Local mitigation of subsynchronous resonance (SSR) permits higher levels of compensation in networks where interactions with turbine-generator torsional vibrations or with other control or measuring systems are of concern.
- Damping of electromechanical (0.5-2 Hz) power oscillations often arises between areas in a large interconnected power network .
- Controlling the current and thus the load flow in parallel transmission lines, which simultaneously improves system stability.

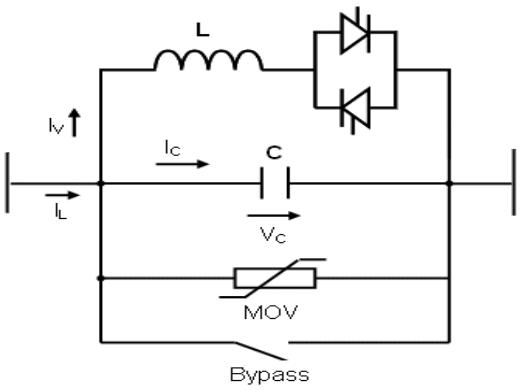

Fig. 1.5 The single line diagram of TCSC [28]

1.3.3 Thyristor- Protected Series Capacitor (TPSC)

Direct-light-triggered thyristors are used by TPSC instead of installing conventional spark gaps or surge arresters. Due to the very short cooling times of the light-triggered thyristor valves, thyristor protected series capacitors can be quickly returned to service after a failure, allowing the transmission lines to be utilized to their maximum capacity. Therefore, TPSC is necessary whenever the transmission lines must be returned to maximum carrying capacity as quickly as possible after a failure [30].

Fixed Series compensation is not without difficulty as series compensation is considered as the main source for subsynchronous resonance phenomenon [26-28]. This thesis investigates the influence of the wind turbines on SSR Occurrence in the steam turbine shafts of the conventional power plant caused by fixed series compensation installed over the transmission line. TCSC and TPSC are not considered in this thesis and is set as further work.

1.4 Research Objectives

The objective of this thesis was an investigation into the capability and the feasibility of the wind turbines integrated into the AC transmission system to damp the SSR occurrence in the steam turbine shafts without using FACTs devices. The main goals of the present thesis were set and achieved as:

- To investigate the possible contribution of wind power plant to damp out the SSR occurrence in the steam turbine caused by fixed capacitor installed over the transmission line system.

- FBM is mathematically analysed and simulated in MATLAB package and PSCAD to study SSR. Then, FBM I modified by featuring wind farm through second transmission line connected to the terminal bus of the synchronous generator.

- To evaluate the effect of the FSIG-WTs on the SSR occurrence at steam turbine because of fixed series compensation.
- To investigate the possibility of utilizing the FRC-WTs to damp SSR by designing an auxiliary controller for the grid-side converters of FRC-WTs. This was achieved by implementing a LQR-type (optimal control) as a supplementary controller with the grid side converters of FRC-WTs.

- To choose the most suitable feedback control signal to damp SSR at the steam turbine shafts. This was achieved by using eigenvalue sensitivity method. Residue method was used to design a lead/lag compensation-type (classical control) as an auxiliary controller within the grid side converter of the FRC-WTs.

1.5 Research Contributions

The main contributions of this thesis are as follows:

- FBM was modified by connecting the wind farm (FSID-WTS and FRC-WTs) to the bus voltage within FBM via second transmission line.

- Connecting FSIG-WTs with FBM increases the range of series compensation at which SSR occurring in the steam turbines.

- If the system is visible, the optimal control via a LQR-type controller implemented as an auxiliary controller with the grid side converters of the FRC-WTs is capable of damping SSR occurring in the steam turbine shafts over a wide range of series compensation percentage.

- Classical control is implementing by designing lead/lag controller as supplementary controller within the grid side converters of the FRC-WTs to damp SSR. By implementing eigenvalue sensitivity technique, the most suitable feedback signal is choosing for the supplementary controller.

1.6 Thesis Structure

The thesis consists of seven chapters. The main core of the thesis is to study the feasibility and capability of wind power plants (FSIG-WTs and FRC-WTs) to contribute to damp SSR in the steam turbine shafts. This been organized as:

Chapter 1 outlines the integration of the wind turbines into the power system and the fixed series compensation. The scope and objectives of the research are also presented in this chapter. The chapter presents the outlines of the thesis structure.

Chapter 2 presents a literature view of previous research into wind turbines, series compensation and SSR phenomenon. The chapter begins with describing the

different types of wind turbines. It contains the fundamental concepts of SSR phenomenon, modern and conventional countermeasures.

Chapter 3 investigates the dynamic modelling of a single machine infinite bus system representing IEEE First Benchmark Model. The system under study is described in details and the dynamic models of its individual components. The comprehensive eigenvalue technique and time domain simulations are used to evaluate the dynamic response of the system model over a wide range of series compensation levels.

Chapter 4 presents the complete dynamic modelling of the FSIG-WTs incorporating into the FBM in details. Eigenvalue results are used to investigate the effect of the level of the series compensation and different ratings of FSIG-WTs on SSR in the steam turbine shafts. The time-domain simulation analysis using MATLAB and PSCAD is investigated to validate the eigenvalue results.

Chapter 5 introduces a dynamic model of complete model of FBM featuring FRC-WTs. Linear Quadratic Regulator (LQR) is used as a supplementary control within the grid side converters of the FRC-WTs to damp SSR in the steam turbine shafts. A full order observer is designed to enable LQR to feedback all the state variables. A comprehensive analysis has made using eigenvalue results and time domain analysis to evaluate the SSR damping controller over wide range of series compensation.

Chapter 6 demonstrates the eigenvalue sensitivity approach to choose the suitable feedback control input signal to damp SSR in the steam turbine. Lead/Lag compensation controller is designed based on the residue method as an auxiliary controller within the grid side converters of FRC-WTs. Eigenvalue technique and time domain simulations are used to evaluate the SSR damping controller.

Chapter 7 summarizes the conclusions from the research described in the thesis. Future work for development of SSR damper using wind turbines is discussed.

Chapter 2-

Literature Review

2.1 Wind Power Generation

During the last decades, wind power has played an important role in generating renewable electricity. Wind turbines have developed rapidly with increasing rotor diameters and the rating of the wind turbines as shown in Figure 2.1 [10].

There are two main types of wind turbines; fixed speed and variable speed-based wind turbines [6].

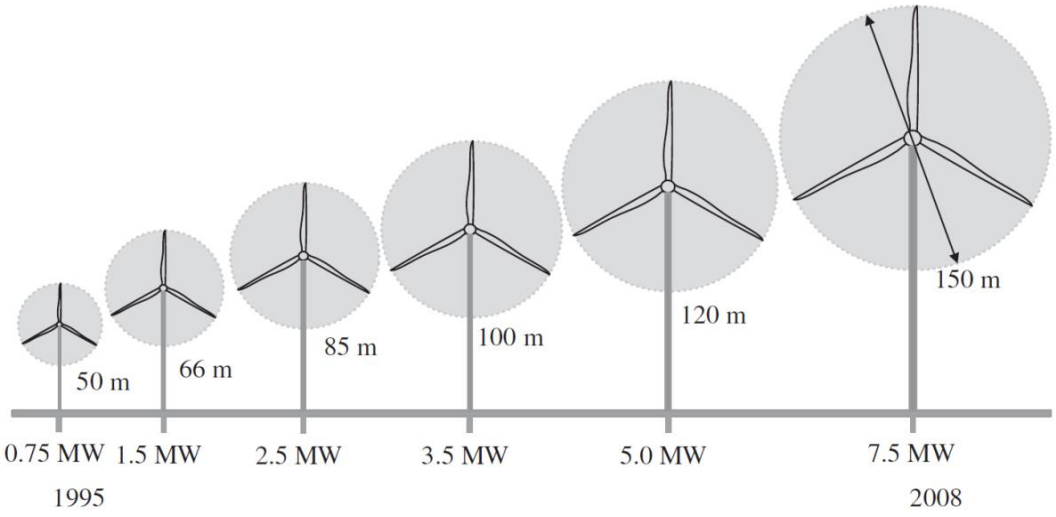

Fig. 2.1 Evaluation of wind turbine dimensions [10]

2.1.1 Fixed speed-based wind turbine

Until the beginning of the 21th century, Fixed Speed Induction Generator (FSIG) was the type most installed because of their simplicity and reliability [31]. FSIG-Based Wind Turbine (FSIG-WT) consists of an aerodynamic driving, a low-speed shaft, a gearbox, a high-speed shaft and squirrel cage induction (asynchronous) generator connected directly to the grid through step up power transformer as shown in Figure 2.2. The amount of power generation is varied by the slip and hence by the rotor speed of induction generator.

This wind turbine type is called fixed speed or constant speed as its rotor speed variations are very small, around 1 to 2%. FSIG-WT consumes reactive power from the grid so it is conventional that power factor correction capacitors provide FSIG-WTs with the reactive power as shown in Figure 2.2.

FSIG-WTs have the advantages of being simple and reliable. On the other hand, FSIG-WT is noisy, and it must be more mechanically robust than variable speed wind turbine. As its speed is constant, the fluctuations in wind speed transfer directly to the drive train torque and cause high structural loads.

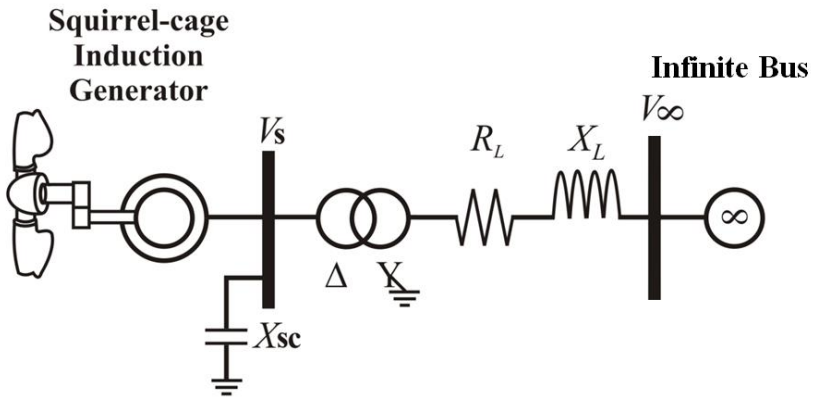

Fig. 2.2 Schematic diagram of a fixed speed induction generator based wind turbine connected to the grid

2.1.2 Variable speed -based wind turbine

In the recent years, the technology has switched from the fixed speed to the variable speed because of the advantages, which are provided by variable speed wind turbines (VSWTs) such as providing simple pitch control, high efficiency and reducing the mechanical stresses [6]. Doubly Fed Induction Generator (DFIG) and Fully Rated Converter (FRC) based on induction or synchronous generator are the most common types of VSWTs.

a- DFIG-based wind turbine

Figure 2.3 shows the schematic diagram of the DFIG based wind turbine [10], [6], [31]. The stator windings of the generator are connected directly to the grid through turbine transformer while the rotor is connected through power converters. The power converters decouple the rotor circuit from the grid in addition to controlling the rotor currents. Depending upon the rotational speed of the generator, DFIG wind turbine can deliver power to the grid through the stator and rotor and the rotor can absorb power. When the rotor speed is lower than the synchronous speed, the rotor circuit absorbs active power from the grid while when the generator operates in the super-synchronous mode, the rotor delivers power to the grid through the converters [16].

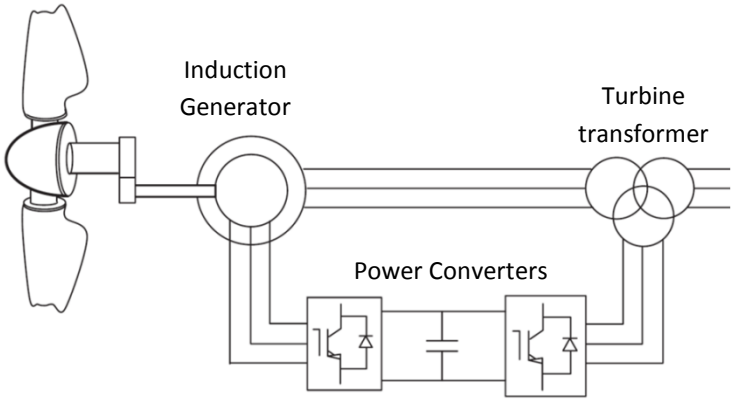

Fig. 2.3 Configuration of a DFIG based wind turbine connected to the grid [10]

b- FRC-based wind turbine

Figure 2.4 shows the typical configuration of the FRC based wind turbine [10], [6], [31]. The generator of FRC-WTs can be either synchronous or asynchronous generator. The generator within FRC-WT is completely decoupled from the grid through back to back converter as shown in Figure 2.4. Therefore, FRC-WTs are influenced by the Sub-Synchronous Resonance (SSR). Moreover, by implementing an effective auxiliary control within FRC-WTs can provide additional support to the network [11].

The generator-side converter can be either a voltage source converter or a diode rectifier while the grid side converter is a voltage source converter [6], [31]. The rating of the power converters equal to the rating of the generator as the full power generated by the generator is transmitted to the grid through the power converters [11].

This thesis investigates the influence of the FSIG-WTs and the FRC-WTs on SSR occurrence in the steam turbine shafts of the conventional power plant caused by fixed series compensation installed over the transmission line. The impact of DFIG-WTs on SSR are not considered in this thesis and is set as further work.

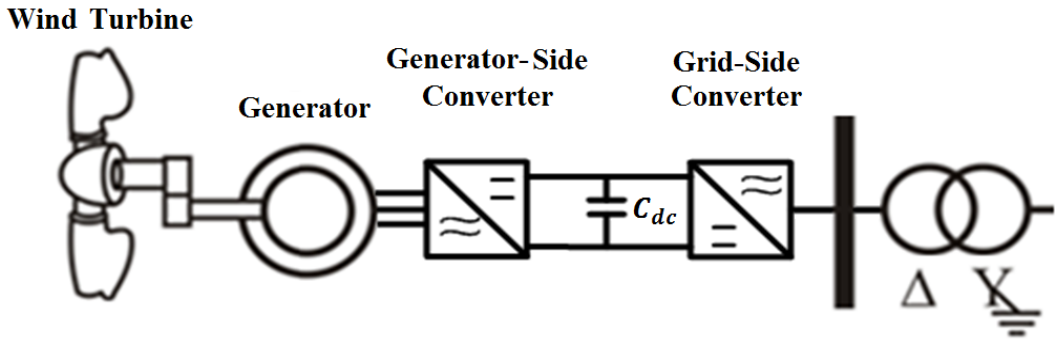

Fig. 2.4 Typical configuration of a Fully Rated Converter-Based Wind Turbine

2.2 Sub-Synchronous Resonance

The mitigation of Subsynchronous Resonance (SSR) caused because of series compensation is a problem of interest in the power industry in which wind turbines could play a major role instead of FACTs devices [32-33].

Since the first appearance of this phenomenon at Mohave plant in USA resulting into two successive shaft failures in 1970 and 1971, it has been analysed, and many countermeasures have been suggested. SSR is a dynamic phenomenon in the power system which has certain characteristics and there are many definitions for this electric phenomenon. The formal definitions of SSR provided by IEEE Subsynchronous Resonance Working Group as follow [34-35]:

"Subsynchronous Resonance (SSR) encompasses the oscillatory attributes of electrical and mechanical variables associated with turbine-generators when coupled to a series capacitor compensated transmission system where the oscillatory energy interchange is lightly damped, undamped, or even negatively damped and growing."

"Subsynchronous oscillation is an electric power system condition where the electric network exchanges significant energy with a turbine-generator at one or more of the natural frequencies of the combined system below the synchronous frequency of the system following a disturbance from equilibrium."

The definition of SSR phenomenon can be explained by considering the large turbine-generator connecting to an infinite bus through a series capacitor compensated transmission line. Figure 2.5 shows a generator driven by multi-stage steam turbine consisting of four stages (HP, IP and LP) where all the steam turbine stages in addition to the generator are mounted in the same shaft. The steam turbine stages, the shaft part connecting the masses and the rotor of the synchronous generator represent mass spring system. For m mass spring system, there are $(m-1)$ torsional oscillation modes. Each natural torsional frequency is functions of the inertia of the corresponding mass and the stiffness of the connected shafts [34], [27-28].

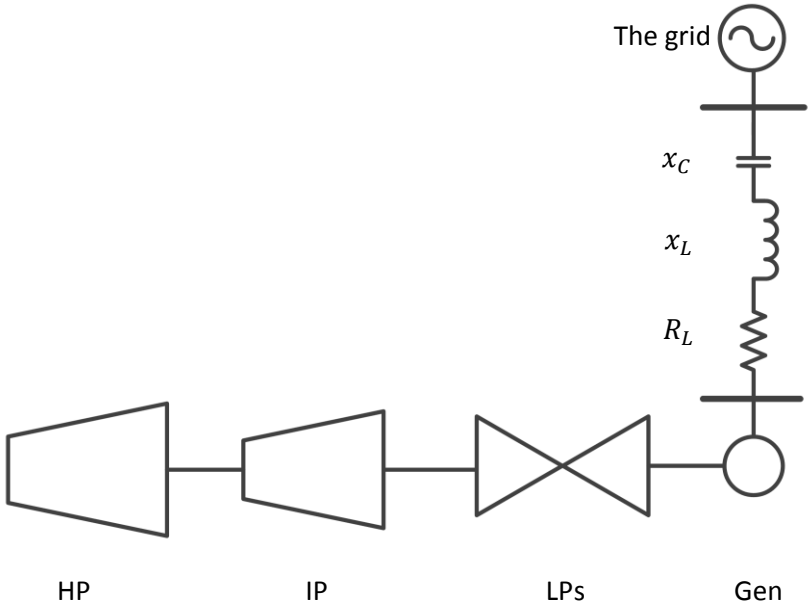

Fig. 2.5 Four stages steam turbine-generator connected to the grid through series compensated transmission line [36].

When the degree of the series compensation is increased, an electrical resonance maybe develop between the total reactance of the line and the reactance of series capacitor at subsynchronous frequency (f_r) which is derived as:

$$f_r = f_0\sqrt{\frac{x_C}{x_L}} \quad Hz \tag{2.1}$$

or

$$\omega_r = \omega_0\sqrt{\frac{x_C}{x_L}} = \sqrt{\frac{1}{LC}} \ \ rad/s \tag{2.2}$$

where ω_0 is the system or the synchronous frequency ($\omega_0 = 2\pi f_0 \ rad/s$, $f_0 = 60 \ Hz$), x_C is the capacitive reactance, and x_L is the total reactance of the line.

The natural frequency (f_r) is called subsynchronous frequency as the value of f_r is lower than that of the synchronous frequency (f_0).

SSR may occur in a system due to any change in system conditions or due to fault. SSR are divided into distinct interactions as [27-28]:

2.2.1 Induction Generator Effect

Induction generator effect occurs due to the electric resonance. When an electric resonance occurs in the series compensated transmission line, there will be a revolving field induced in the armature windings due to the electric resonance at the subsynchronous frequency (f_r). This revolving field will induce oscillation torque with frequency equal to the complementary of the subsynchronous frequency (f_r) as:

$$f_{er} = f_0 - f_r \tag{2.3}$$

Since the rotor of generator rotates at a synchronous speed which is higher than the speed of the induced revolving field in the armature due to electric resonance ($f_r < f_0$), the synchronous generator behaves like an induction generator. Figure 2.6 shows the equivalent circuit of the induction generator, as the slip (s) is negative:

$$s = \frac{f_r - f_0}{f_r}, \qquad s < 0 \tag{2.4}$$

The rotor resistance, viewed from the armature terminals, is a negative resistance. However, if the negative rotor resistance of the generator is greater in magnitude than the total positive resistance of the network in addition to the armature resistance there will be sustained subsynchronous currents [27].

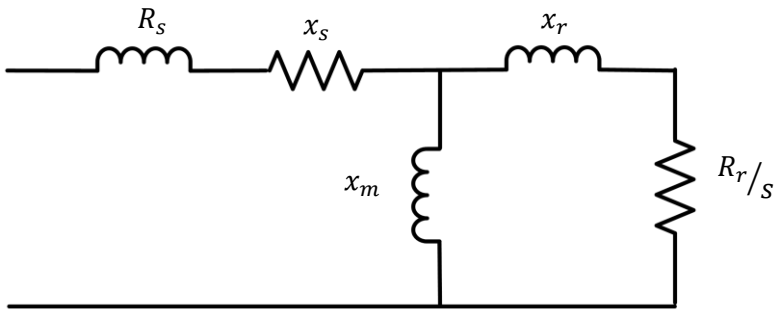

Fig. 2.6 Equivalent circuit of the induction generator [10].

2.2.2 Torsional Interaction Effect

Torsional interaction effect occurs due to the mechanical modes of the multi-mass turbine generator system [28]. Regarding Figure (2.5), there are $(m-1)$ torsional oscillation modes for m mass spring system in addition to power oscillation mode, zero mode, by which all the entire mass spring system oscillates in unison. These torsional oscillations occur at frequencies lower than the value of the synchronous frequency. The field winding of the generator on the rotor is rotating at the synchronous speed while the torsional oscillation occurs at a subsynchronous frequency (f_m). Therefore, there are induced voltages and currents in the armature winding of the generator at frequency ($f_{em} = f_0 - f_m$) called complementary of the torsional frequency.

If one of the natural torsional modes of the turbine-generator shaft coincides or is close to the complementary of the subsynchronous frequency (f_{er}), Torsional interaction effect occurs. As a result, generator rotor oscillations will increase and this motion will induce armature voltage components at both subsynchronous and super-synchronous frequencies. Moreover, the induced subsynchronous frequency voltage sustains the subsynchronous torque and the system will become self-excited [27-28].

Torsional interaction acts as a negative resistance to the induction generator effect while induction generator effect acts as a negative damping to the torsional oscillation and the two types of the SSR are called self-excited effects [27].

2.2.3 Transient torque

Transient torque occurs when a fault on a series compensated power system occurs. Unlike torsional interaction and induction generator effect, the growth rate for torque amplification is very high and oscillating shaft torques might be expected to reach a damaging level [27].

2.3 SSR Analysis Tools

There are several analytical tools in order to study SSR. Frequency scanning and eigenvalue analysis are the most common tools used to evaluate SSR [27].

The frequency scanning technique is effective in the study of induction generator effects. This method computes the equivalent resistance and inductance, seen looking into the network from a point behind the stator winding of the generator as a function of frequency [27], [36].

Eigenvalue analysis studies the stability of the system without solving the differential equations of the system. To perform the eigenvalue analysis, the nonlinear model of the network and the generators are linearized around the operating point. It studies the dynamic stability of the system by giving the frequencies of the oscillations and the damping of each frequency. The eigenvalues are determined for a linearized system written in stand state space form as [27-28]:

$$\Delta\dot{x} = A\Delta x + B\Delta u \quad (2.5)$$

$$Det(\lambda I - A) = 0 \quad (2.6)$$

where the prefix Δ denotes a small deviation about the initial operating point, Δx and Δu represent the state vector and the input vector, A and B are the system matrix and the input or the control matrix, I denotes the identity matrix its size equals the size of the system matrix and λ denotes the eigenvalues of the linearized system.

The eigenvalues of the system matrix A describe the stability of the system as [28]:

- The real part of the eigenvalues represents the damping and the imaginary part represents the frequency of the oscillations.
- The system is unstable if there is at least one eigenvalue with a positive real part.
- The system is stable if the real parts of all eigenvalues are negative. The more negative the real part is, the sooner the oscillation of the associated mode dies.

This thesis investigated the SSR due to the torsional interaction effect which involves the energy interchange between the turbine-generator and the electric network. Eigenvalue analysis is used in this thesis to investigate the effect of the wind turbines on the SSR occurrence in the steam turbine shafts in addition to the time domain simulation using MATLAB and PSCAD programs.

2.4 Countermeasures of Subsynchronous Resonance

Since the first SSR occurrence in 1970 at Mohave station in USA, wide varieties of countermeasures and methods have been employed by utilities to damp SSR oscillations. Unit-Tripping SSR Countermeasures make the generator be electrically separated from the network when a dangerous condition is detected such as armature current relay [37], torsional motion relay [38] and unit-tripping logic schemes [39]. Non-unit-Tripping SSR Countermeasures protect the generator from SSR without electrically separating the generator from the power system such as static blocking filter and Pole face amortisseur winding [40].

In the recent three decades, studies on the mitigation of the SSR oscillations have focused on Flexible AC Transmission System (FACTS) devices such as Thyristor Switched Resistor (NGH Scheme), Thyristor Controlled Series Capacitor (TCSC), Static Synchronous Series Compensator (SSSC), Static VAR Compensator (SVC), and Static Synchronous Compensator (STATCOM) [41-50].

The proposed reinforcements for the transmission networks for many countries incorporate HVDC systems and series compensation [25]. There are some studies based on the application of HVDC systems in damping SSR oscillations [51-53].

2.5 The Impact of SSR on the Wind Turbine

There is need for upgrading of grid transmission infrastructures including the installing of fixed series compensation in order to accommodate the increased power flow from the wind plants [54-56]. The presence of series capacitors in the line may potentially cause SSR in induction generator based wind turbine generators [54]. In [53], [57], a detailed analytical and experimental result of SSR occurring in a squirrel cage induction motor and a deep bar induction motor fed by a series compensated feeder were presented.

In [54], wind farm interaction with series compensated transmission line was discussed for the first time. The impact of a large-scale integration of wind farms, both conventional FSIG-based wind farms and DFIG-based wind farms, into a utility grid was studied, which focused on major interconnection issues. Based on the simulation studies, induction generator effect was detected in FSIG-based wind farms in the presence of the series capacitor.

In [58], a report was carried out by Xcel energy on the study of a series capacitor in the Wilmarth-Lakefield transmission system. This report specifically discussed the impact of the series capacitor on the interconnected network and turbine generators connected at various points in the network. A 107 MVA wind farm based on 100 DFIGs was proposed at the Lakefield system. This study suggested that when a large number of wind turbines are aggregated, the SSR issue might become more prominent.

In [59-63], SSR was discussed issues in wind farms and its mitigation using Flexible AC Transmission system (FACTS) devices. In [59], the potential of SSR through a frequency domain model of the induction generator based wind farm was investigated. It concluded that torsional modes may be excited by an electrical fault in the network but any unstable torsional interaction was not indicated. In [60], the potential of SSR on a DFIG-based 500 MW wind farm connected to a series compensated transmission line was studied. It indicated the potential of induction

generator effect in the wind farm following a fault in the network with a high level of series compensation. Static Var Compensator (SVC) was proposed to mitigate the SSR oscillation in the FSIG-based wind farm [61]. Another paper [62] showed the mitigation of SSR occurring in the FSIG-WTs using Thyristor Controlled Series Capacitor (TCSC). A further paper [63] presented a comparative study of mitigation of SSR occurring in FSIG-based wind farms of size between 100 MW to 500 MW using two FACTS devices: a) SVC and b) TCSC. TCSC was found to be superior over the SVC with a similar damping controller for mitigation of the SSR oscillation in the wind farm following a symmetrical fault in the network.

In [64-65], Static Synchronous Compensators (STATCOM) and Static Synchronous Series Compensators (SSSC) were installed to damp SSR in 100 MW FSIG-based wind farm connected to a series compensated transmission line. In these two papers, SSR happened because of torsional interaction and no induction generator effect was reported.

[66] presented modelling of DFIG-based wind farm connected to a series compensated transmission line. Impact of a series capacitor and control parameters on the SSR oscillation were investigated. Further studies of SSR with DFIG based wind farms were reported in [67-70]. A detailed modelling of the DFIG based wind farm connected to a series compensated transmission line was reported in these papers. In [70], The ability of the power converters in doubly-fed induction generator (DFIG) wind farms in mitigating SSR within the wind farm has been investigate. DFIG converter controller design and its interactions with series capacitor were studied.

Although many papers investigated the effect of SSR on wind farms, both conventional FSIG-based wind farms and DFIG-based wind farms, no paper investigates the effect of wind turbines on damping SSR occurring in the steam turbine shafts. The ability of the power converters in FRC-based wind farms in mitigating SSR occurring in the steam turbine shafts has rarely been investigate.

2.6 Conclusion

This chapter presented a literature view of previous research into wind turbines, series compensation and SSR phenomenon. A brief describing of the different types of wind turbines were mentioned. The fundamental concepts of SSR phenomenon, modern and conventional countermeasures were also presented in this chapter.

Although many papers investigated the effect of SSR on wind farms, the effect of wind turbines on damping SSR, which occurs in the steam turbine shafts, has rarely been investigated. The ability of the power converters in FRC-based wind farms in mitigating SSR occurring in the steam turbine shafts has rarely been investigated.

Regarding the survey done in this chapter, studying the effect of the wind turbines on damping SSR occurrence in the steam turbines is interesting and new point for research. It also contributes to reduce the cost of installing FACTs devices in order to damp the SSR by exchanging it with wind farms, which are already connected to the grid.

Chapter 3

Model and Analysis of Subsynchronous Resonance in the Power System

3.1 Introduction

In recent years, electrical power generation from renewable sources, especially wind turbine, has increased. Most of those generation capacity is connected to the existed power networks. As a result, this requires increasing the power transfer capability of the current network, which is originally not designed for this purpose. Fixed series compensation is considered as one of the economic solutions to increase power transfer capability through transmission lines. However, as mentioned in Chapter "2", fixed series compensation results in the problem of Subsynchronous Resonance (SSR).

This chapter presents a mathematical model of the IEEE First Benchmark Model and an eigenvalue analysis method for the study of the SSR. The dynamic performance of a synchronous generator and a transmission network are described by a set of nonlinear differential and algebraic equations. These equations were linearized around the operating point so that a linearized model could be established and the performance of the SSR studied.

3.2 IEEE First Benchmark Model

The system used in the small-signal analysis of SSR in this thesis is the IEEE First Benchmark Model (FBM) for computer simulation of SSR. This model was created by the IEEE SSR Task Force group to study SSR and test SSR countermeasures [72].

FBM is simple model as it consists of a single synchronous generator connected to infinite bus through a series compensated transmission line as shown in Figure 3-1. From the synchronous generator on the left, there is the transformer, the line impedance, the series capacitor and the infinite bus. Also in the figure there are two different locations at which fault reactance (X_F) may occur. A fault may be assumed either at bus A or bus B, but not simultaneously. The parameters of the shaft are the same as the ones used in the FBM and can be found in [72] and next page.

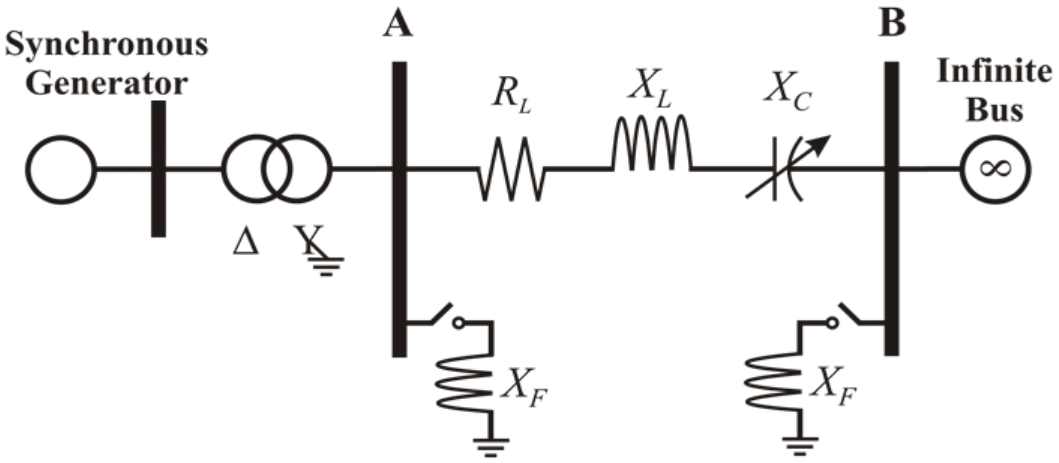

Fig. 3.1 IEEE first benchmark model [72]

IEEE First Benchmark Model

Parameters (in p.u)

(a) Mass-spring system (M: s, K: p.u., torque per rad, D: p.u.)

M_H = 0.185794 K_{HI} = 19.303

M_I = 0.311178 K_{IA} = 34.929

M_A = 1.717340 K_{AB} = 52.038

M_B = 1.768430 K_{BG} = 70.858

M_G = 1.736990 K_{GX} = 2.822

M_X = 0.068433

$D_H = D_I = D_A = D_B = D_G = D_X$ = 0.1

(b) Turbine torques and governor

F_H = 0.3 T_{CH} = 0.3s K_G = 25

F_I = 0.26 T_{RH} = 7.0s T_{SR} = 0.2s

F_A = 0.22 T_{CO} = 0.2s T_{SM} = 0.3s

F_B = 0.22

(c) Exciter and voltage regulator

K_A = 50 T_A = 0.01s T_E = 0.002s

$E_{FD\ max}$ = 7.3 p.u. $E_{FD\ min}$ = -7.3s

(d) Synchronous generator (p.u.)

X_d = 1.790 X_q = 1.710 X_F = 1.700

X_D = 1.666 X_Q = 1.695 X_S = 1.825

X_{md} = 1.660 X_{mq} = 1.580 R_a = 0.0015

R_F = 0.001 R_D = 0.0037

R_S = 0.0182 R_Q = 0.0053

(f) Transformer and transmission line (p.u.)

R_T = 0.01 X_T = 0.14 $X_{C/XL}$ = 0-100%

X_L = 0.56 R_L = 0.02

(g) the initial operating condition of synchronous generator

P_G = 0.9 p.u. *P.F.*= 0.9 (lagging)

Vt =1.05 p.u.

3.3 System Modelling for the Eigenvalue Analysis

The eigenvalue analysis is used in this thesis to investigate SSR, as it gives information of both resonant frequency and damping at that frequency. A detailed mathematical model of the FBM is established for the eigenvalue analysis to understand the effect of series compensation on SSR. First, individual mathematical models describing the turbine-generator mechanical system, the synchronous generator, and electric network are presented. The obtained nonlinear model is linearized at one operating point and a linear state space model is obtained for the computation of the eigenvalues.

3.3.1 Basic equation of the mass-spring system

The turbine-generator mechanical system consists of six masses: a high-pressure turbine (*HP*), an intermediate-pressure turbine (*IP*), low pressure turbine A (*LPA*) and low pressure turbine B (*LPB*), a generator (GEN) and its rotating exciter (*EXC*) coupled to a common shaft as shown in Figure 3.2. The turbine masses, generator rotor and exciter are considered as lumped masses connected to each other via massless springs and together they constitute a linear-mass-spring system. The system data and the initial operating conditions of the system are given in the end of this chapter.

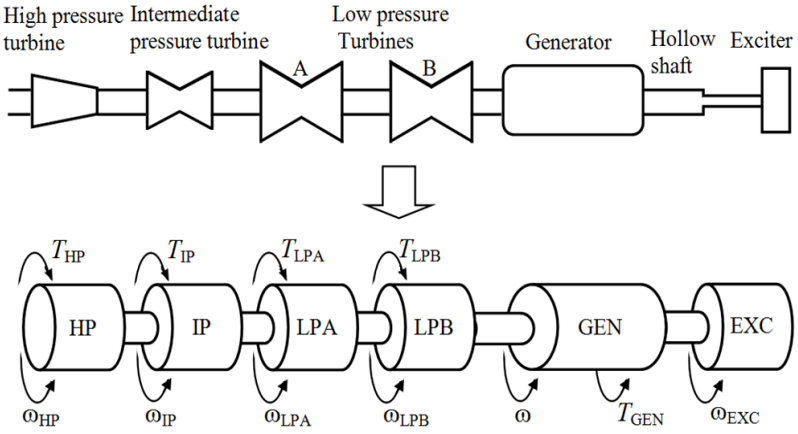

Fig. 3.2 Mechanical structure of six masses FBM system [73].

For clarity of the dynamic expressions, one mass with details of the torques acting on it presents the torsional relation of the i^{th} mass-spring system as shown in Figure 3.3. The shaft torque on the left in addition to the external torque input are together in one direction; and the shaft torque on the right, the damping torque ($D_i\omega_i$) on the mass and the accelerating torque ($M_i\omega_i$) are together in the opposite direction.As shown in Figure 3.3, the torques acting on the i^{th} mass are:

Input torque $K_{i-1,i}(\theta_{i-1} - \theta_i)$

Output torque $T_i - K_{i,i+1}(\theta_i - \theta_{i+1})$

Damping torque $D_i\omega_i$

Accelerating torque $M_i\omega_i$

where

K the stiffness of the shaft section in p.u. torque/rad

θ_i the twist angle of mass i in rad/s

ω_i the speed of mass i in p.u.

M_i the inertia constant of mass i in seconds

D the damping coefficient of each mass in p.u. torque/p.u. speed

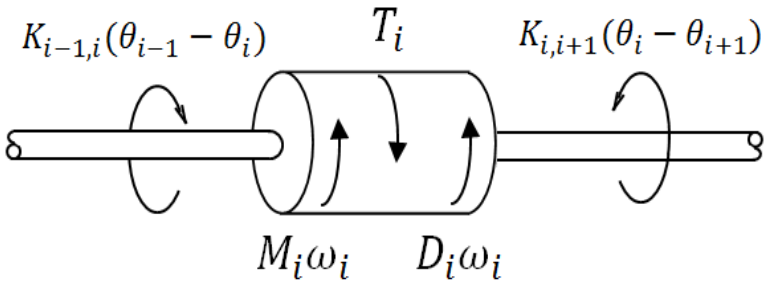

Fig. 3.3 The i^{th} mass-spring system [26].

Therefore, the linearized differential equations that describe the torque equilibrium and the motion of the i^{th} mass are [26-28]:

$$\frac{M_i}{\omega_0}\Delta\dot{\omega}_i = K_{i-1,i}(\Delta\theta_{i-1} - \Delta\theta_i) - \Delta T_i - K_{i,i+1}(\Delta\theta_i - \Delta\theta_{i+1}) - D_i\Delta\omega_i \quad (3.1)$$

$$\Delta\dot{\theta}_i = \omega_0\Delta\omega_i \quad (3.2)$$

$$K_{i-1,i}\big|_{i=1} = 0,\ \ K_{i,i+1}\big|_{i=n} = 0,\ \ i = 1,2,\dots,n \quad (3.3)$$

Equations (3.1) to (3.3) are applied to the linear six mass spring system depicted in Figure 3.2.The sections of the steam turbine, generator and the rotating exciter are identified by subscripts $H,\ I, A, B, G$ and X respectively. The shaft stiffness is identified by K_{HI}, K_{IA}, ...etc. The linearized differential equations of the linear six-mass-spring system are as:

$$\Delta\dot{\omega}_H = \frac{1}{M_H}[\Delta T_H - D_H\Delta\omega_H - K_{HI}(\Delta\theta_H - \Delta\theta_I)] \quad (3.4a)$$

$$\Delta\dot{\theta}_H = \omega_b\Delta\omega_H \quad (3.4)$$

$$\Delta\dot{\omega}_I = \frac{1}{M_I}[\Delta T_I - D_I\Delta\omega_I + K_{HI}(\Delta\theta_H - \Delta\theta_I) - K_{IA}(\Delta\theta_I - \Delta\theta_A)] \quad (3.5a)$$

$$\Delta\dot{\theta}_I = \omega_b\Delta\omega_I \quad (3.5)$$

$$\Delta\dot{\omega}_A = \frac{1}{M_A}[\Delta T_A - D_A\Delta\omega_A + K_{IA}(\Delta\theta_I - \Delta\theta_A) - K_{AB}(\Delta\theta_A - \Delta\theta_B)] \quad (3.6a)$$

$$\Delta\dot{\theta}_A = \omega_b\Delta\omega_A \quad (3.6)$$

$$\Delta\dot{\omega}_B = \frac{1}{M_B}[\Delta T_B - D_B\Delta\omega_B + K_{AB}(\Delta\theta_A - \Delta\theta_B) - K_{BG}(\Delta\theta_B - \Delta\delta)] \quad (3.7a)$$

$$\Delta\dot{\theta}_B = \omega_b\Delta\omega_B \quad (3.7)$$

$$\Delta\dot{\omega} = \frac{1}{M_G}[-\Delta T_e - D_G\Delta\omega + K_{BG}(\Delta\theta_B - \Delta\delta) - K_{GX}(\Delta\delta - \Delta\theta_X)] \quad (3.8a)$$

$$\Delta\dot{\delta} = \omega_b\Delta\omega \quad (3.8)$$

$$\Delta\dot{\omega}_{EXC} = \frac{1}{M_X}[-\Delta T_x - D_X\Delta\omega_X + K_{GX}(\Delta\delta - \Delta\theta_X)] \quad (3.9a)$$

$$\Delta\dot{\theta}_{EXC} = \omega_b\Delta\omega_X \quad (3.9)$$

where the $\omega's$ are the speeds in per unit value, ω_b is the base speed (2πf rad/s), the $\theta's$ are the mechanical angles in mechanical radians, and δ is the electrical angle in electrical radians [36], [74]. Superscript "." is used to indicate the differential operator and Δ represents an incremental value.

The exciter torque (ΔT_x) may be neglected, as it is relatively small and difficult to calculate [75].

The overall shaft equations are given by the following matrix equation:

$$[\Delta \dot{x}_{ms}] = [A_{ms}][\Delta x_{ms}] + [B_{ms}][\Delta U_{ms}] \quad (3.10)$$

where

$$[\Delta x_{ms}] = [\Delta\omega_H, \Delta\theta_H, \Delta\omega_I, \Delta\theta_I, \Delta\omega_{LPA}, \Delta\theta_{LPA}, \Delta\omega_{LPB}, \Delta\theta_{LPB}, \Delta\omega, \Delta\delta, \Delta\omega_{EXC}, \Delta\theta_{EXC}]^T$$

$$[\Delta U_{ms}] = [\Delta t_H, \Delta T_I, \Delta T_{LPA}, \Delta T_{LPB}, \Delta T_e]^T$$

$$[A_{ms}] =$$

$$\begin{bmatrix}
-D_H/M_H - K_{HI}/M_H & 0 & K_{HI}/M_H & 0 & 0 & 0 & 0 & 0 & 0 & 0 & 0 \\
\omega_b & 0 & 0 & 0 & 0 & 0 & 0 & 0 & 0 & 0 & 0 \\
0 & K_{HI}/M_I & -D_I/M_I - (K_{HI} + K_{IA})/M_I & 0 & K_{HI}/M_I & 0 & 0 & 0 & 0 & 0 & 0 \\
0 & 0 & \omega_b & 0 & 0 & 0 & 0 & 0 & 0 & 0 & 0 \\
0 & 0 & 0 & K_{IA}/M_A & -D_A/M_A - (K_{IA} + K_{AB})/M_A & 0 & K_{AB}/M_A & 0 & 0 & 0 & 0 \\
0 & 0 & 0 & 0 & \omega_b & 0 & 0 & 0 & 0 & 0 & 0 \\
0 & 0 & 0 & 0 & 0 & K_{AB}/M_B & -D_B/M_B - (K_{AB} + K_{BG})/M_B & 0 & K_{BG}/M_B & 0 & 0 \\
0 & 0 & 0 & 0 & 0 & 0 & \omega_b & 0 & 0 & 0 & 0 \\
0 & 0 & 0 & 0 & 0 & 0 & 0 & K_{BG}/M_G & -D_G/M_G - (K_{BG} + K_{GE})/M_G & 0 & K_{GE}/M_G \\
0 & 0 & 0 & 0 & 0 & 0 & 0 & 0 & \omega_b & 0 & 0 \\
0 & 0 & 0 & 0 & 0 & 0 & 0 & 0 & 0 & K_{GE}/M_E & -D_E/M_E - K_{GE}/M_E \\
0 & 0 & 0 & 0 & 0 & 0 & 0 & 0 & 0 & \omega_b & 0
\end{bmatrix}$$

$$[B_{ms}] = \begin{bmatrix}
1/M_H & 0 & 0 & 0 & 0 \\
0 & 0 & 0 & 0 & 0 \\
0 & 1/M_I & 0 & 0 & 0 \\
0 & 0 & 0 & 0 & 0 \\
0 & 0 & 1/M_A & 0 & 0 \\
0 & 0 & 0 & 0 & 0 \\
0 & 0 & 0 & 1/M_B & 0 \\
0 & 0 & 0 & 0 & 0 \\
0 & 0 & 0 & 0 & -1/M_G \\
0 & 0 & 0 & 0 & 0 \\
0 & 0 & 0 & 0 & 0 \\
0 & 0 & 0 & 0 & 0
\end{bmatrix}$$

3.3.2 Turbine torque and governor system

Figure 3.4 shows the block diagram of the steam turbine and the speed governor. There are four turbine torques with a total output of T_m. All the turbine torques are proportional, with each turbine contributing a fraction and the sum of the fractions is calculated as:

$$F_H + F_I + F_A + F_B = 1 \quad (3.12)$$

where F_H, F_I, F_A and F_B represent the fraction of mechanical power delivered by high pressure, intermediate pressure, low pressure A and low-pressure B turbine respectively.

The speed of the shaft between the low pressure turbine and the generator rotor is sensed and combined with the reference speed to have input signal for the governor. This speed deviation is relayed to activate the servomotor to control the steam flow by opening or closing the steam valves [74-75]. As shown in Figure 3.4, the governor is modelled as:

$$(1 + sT_{SR})a = K_g \Delta\omega \quad (3.13)$$

$$(1 + sT_{SM})g = a \quad (3.14)$$

where a and g denote the speed relay position and the governor opening. K_g, T_{SR} and T_{SM} are the governor gain and the two time constants of the governor.

There are three time constants due to the steam flow, T_{CH} in the chamber in the front of the pressure turbine, T_{RH} in the reheater between the high and intermediate pressure turbines, and T_{CO} in the crossover connection between the intermediate and low pressure turbines. Therefore, three differential equations are used to model the turbine torques as:

$$(1 + sT_{CH})\Delta T_H = F_H g \quad (3.15)$$

$$(1 + sT_{RH})\Delta T_I = \frac{F_I}{F_H}\Delta T_H \quad (3.16)$$

$$(1 + sT_{CO})\Delta T_A = \frac{F_A}{F_I}\Delta T_I \quad (3.17)$$

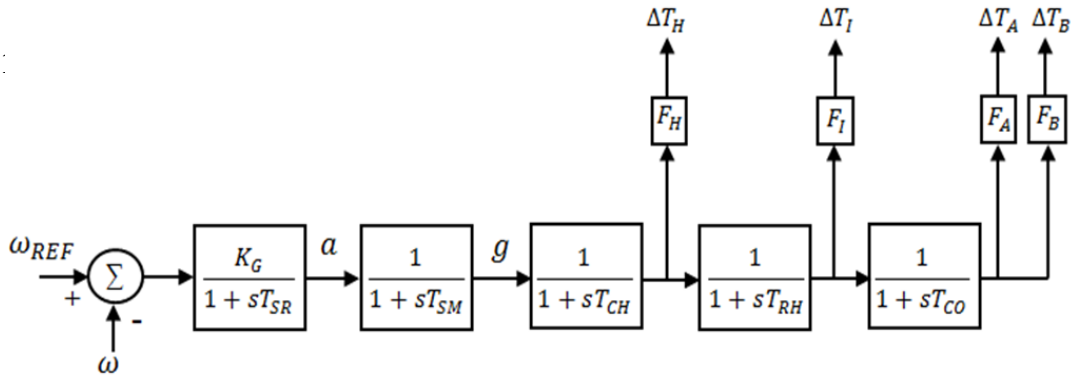

Fig. 3.4 Block diagram of the governor and the steam turbine [6].

$$\Delta T_B = \frac{\boldsymbol{F_B}}{\boldsymbol{F_A}} \Delta T_A \tag{3.18}$$

Equations (3.13) to (3.18) are linearized and written in the time domain in the standard state variable form as:

$$\Delta \dot{T}_H = \frac{F_H}{T_{CH}} \Delta g - \frac{1}{T_{CH}} \Delta T_H \tag{3.19}$$

$$\Delta \dot{T}_I = \frac{F_I}{T_{RH} F_H} \Delta T_H - \frac{1}{T_{RH}} \Delta T_I \tag{3.20}$$

$$\Delta \dot{T}_A = \frac{F_A}{T_{CO} F_I} \Delta T_I - \frac{1}{T_{CO}} \Delta T_A \tag{3.21}$$

$$\Delta \dot{a} = \frac{K_g}{T_{SR}} \Delta \omega - \frac{1}{T_{SR}} \Delta a \tag{3.22}$$

$$\Delta \dot{g} = \frac{1}{T_{SM}} \Delta a - \frac{1}{T_{SM}} \Delta g \tag{3.23}$$

The corresponding state space equation is given as:

$$[\Delta \dot{x}_g] = [A_g][\Delta x_g] + [B_g][\Delta U_g] \tag{3.24}$$

where

$$[\Delta x_g] = [\Delta T_H, \Delta T_H, \Delta T_H, \Delta a, \Delta g\ ]^T \tag{3.25}$$

$$[\Delta U_g] = [\Delta \omega\ ]^T \tag{3.26}$$

$$A_g = \begin{bmatrix} -1/T_{CH} & 0 & 0 & 0 & F_H/T_{CH} \\ F_I/(T_{RH}F_H) & -1/T_{RH} & 0 & 0 & 0 \\ 0 & F_A/(T_{CO}F_I) & -1/T_{CO} & 0 & 0 \\ 0 & 0 & 0 & -1/T_{SR} & 0 \\ 0 & 0 & 0 & 1/T_{SM} & -1/T_{SM} \end{bmatrix}$$

$$B_g = \begin{bmatrix} 0 \\ 0 \\ 0 \\ K_g/T_{SR} \\ 0 \end{bmatrix}$$

3.3.3 Modelling of the synchronous generator.

Figure 3.5 depicts a schematic diagram of a conventional synchronous machine which consists of stator and rotor. The stator circuit consists of three-phase windings (a, b and c) which produce a sinusoidal space distributed magneto-motive force. The rotor circuit carries the field (excitation) winding which is excited by DC voltage and the damper windings. The damper winding is represented by three equivalent damper circuits; one (D damper) on the direct axis (d-axis) and two (Q and S dampers) on the quadratic axis (q-axis) [3-5].

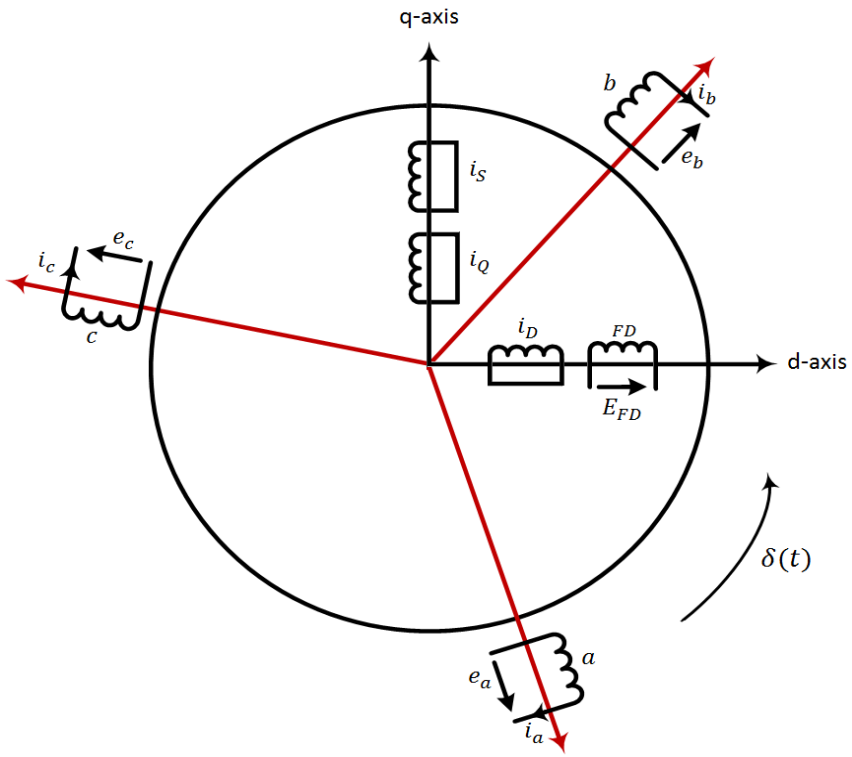

Fig. 3.5 Schematic diagram of a conventional synchronous generator [68]

where

a, b, c: Stator windings

e_a, e_b, e_c: Stator three phase winding voltages

i_a, i_b, i_c: Stator three phase winding currents

v_f, E_{FD}: Field winding, Field voltage

i_D: d-axis damping winding

i_Q, i_S: q-axis damping windings

$\delta(t)$: the electric angle by which d-axis leads the axis of phase a winding

For the SSR study, it is more convenient to choose the generator currents instead of the flux linkages as state variables. Therefore, the synchronous generator voltage equations in linear form become:

2- d- axis:

$$\frac{1}{\omega_b}\left(-x_d\Delta\dot{i}_d + x_{md}\Delta\dot{i}_f + x_{md}\Delta\dot{i}_D\right) = \Delta v_{td} + r_a\Delta i_d - x_q\Delta i_q + x_{mq}\Delta i_Q + x_{mq}\Delta i_S + \psi_{qo}\Delta\omega \quad (3.27)$$

$$\frac{1}{\omega_b}\left(-x_{md}\Delta\dot{i}_d + x_f\Delta\dot{i}_f + x_{md}\Delta\dot{i}_D\right) = \Delta v_f - r_f\Delta i_f \quad (3.28)$$

$$\frac{1}{\omega_b}\left(-x_{md}\Delta\dot{i}_d + x_{md}\Delta\dot{i}_f + x_D\Delta\dot{i}_D\right) = r_D\Delta i_D \quad (3.29)$$

3- q-axis:

$$\frac{1}{\omega_b}\left(-x_q\Delta\dot{i}_q + x_{mq}\Delta\dot{i}_Q + x_{mq}\Delta\dot{i}_S\right) = \Delta v_{tq} + r_a\Delta i_q + x_d\Delta i_d - x_{md}\Delta i_f - x_{md}\Delta i_D - \psi_{do}\Delta\omega \quad (3.30)$$

$$\frac{1}{\omega_b}\left(-x_{mq}\Delta\dot{i}_q + x_Q\Delta\dot{i}_Q + x_{mq}\Delta\dot{i}_S\right) = r_Q\Delta i_Q \quad (3.31)$$

$$\frac{1}{\omega_b}\left(-x_{mq}\Delta\dot{i}_q + x_{mq}\Delta\dot{i}_Q + x_S\Delta\dot{i}_S\right) = r_S\Delta i_S \quad (3.32)$$

Air-gap torque equation:

$$\Delta T_e = -(x_{mq}i_{Q0} + x_{mq}i_{S0})\Delta i_d + \left(x_{md}i_{f0} + x_{md}i_{D0}\right)\Delta i_q + x_{md}i_{q0}\Delta i_f + x_{md}i_{q0}\Delta i_D - x_{mq}i_{d0}\Delta i_Q - x_{mq}i_{d0}\Delta i_S \quad (3.33)$$

where v_{td} and v_{tq} are the d-q components of synchronous generator terminal voltage. Subscript "0" is used to indicate initial value and superscript "." represents differential operator. v_f is the field voltage and is defined using output field voltage as:

$$v_f = \frac{r_f}{x_{md}}E_{FD} \quad (3.34)$$

The corresponding state space equation in the linear form is given as:

$$[\Delta\dot{x}_e] = [A_e][\Delta x_e] + [B_e][\Delta U_e] \quad (3.35)$$

where

$$[\Delta x_e] = \left[\Delta i_d, \Delta i_q, \Delta i_f, \Delta i_D, \Delta i_Q, \Delta i_S\right]^T \quad (3.36)$$

$$[\Delta U_e] = \left[\Delta\omega, , \Delta E_{fd}, \Delta v_{td}, \Delta v_{tq}\right]^T \tag{3.37}$$

$$[A_e] = [L]^{-1}[Q]$$

$$[B_e] = [L]^{-1}[R]$$

$$[L] = \omega_b \begin{bmatrix} -x_d & 0 & x_{md} & x_{md} & 0 & 0 \\ 0 & -x_q & 0 & 0 & x_{mq} & x_{mq} \\ -x_{md} & 0 & x_f & x_{md} & 0 & 0 \\ -x_{md} & 0 & x_{md} & x_D & 0 & 0 \\ 0 & -x_{mq} & 0 & 0 & x_Q & x_{mq} \\ 0 & -x_{mq} & 0 & 0 & x_{mq} & x_S \end{bmatrix}$$

$$[Q] = \begin{bmatrix} r_a & -x_q & 0 & 0 & x_{mq} & x_{mq} \\ x_d & r_a & -x_{md} & -x_{md} & 0 & 0 \\ 0 & 0 & -r_f & 0 & 0 & 0 \\ 0 & 0 & 0 & r_D & 0 & 0 \\ 0 & 0 & 0 & 0 & r_Q & 0 \\ 0 & 0 & 0 & 0 & 0 & r_S \end{bmatrix}$$

$$[R] = \begin{bmatrix} \psi_{qo} & 0 & 1 & 0 \\ 0 & -\psi_{do} & 0 & 1 \\ r_f/x_{md} & 0 & 0 & 0 \\ 0 & 0 & 0 & 0 \\ 0 & 0 & 0 & 0 \\ 0 & 0 & 0 & 0 \end{bmatrix}$$

3.3.4 Modelling of the transmission line.

Figure 3.6 shows a single line diagram of the series compensation representing by RLC circuit. The synchronous generator is represented by constant voltage source behind the transient reactance [36]. R_L and x_L represent the total resistance and inductance of the transformer and the transmission line. E_g and V_b are the generator terminal voltage behind the transient reactance and infinite bus voltage. x_C is series capacitance and its value is calculated as a percentage of the inductance of the transmission line as:

$$x_C = \%\, compensation \times x_L \tag{3.38}$$

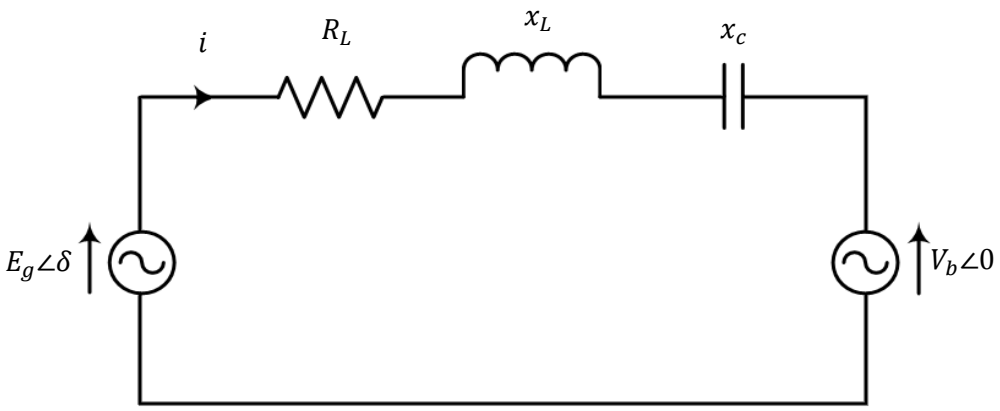

Fig. 3.6 Equivalent single line diagram of the FBM system [68].

Figure 3.7 depicts the voltages phasor for synchronous generator connecting to the grid in the rotor frame reference, d-q axes, regarding to the voltage reference. In Figure 3.7, δ is the rotor angle by which the q-axis of the rotor frame reference leads the infinite bus voltage. By applying Park's transformation [26], the differential equations for the series compensated transmission line are expressed in the d-q reference frame as:

$$v_{td} = R_L i_d - x_L i_q + \frac{x_L}{\omega_b} P i_d + e_{cd} + V_{bd} \tag{3.39}$$

$$v_{tq} = x_L i_d + R_L i_q + \frac{x_L}{\omega_b} P i_q + e_{cq} + V_{bq} \tag{3.40}$$

$$i_d = \frac{1}{\omega_b x_c} P e_{cd} - \frac{1}{x_c} e_{cq} \tag{3.41}$$

$$i_q = \frac{1}{\omega_b x_c} P e_{cq} + \frac{1}{x_c} e_{cd} \tag{3.42}$$

where e_{cd} and e_{cq} are the d-q components of the voltage across the series capacitance. "P" is the differential operator.

As shown in Figure 3.7, V_{bd} and V_{bq} are the d-q components of the infinite bus as:

$$V_{bd} = V_{b0}\sin(\delta),\ V_{bq} = V_{b0}\cos(\delta) \tag{3.43}$$

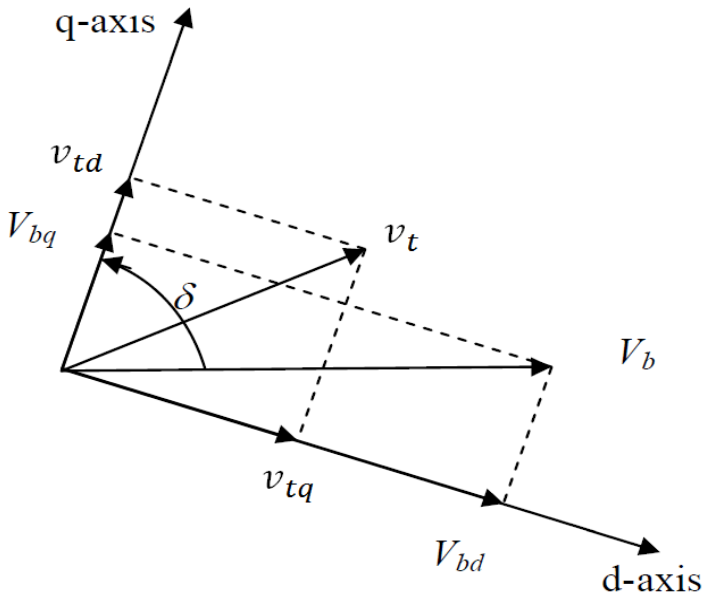

Fig. 3.7 Voltage phasor diagram between the terminal voltage of the synchronous generator and the infinite bus voltage in d-q frame.

By substituting equation (3.43) in equations (3.39) and (3.40), the linearized forms of equations (3.39) to (3.42) are written as:

$$\Delta v_{td} = R_L \Delta i_d - x_L \Delta i_q + \frac{x_L}{\omega_b} \Delta \dot{i}_d + \Delta e_{cd} + V_{b0} \cos(\delta_0)\, \Delta\delta \tag{3.44}$$

$$\Delta v_{tq} = x_L \Delta i_d + R_L \Delta i_q + \frac{x_L}{\omega_b} \Delta \dot{i}_q + \Delta e_{cq} - V_{b0} \sin(\delta_0)\, \Delta\delta \tag{3.45}$$

$$\Delta i_d = \frac{1}{\omega_b x_c} \Delta \dot{e}_{cd} - \frac{1}{x_c} \Delta e_{cq} \tag{3.46}$$

$$\Delta i_q = \frac{1}{\omega_b x_c} \Delta \dot{e}_{cq} + \frac{1}{x_c} \Delta e_{cd} \tag{3.47}$$

The state space form for series compensated transmission line is given as:

$$\begin{bmatrix} \Delta v_{td} \\ \Delta v_{tq} \end{bmatrix} = \begin{bmatrix} 1 & 0 \\ 0 & 1 \end{bmatrix} \begin{bmatrix} \Delta e_{cd} \\ \Delta e_{cq} \end{bmatrix} + \begin{bmatrix} R_L & -x_L \\ x_L & R_L \end{bmatrix} \begin{bmatrix} \Delta i_d \\ \Delta i_q \end{bmatrix} + \frac{x_L}{\omega_b} \begin{bmatrix} \Delta \dot{i}_d \\ \Delta \dot{i}_q \end{bmatrix} + \begin{bmatrix} V_{b0} \cos(\delta_0) \\ -V_{b0} \sin(\delta_0) \end{bmatrix} \Delta\delta \tag{3.48}$$

$$\begin{bmatrix} \Delta \dot{e}_{cd} \\ \Delta \dot{e}_{cq} \end{bmatrix} = \begin{bmatrix} 0 & \omega_b \\ -\omega_b & 0 \end{bmatrix} \begin{bmatrix} \Delta e_{cd} \\ \Delta e_{cq} \end{bmatrix} + \begin{bmatrix} \omega_b x_c & 0 \\ 0 & \omega_b x_c \end{bmatrix} \begin{bmatrix} \Delta i_d \\ \Delta i_q \end{bmatrix} \tag{3.49}$$

3.3.5 The excitation system

Figure 3.8 shows the block diagram of the exciter mass and voltage regulator model. The synchronous generator in FBM has rotating exciter and is used to regulate the terminal voltage of the synchronous generator. The corresponding data are given in the end of the chapter [26-28]. The regulator input filter, the saturation function and the stabilizing feedback loop are neglected for simplification. Regarding the relation between the excitation output voltage and the field voltage in equation (3.34), the excitation system can be derived from its block diagram in Figure 3.8 as:

$$\dot{V}_R = \frac{K_A}{T_A} V_R - \frac{1}{T_A} \Delta v_t \tag{3.50}$$

$$\dot{E}_{FD} = \frac{1}{T_E} E_{FD} - \frac{1}{T_E} V_R \tag{3.51}$$

where

K_A, T_A: The voltage regulator gain and its time constant

T_E: The exciter time constant

v_t: The terminal voltage of the synchronous generator

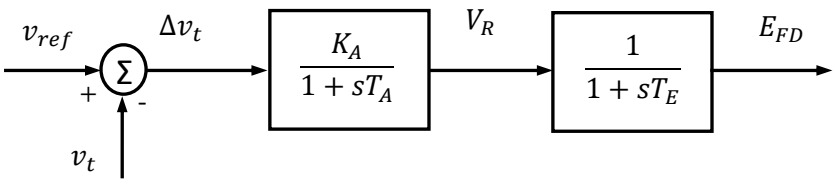

Fig. 3.8 Block diagram of the excitation system [26].

The linearized form of the terminal voltage of the synchronous generator is derived as:

$$\Delta v_t = \frac{v_{d0}}{v_{t0}}\Delta v_{td} + \frac{v_{q0}}{v_{t0}}\Delta v_{tq} \tag{3.52}$$

The state-space equation of the excitation system in the linearized form is:

$$\begin{bmatrix} \Delta \dot{V}_R \\ \Delta \dot{E}_{FD} \end{bmatrix} = \begin{bmatrix} \frac{K_A}{T_A} & 0 \\ \frac{1}{T_E} & \frac{-1}{T_E} \end{bmatrix} \begin{bmatrix} \Delta V_R \\ \Delta E_{FD} \end{bmatrix} + \frac{1}{T_A} \begin{bmatrix} \frac{-v_{d0}}{v_{t0}} & \frac{-v_{q0}}{v_{t0}} \\ 0 & 0 \end{bmatrix} \begin{bmatrix} \Delta v_{td} \\ \Delta v_{tq} \end{bmatrix} \tag{3.53}$$

3.3.6 The state space equations for the complete system

The overall model of the system under study, IEEE First Benchmark Model, was derived by performing the following mathematical manipulations for the interactions among the various components of the system [36], [74].

The electrical parts of the system are gathered by combining Equations (3.35), (3.48) and (3.49) to form the following equations:

$$\begin{bmatrix} \Delta \dot{x}_e \\ \Delta \dot{e}_{cd} \\ \Delta \dot{e}_{cq} \end{bmatrix} = [AE] \begin{bmatrix} \Delta x_e \\ \Delta e_{cd} \\ \Delta e_{cq} \end{bmatrix} + [BE] \begin{bmatrix} \Delta \omega \\ \\ \Delta \delta \end{bmatrix} \tag{3.54}$$

$$\begin{bmatrix} \Delta v_{td} \\ \\ \Delta v_{tq} \end{bmatrix} = [CE] \begin{bmatrix} \Delta x_e \\ \Delta e_{cd} \\ \Delta e_{cq} \end{bmatrix} \tag{3.55}$$

where AE is the system matrix, BE represents the input matrix and CE is the output matrix.

In the same way, the mechanical parts of the system are gathered by combining Equation (3.10), (3.21), and (3.52) to form the following equations:

$$\begin{bmatrix} \Delta \dot{x}_{ms} \\ \Delta \dot{V}_R \\ \Delta \dot{E}_{FD} \end{bmatrix} = [AM] \begin{bmatrix} \Delta x_{ms} \\ \Delta V_R \\ \Delta E_{FD} \end{bmatrix} + [BM] \begin{bmatrix} \Delta T_e \\ \Delta v_{td} \\ \Delta v_{tq} \end{bmatrix} \tag{3.56}$$

$$\begin{bmatrix} \Delta \omega \\ \\ \Delta \delta \end{bmatrix} = [CM] \begin{bmatrix} \Delta x_{ms} \\ \Delta V_R \\ \Delta E_{FD} \end{bmatrix} \tag{3.57}$$

where AM is the system matrix, while BM and CM represent the input and output vectors. The vectors $[DE]$ and $[DM]$ equal zero.

Combining Equation (3.54), (3.55), (4.56) and (4.57), the overall linearized equations of the system under study, IEEE First Benchmark model, are given by:

$$[\Delta \dot{x}_{sys}] = [At_{sys}][\Delta x_{sys}] \quad (4.58)$$

where

$$[\Delta X_{sys}] = [\Delta\omega_H\ \Delta\theta_H\ \Delta\omega_I\ \Delta\theta_I\ \Delta\omega_{LPA}\ \Delta\theta_{LPA}\ \Delta\omega_{LPB}\ \Delta\theta_{LPB}\ \Delta\omega\ \Delta\delta\ \Delta\omega_{EXC}\ \Delta\theta_{EXC}\ \ldots$$
$$\Delta T_H\ \Delta T_i\ \Delta T_A\ \Delta a\ \Delta g\ \Delta e_{cd}\ \Delta e_{cq}\ \Delta i_d\ \Delta i_q\ \ \Delta i_F\ \Delta i_D\ \Delta i_Q\ \Delta i_S\ \ \Delta V_R\ \Delta E_{ED}]$$

The complete linearized electrical and mechanical model of the system to study SSR is a 27th-order system.

3.4 Effect of Series Capacitor Compensation on SSR

The six-mass model of the turbine-generator shaft system shown in Figure 3.2 has five torsional modes in addition to the rigid body mode (0 mode). 0 Mode with the lowest frequency, 1.5 Hz, is the mode usually considered in power-system stability analysis as it represents the oscillation of the entire rotor against the power system. It is called the swing or electro-mechanical mode because the turbine sections, generator, and exciter oscillate together as a rigid body without a shaft twist [26-28].

The other 5 mechanical modes are called torsional modes because they indicate that some of the shaft masses oscillate against the others as shown in Figure 3.9.The “n” torsional modes are numbered sequentially according to mode frequency and number of phase reversals in the mode shape. In general, mode n has the n^{th} lowest frequency and a mode shape with n shaft twists. Mode 1 has one shaft twist and its frequency is the lowest torsional mode frequency, mode 2 has two shaft twists, and so on.

The mode shapes are found from the eigenvectors, which in turn are determined from calculating the eigenvalues of the mass spring system. For each eigenvalue, there is an eigenvector consisting of six components. These six components are normalized with respect to the largest component, the six mode shapes of the torsional oscillations of all eigenvectors emerge as in Figure 3.9.

Figure 3.9 is obtained by calculating the eigenvectors of the linearized model of FBM and these data were verified by comparing it with references used FBM in their system such as [26-28]. To sketch the mode shapes for the torsional oscillation modes as shown in Figure 3.9. The steps, which were followed to sketch the mode shapes are as:

- Obtain the eigenvalues of the linearized model.
- Obtain the right eigenvectors corresponding to the these eigenvalues.
- Select the columns associated to the torsional modes and select the elements from these columns corresponding to state variables of the speed of the masses or the twist angle of masses.
- Separate the real parts of these elements of these eigenvectors and make normalization to it.

It is noticeable from Figure 3-9 that, the rotors of the generator, LPB section and exciter have very low relative amplitudes of rotational displacement in torsional mode 5. Therefore, this mode cannot be easily excited by applying torques to the generator, LPA and exciter rotor.

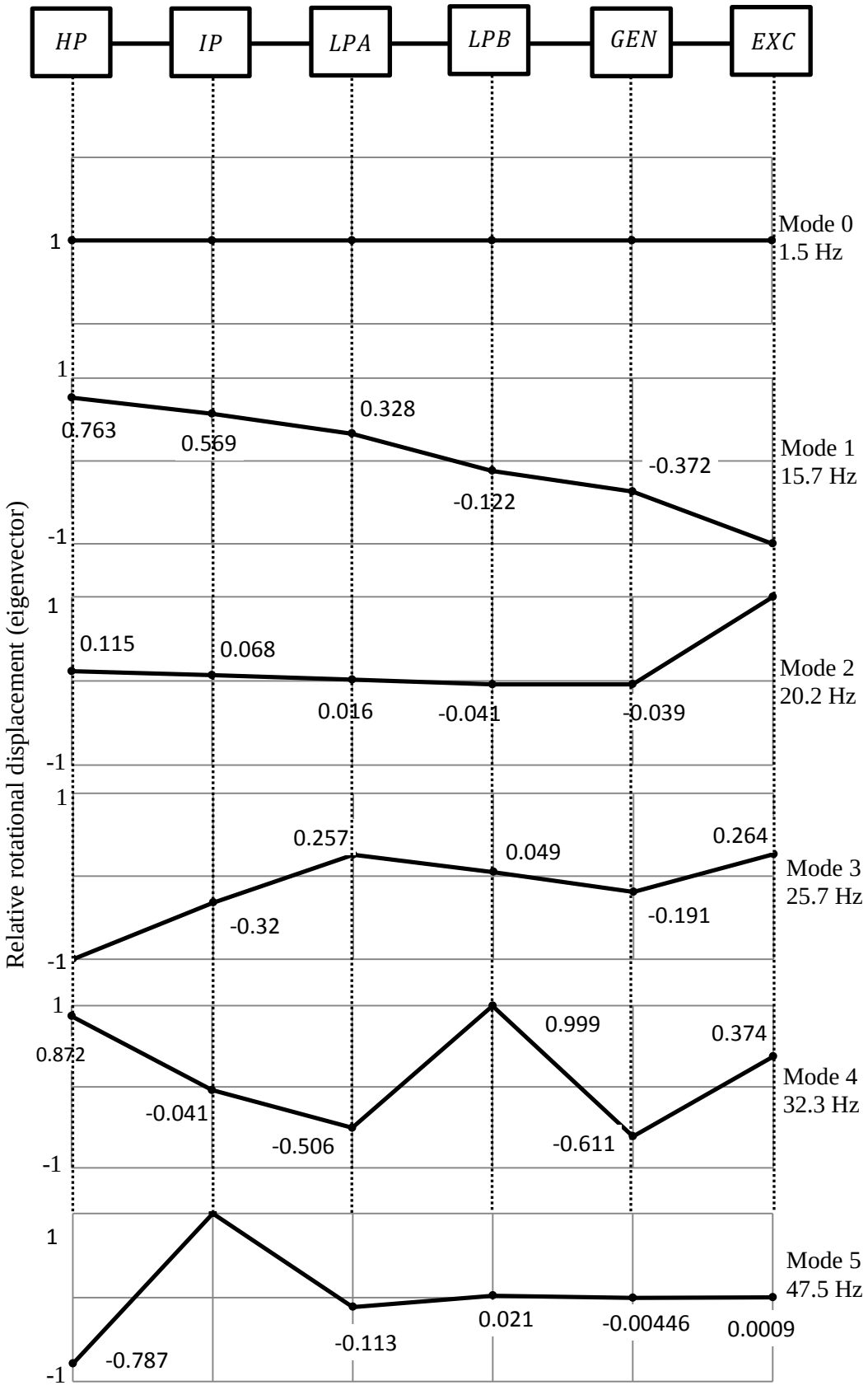

Fig. 3.9 Natural frequencies and mode shapes of the turbine-generator shaft system of FBM

To study how these oscillatory modes interact with each other, the variation of the real and imaginary parts of the eigenvalues is investigated over a wide range of series compensation levels. Results are listed in Table 3-1for 20%, 30% and 50% series compensation. Figure 3.10 shows the ranges of series compensation levels for which torsional instability arises. Figure 3.10a shows the real parts of eigenvalues of the torsional modes in addition to mode 0, while Figure 3.10b the imaginary parts of the eigenvalues of torsional modes, mode 0 and subsynchronous mode (SUB mode) as a function of the compensation level from 0% to 100%. The torsional instability of the FBM is directly related to the mode SUB whose frequency decreases as the series compensation increases.

Examining the Table 3-1 and Figure 3.10 shows that:

- The frequency of the SUB mode decreases with the increase of the compensation level.Therefore, there is an increased risk that the frequency of the SUB mode will match one of the frequencies of the torsional oscillation modes as the compensation level is increased.
- There are four unstable torsional modes (4, 3, 2 and 1 modes). Each of these modes is excited and becomes unstable whenever the frequency of mode SUB coincides or is close with its frequency.
- Up to 27% series compensation, none of the torsional modes oscillate as the frequency of SUB mode is far away from their natural frequencies although the system is unstable because it’s the real part of 0 mode is positive.
- Mode 1 shows the most severe undamping with a peak at 85% series compensation. As the amplitude of the torsional oscillation of 1mode is the highest among the five torsional modes.
- 5 Mode is stable over the whole range of series compensation as its modal inertia is high.
- The other eigenvalue modes listed in Table 3-1, relating to the generator windings, the excitation system and the governor system and the turbine, are stable.

Table 3-1: Eigenvalues of the IEEE FBM.

modes	Series compensation level		
	20%	**30%**	**50%**
5	-0.182 ±J 298.18	-0.182±J298.18	-0.182 ±J298.18
4	-0.202 ±J 203.25	**+0.278 ±J 204.45**	+0.159 ±J 202.65
3	-0.225 ±J 160.68	-0.246 ±J 160.75	**+1.014 ±J161.45**
2	-0.667 ±J 127.03	-0.670 ±J 127.04	-0.678 ±J 127.09
1	-0.264 ±J 99.188	-0.285 ±J 99.274	-0.348 ±J 99.579
0	-0.140 ±J 8.5706	-0.215 ±J9.0368	-0.407±J 10.123
SUB	-6.070 ±J 241.11	**-6.316 ±J 209.27**	**-6.947 ±J161.68**
Other modes	-6.963 ±J 512.11 -499.98 -101.86 -31.058 -24.764 -8.4711 -0.144 -5.541 -4.811 -2.987 ±J 0.585 -2.2641	-7.006 ±J542.58 -499.98 -101.8 -31.391 -24.776 -8.344 -0.144 -5.490 -4.817 -2.272 -2.997 ±J 0.449	-7.063 ±J 590.87 -499.98 -101.66 -32.255 -24.804 -8.035 -0.144 -5.371 -4.836 -2.25 -2.758 -3.301

Examining the Table 3-1 shows that:

- At 20% series compensation, the frequency of the SUB mode is far away from the frequencies of the torsional modes. Therefore, all the torsional modes are stable as the real parts of the torsional modes are negative.
- At 30%, the frequency of SUB mode is close to 4 mode. Therefore, 4 mode is exciting and becomes unstable. In the same sequence, at 50% series compensation, the frequency of SUB mode is close to 3 mode. As a result, 3 mode becomes unstable and causes SSR at frequency 161.45 rad/s.

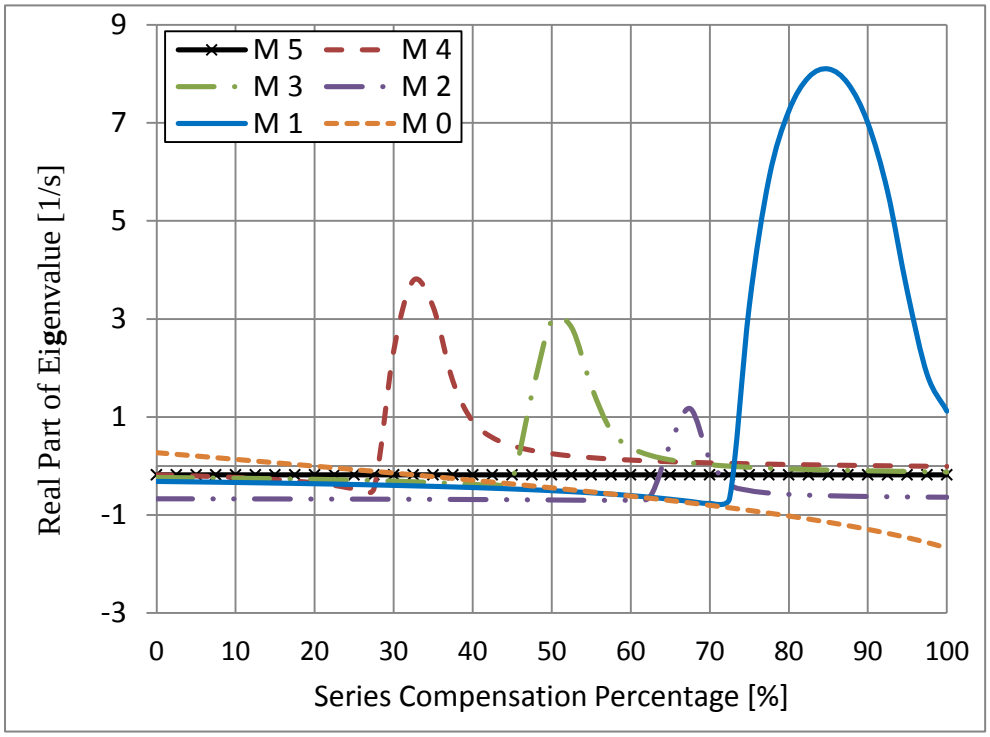

(a)

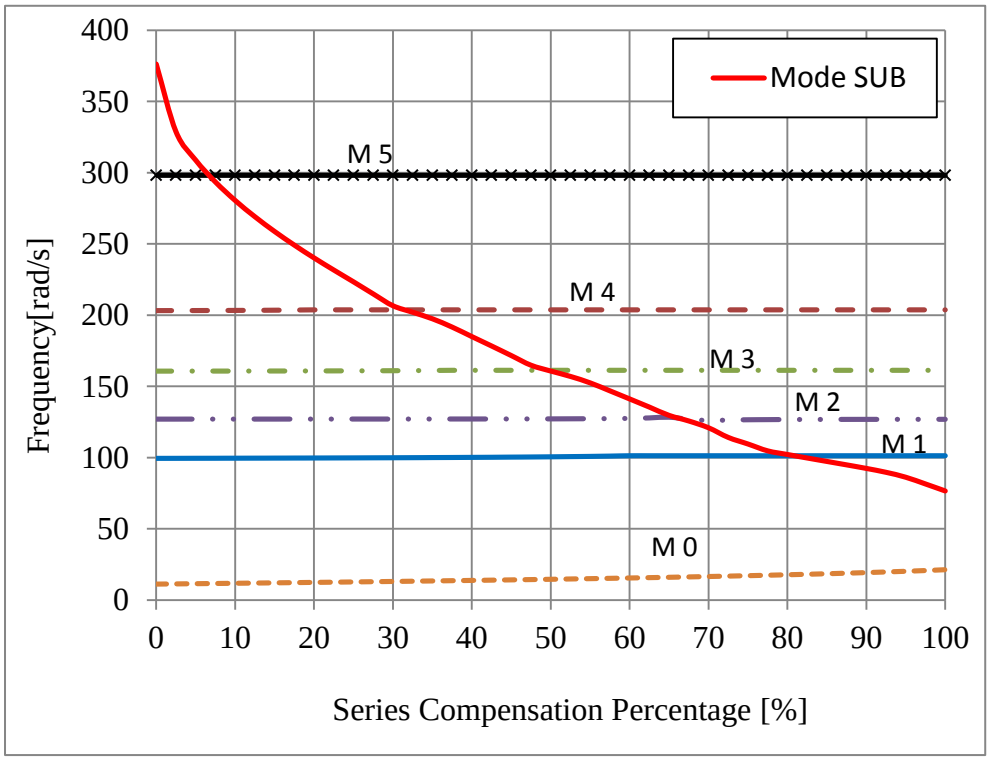

(b)

Fig. 3.10 Stability of the torsional modes in terms of the series compensation level for FBM: (a) Real parts of the torsional modes (b) Imaginary parts of the torsional modes

3.5 Conclusion

This chapter studied the subsynchronous resonance phenomenon and the torsional interaction effect. This study was based on the IEEE first benchmark model. The analysis was performed by modelling the individual sub-systems (turbine-generator mechanical system, synchronous generator, and electric network) separately, with linearized equations. The set of linearized equations were grouped to obtain the overall system model in a state-space form.

The effect of the series capacitor compensation on SSR was investigated using eigenvalue analysis. The eigenvalue analysis shows that the FBM system exhibits SSR phenomenon for a wide range of compensation levels. As a result, FBM is suitable for testing the effect of any technique on SSR.

Reducing the fixed series compensation level to be equal or be less than 25% can solve the torsional interaction problem by avoiding the interaction with SSR but is not an economic solution.

Chapter 4-

The Influence of Fixed Speed Induction Generator-Based Wind Turbines on SSR

4.1 Introduction

Fixed Speed Induction Generator based Wind turbines (FSIG-WTs) have been installed in large numbers in power grids. Wind parks of these turbines have been installed in many European countries, USA, China and India [14-15], [71]. About 15% of the operating wind parks in the Europe are of fixed speed type using asynchronous generators connected directly to the grid. These wind parks have a life time of over 20 years [72]. Squirrel cage induction generators are used in wind generators because of their low cost, asynchronous operation, and low maintenance because of rugged brushless construction. Although FSIG-WTs are vulnerable to network faults, they make a significant contribution to network damping [12]. For the reasons mentioned above, it is a matter of interest to investigate the interaction of FSIG-WTs with the power systems, especially to study their effect on SSR created in synchronous generators because of fixed series compensation.

In this chapter, the influence of FSIG-WTs on SSR occurrence in steam shafts is analyzed and a detailed analysis of FSIG-WTs connected to IEEE First Benchmark Model (FBM) is presented. A range of series compensation level and power rating of the wind farm are assessed. A detailed state space model of the system under study is developed for small-signal analysis using eigenvalue analysis. Time domain simulations are carried out to validate the eigenvalue analysis results. The simulations are performed in MATLAB and PSCAD/EMTDC.

4.2 System Description

The system under study is shown in Figure 4.1 and represents a large FSIG-Based Wind Farm (FSIG-WF) connected to the FBM via a short transmission line. Figure 4-2 presents the configuration of a typical FSIG-WF, where there are n identical wind turbines connected to the grid through the collector cables [12].

As the wind turbine rotor speed is much less than that of the generator, a gearbox is used to connect the low speed shaft of the turbine to the high-speed shaft of the generator. The nominal operating voltage of the generator is 690 V (line-line). The power is transmitted via a cable to a switchboard and a local step-up transformer is usually located at the tower base. As induction generators always consume reactive power, capacitor banks are employed to provide the reactive power consumption of the FSIG and improve the power factor [10]. The rating of the capacitor bank is selected to compensate for the no-load reactive power demand of the generator [11]. For simplicity, the mechanical drive train of the FSIG-WTs is simulated as one mass. The parameters used in the FBM and can be found in [72] and in the Chapter '3' while the parameters used in FSIG-WTs can be found in [10] and in the next page.

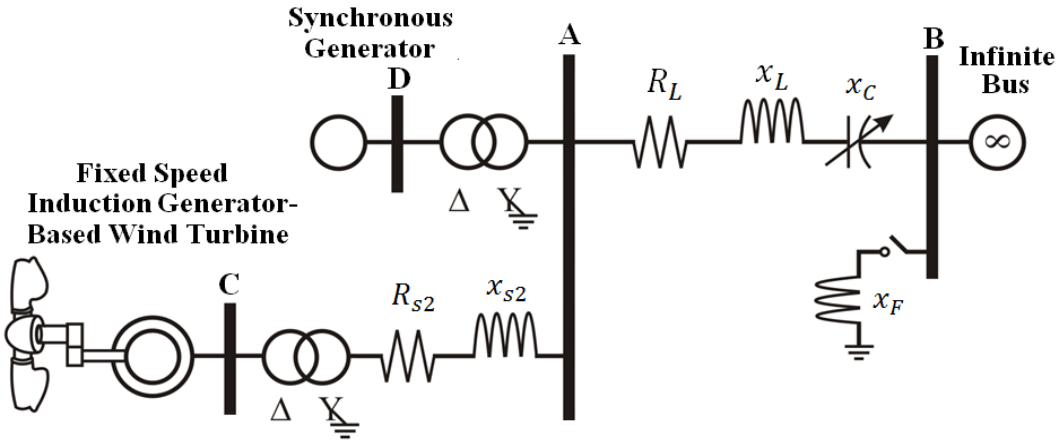

Fig. 4.1 FSIG connecting to IEEE first benchmark model.

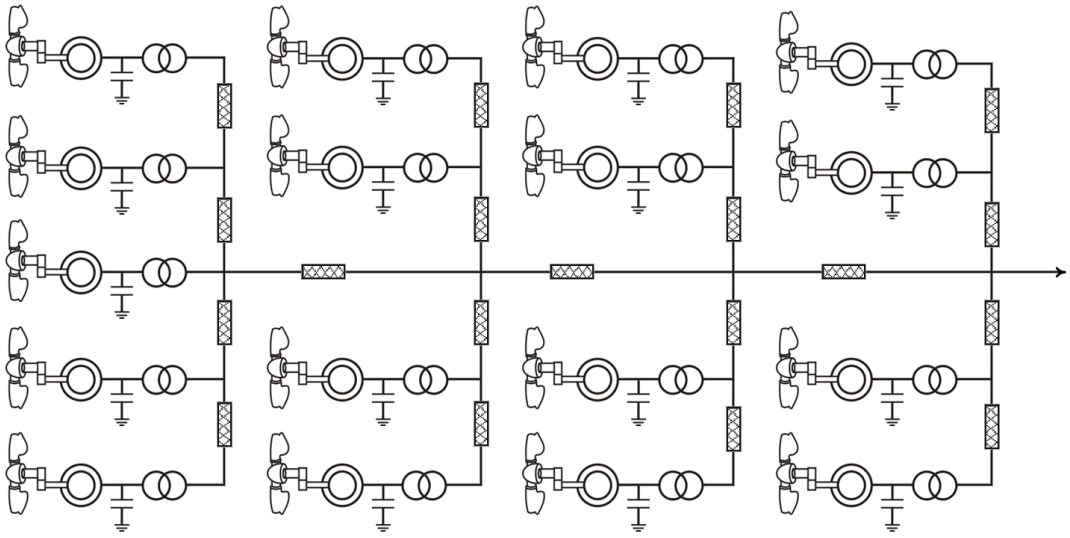

Fig. 4.2 Typical wind farm connection [12]

Parameters of Fixed Speed Induction Generator-Based Wind Turbine (FSIG-WT)

(a) Generator (p.u.)

R_s = 0.00488 X_{ls} = 0.09241 X_{lm} = 3.95279

R_r = 0.00549 X_{lr} = 0.09955 H= 3.5 s

(b) Transformer and transmission line (Line II) (p.u.)

X_{L2} = 0.23 R_{L2} = 0.01

(c) the initial operating condition of synchronous generator

P_G = 0.9 p.u. $P.F.$= 0.9 (lagging)

Vt =1.05 p.u.

4.3 The Modelling of the System under Study

The system under study consists of FSIG-WF connected to FBM through a short transmission line as shown in Figure 4.1. The FSIG-WF is represented by an equivalent induction generator model, which is represented by the aggregation of large numbers of identical induction generator-based wind turbine as shown in Figure 4.2. The size of the FSIG-WF is varied between 200 MW and 750 MW by changing the numbers of wind turbine connected. The rating of each wind turbine is maintained at 2 MW. The model consists of FBM and 4 sub-systems: (I) Fixed Speed Induction Generator Model, (II) Drive train system, (III) Shunt capacitor at induction generator terminal and (IV) second transmission line (Line II). The mathematical analysis of the FBM given in Chapter 3 is used here.

4.3.1 The fixed speed induction generator model

The stator of an induction machine consists of symmetrical three phase windings distributed 120^{o} apart in space, while the rotor windings are forged and short-circuited. As the stator is connected to a three-phase voltage source, a magnetic field rotating at synchronous speed (ω_s) is produced. ω_s is defined as:

$$\omega_s = \frac{4\pi f_s}{p_f} \quad \text{rad/sec.} \tag{4.1}$$

where f_s is the frequency in Hz and p_f is the number of poles.

Once the stator magnetic field cuts the rotor conductors, three-phase voltages of slip frequency (sf_s) are induced on the rotor where 's' is the slip and is calculated as:

$$s = \frac{\omega_s - \omega_r}{\omega_s} \tag{4.2}$$

where ω_r is the rotor angular speed in rad/sec.

As the rotor conductors are short-circuited, three-phase currents flow on the rotor at slip frequency. These currents also produce a rotating magnetic field which is rotating at slip speed ($s\omega_s$) with respect to the rotor [10]. When the machine is driven by an external prime mover at speed higher than the synchronous speed, the direction of the induced torque will reverse and the machine will act as induction generator. The amount of power produced by the induction generator increases with the mechanical

torque applied to its shaft by the prime mover. Figure 4.3 shows the single-line equivalent circuit of the induction generator in the d-q frame reference [10]. The machine voltages and the flux equations can be expressed in the d-q axes as shown in Table 4.1.

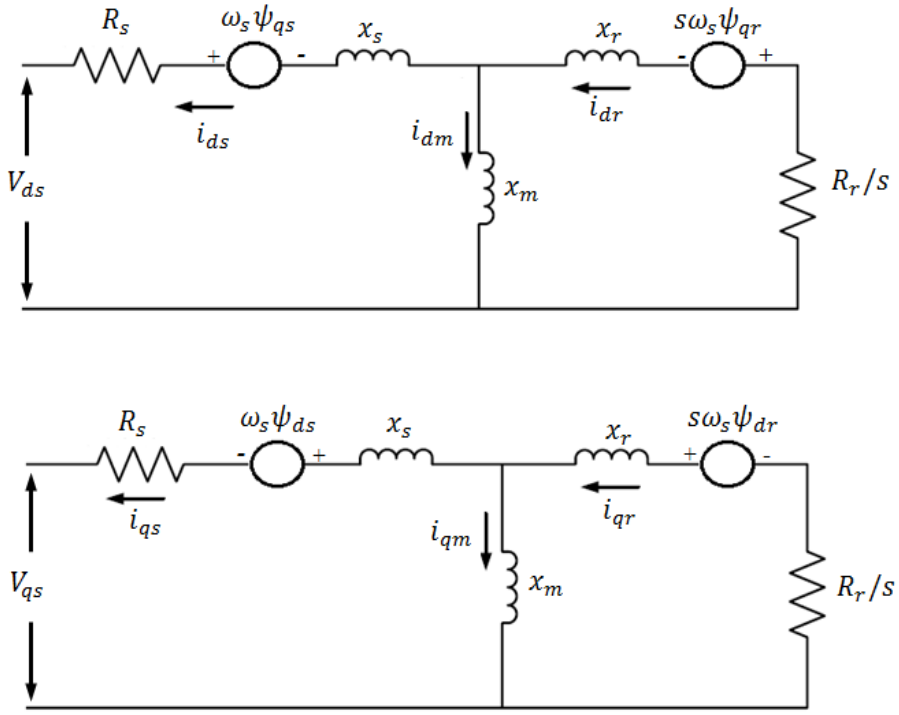

Fig. 4.3 Single-line equivalent circuit of an induction machine [10]

Table 4-1. The induction generator equations in the d-q axes (in per unit) [10]:

Voltage equations:	Flux equations:
$v_{ds} = -r_s i_{ds} - \omega_s\psi_{qs} + \frac{1}{\omega_s}\frac{d}{dt}\psi_{ds}$ (4.3)	$\psi_{ds} = -L_{ss} i_{ds} + L_m i_{dr}$ (4.7)
$v_{qs} = -r_s i_{qs} + \omega_s\psi_{ds} + \frac{1}{\omega_s}\frac{d}{dt}\psi_{qs}$ (4.4)	$\psi_{qs} = -L_{ss} i_{qs} + L_m i_{qr}$ (4.8)
$0 = r_r i_{dr} - s\omega_s\psi_{qr} + \frac{1}{\omega_s}\frac{d}{dt}\psi_{dr}$ (4.5)	$\psi_{dr} = L_{rr} i_{dr} - L_m i_{ds}$ (4.9)
$0 = r_r i_{qr} + s\omega_s\psi_{dr} + \frac{1}{\omega_s}\frac{d}{dt}\psi_{qr}$ (4.6)	$\psi_{qr} = L_{rr} i_{qr} - L_m i_{qs}$ (4.10)

The stator voltages are expressed in terms of currents by substituting the stator and rotor fluxes ψ_{ds}, ψ_{qs}, ψ_{dr}, and ψ_{qr} given in Equation (4.7) to Equation (4.10), into the stator and rotor voltage equations. Thus the voltage equations in terms of currents become:

$$v_{ds} = -r_s i_{ds} + x_s i_{qs} - x_m i_{qr} + \frac{1}{\omega_s}\left(-x_s \frac{di_{ds}}{dt} + x_m \frac{di_{dr}}{dt}\right) \quad (4.11)$$

$$v_{qs} = -r_s i_{qs} - x_s i_{ds} + x_m i_{dr} + \frac{1}{\omega_s}\left(-x_s \frac{di_{qs}}{dt} + x_m \frac{di_{qr}}{dt}\right) \quad (4.12)$$

$$0 = r_r i_{dr} - s\omega_s x_r i_{qr} + s\omega_s x_m i_{qs} + \frac{1}{\omega_s}\left(-x_m \frac{di_{ds}}{dt} + x_r \frac{di_{dr}}{dt}\right) \quad (4.13)$$

$$0 = r_r i_{qr} + s\omega_s x_r i_{dr} - s\omega_s x_m i_{ds} + \frac{1}{\omega_s}\left(-x_m \frac{di_{qs}}{dt} + x_r \frac{di_{qr}}{dt}\right) \quad (4.14)$$

The linearized voltage equations of the FSIG in matrix form can be written as:

$$\frac{1}{\omega_s}\begin{bmatrix} -x_s & 0 & x_m & 0 \\ 0 & -x_s & 0 & x_m \\ -x_m & 0 & x_r & 0 \\ 0 & -x_m & 0 & x_r \end{bmatrix}\begin{bmatrix} \Delta\dot{i}_{ds} \\ \Delta\dot{i}_{qs} \\ \Delta\dot{i}_{dr} \\ \Delta\dot{i}_{qr} \end{bmatrix} =$$

$$\begin{bmatrix} r_s & -x_s & 0 & x_m \\ x_s & r_s & -x_m & 0 \\ 0 & (\omega_{ro}-\omega_s)x_m & -r_r & (\omega_s-\omega_{ro})x_r \\ (\omega_s-\omega_{ro})x_m & 0 & (\omega_{ro}-\omega_s)x_r & -r_r \end{bmatrix}\begin{bmatrix} \Delta i_{ds} \\ \Delta i_{qs} \\ \Delta i_{dr} \\ \Delta i_{qr} \end{bmatrix} +$$

$$\begin{bmatrix} 1 & 0 & 0 \\ 0 & 1 & 0 \\ 0 & 0 & (x_m i_{qso} - x_r i_{qro}) \\ 0 & 0 & (x_r i_{dro} - x_m i_{dso}) \end{bmatrix}\begin{bmatrix} \Delta v_{ds} \\ \Delta v_{qs} \\ \Delta\omega_r \end{bmatrix} \quad (4.15)$$

4.3.2 Drive train system

The representation of the wind turbine in a power system has been investigated in [10-11]. The drive train of the wind turbine consists of blades, hub, low-speed shaft, high-speed shaft and induction generator. In this research, the influence of the FSIG-WTs on SSR has been studied, so the representation of drive train as a single-mass system is sufficient. All the components of the drive train system are lumped together to a single mass as shown in Figure 4.4.

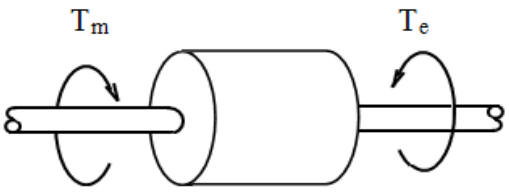

Fig. 4.4 Single mass drive train system of FSIG-WTs

The swing equation for the single mass wind turbine is very important as it describes the balance between the electromagnetic and mechanical torques of FSIG [12]. The swing equation is given as:

$$\frac{d\omega_r}{dt} = \frac{1}{2H}(T_m - T_e) \tag{4.16}$$

where H is the overall inertia constant of FSIG-WT in seconds, T_m is the mechanical torque and T_e is the electromagnetic torque.

The electromagnetic torque is calculated in terms of the stator and rotor currents as follows:

$$T_e = x_m(i_{dr}i_{qs} - i_{qr}i_{ds}) \tag{4.17}$$

By substituting Equation (4.17) into Equation (4.16), the rotor mechanic equation can be written in terms of currents as:

$$\frac{d\omega_r}{dt} = \frac{1}{2H}(T_m - x_m i_{dr}i_{qs} + x_m i_{qr}i_{ds}) \tag{4.18}$$

The linearized form of the rotor mechanic equation around the operating point is given by:

$$\Delta\dot{\omega}_r = \frac{x_m}{2H}(i_{qro}\Delta i_{ds} - i_{dro}\Delta i_{qs} - i_{qso}\Delta i_{dr} + i_{dso}\Delta i_{qr}) \tag{4.19}$$

The complete FSIG dynamic model is represented in state-space matrices as follows:

$$\left[\Delta\dot{X}_{FSIG}\right] = [At_{FSIG}][\Delta X_{FSIG}] + [Bt_{FSIG}]\begin{bmatrix}\Delta v_{ds}\\ \\ \Delta v_{qs}\end{bmatrix} \tag{4.20}$$

where

$$\left[\Delta\dot{X}_{FSIG}\right] = \left[\Delta\dot{i}_{ds} \quad \Delta\dot{i}_{qs} \quad \Delta\dot{i}_{dr} \quad \Delta\dot{i}_{qr} \quad \Delta\dot{\omega}_r\right]^T$$

$$[At_{FSIG}] = \begin{bmatrix} zoz(1,1) & zoz(1,2) & zoz(1,3) & zoz(1,4) & zoz(1,5)\\ zoz(2,1) & zoz(2,2) & zoz(2,3) & zoz(2,4) & zoz(2,5)\\ zoz(3,1) & zoz(3,2) & zoz(3,3) & zoz(3,4) & zoz(3,5)\\ zoz(4,1) & zoz(4,2) & zoz(4,3) & zoz(4,4) & zoz(4,5)\\ (x_m i_{qro}/2H) & (-x_m i_{dro}/2H) & (-x_m i_{qso}/2H) & (x_m i_{dso}/2H) & 0 \end{bmatrix}, \quad [Bt_{FSIG}] = \begin{bmatrix} zoq(1,1) & zoq(1,2)\\ zoq(2,1) & zoq(2,2)\\ zoq(3,1) & zoq(3,2)\\ zoq(4,1) & zoq(4,2)\\ 0 & 0 \end{bmatrix}$$

$$zoz = \omega_b \begin{bmatrix} -x_s & 0 & x_m & 0\\ 0 & -x_s & 0 & x_m\\ -x_m & 0 & x_r & 0\\ 0 & -x_m & 0 & x_r \end{bmatrix}^{-1} \begin{bmatrix} r_s & -x_s & 0 & x_m & 0\\ x_s & r_s & -x_m & 0 & 0\\ 0 & (\omega_{ro}-\omega_s)x_m & -r_r & (\omega_s-\omega_{ro})x_r & (x_m i_{qso} - x_r i_{qro})\\ (\omega_s-\omega_{ro})x_m & 0 & (\omega_{ro}-\omega_s)x_r & -r_r & (x_r i_{dro} - x_m i_{dso}) \end{bmatrix} \tag{4.21}$$

$$zoq = \omega_b \begin{bmatrix} -x_s & 0 & x_m & 0\\ 0 & -x_s & 0 & x_m\\ -x_m & 0 & x_r & 0\\ 0 & -x_m & 0 & x_r \end{bmatrix}^{-1} \begin{bmatrix} 1 & 0\\ 0 & 1\\ 0 & 0\\ 0 & 0 \end{bmatrix} \tag{4.22}$$

4.3.3 Shunt capacitor at the induction generator terminal

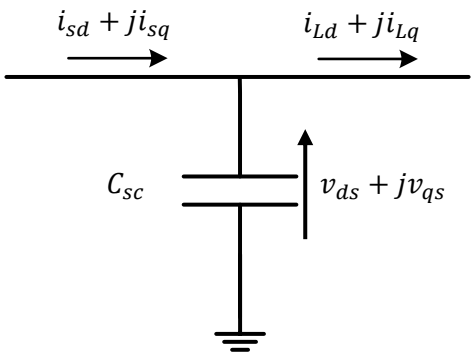

Fig. 4.5 Power factor capacitor bank across the terminals the FSIG-WT.

The power factor capacitor banks are connected across the terminals of the induction generator to provide it with the reactive power. Figure 4.5 shows a simple shunt capacitor. The voltage across the shunt capacitor in the d-q reference frame is written as follows [23**]**:

$$\frac{C_{sc}}{\omega_s}\frac{dv_{ds}}{dt} = i_{sd} - i_{Ld} + C_{sc}v_{qs} \tag{4.23a}$$

$$\frac{C_{sc}}{\omega_s}\frac{dv_{qs}}{dt} = i_{sq} - i_{Lq} - C_{sc}v_{ds} \tag{4.23}$$

Since in the per unit system, $x_{sc} = \frac{1}{C_{sc}}$, equations (4.22) and (4.23) are written as follows:

$$\begin{bmatrix} \frac{dv_{ds}}{dt} \\ \frac{dv_{qs}}{dt} \end{bmatrix} = \begin{bmatrix} 0 & \omega_s \\ -\omega_s & 0 \end{bmatrix} \begin{bmatrix} v_{ds} \\ v_{qs} \end{bmatrix} + \begin{bmatrix} \omega_s x_{sc} & 0 & -\omega_s x_{sc} & 0 \\ 0 & \omega_s x_{sc} & 0 & -\omega_s x_{sc} \end{bmatrix} \begin{bmatrix} i_{sd} \\ i_{sq} \\ i_{Ld} \\ i_{Lq} \end{bmatrix} \tag{4.24}$$

where,

C_{sc}, x_{sc} : Shunt capacitor across the induction generator terminals

i_{sd} , i_{sq} : The d-q components of the output FSIG-WT current

i_{Ld} , i_{Lq} : The d-q components of the short transmission line current

4.3.4 Transmission line connecting wind farm with FBM

The FSIG_WF is connected to a FBM via a step-up voltage transformer and a short transmission line, line AC, as shown in Figure 4.1. The resistance and the inductance of the short transmission line are chosen to be one third of the main transmission line, line AB, at the FBM not to affect the dynamic analysis of the SSR. The d-q components of the FSIG terminal voltage, v_{sd} and v_{sq}, are written in per unit as:

$$v_{sd} = v_d + R_{s2} i_{Ld} - x_{s2} i_{Lq} + \frac{x_{s2}}{\omega_s} \dot{i}_{Ld} \tag{4.25}$$

$$v_{sq} = v_q + R_{s2} i_{Lq} + x_{s2} i_{Ld} + \frac{x_{s2}}{\omega_s} \dot{i}_{Lq} \tag{4.26}$$

where v_d and v_q are the per unit d-q voltage components at bus 'A' in Figure 4.1, while R_{s2} and x_{s2} are the resistance and reactance of the line AC in per unit.

The linearized equations, which represent the short transmission line, are given as:

$$\Delta \dot{i}_{Ld} = \frac{\omega_b}{x_{s2}} \Delta v_{ds} - \frac{\omega_b}{x_{s2}} v_d - \frac{\omega_b R_{s2}}{x_{s2}} \Delta i_{Ld} + \omega_b \Delta i_{Lq} \tag{4.27}$$

$$\Delta \dot{i}_{Lq} = \frac{\omega_b}{x_{s2}} \Delta v_{qs} - \frac{\omega_b}{x_{s2}} v_q - \frac{\omega_b R_{s2}}{x_{s2}} \Delta i_{Lq} + \omega_b \Delta i_{Ld} \tag{4.28}$$

The state space equations for the short transmission line in addition to the power factor correction capacitors connected at the terminal bus of the FSIG are given as:

$$[\Delta \dot{X}_{stl}] = [At_{stl}][\Delta X_{stl}] + [Bt_{stl}] \begin{bmatrix} \Delta v_d \\ \Delta \boldsymbol{v}_q \\ \Delta i_{ds} \\ \Delta i_{qs} \end{bmatrix} \tag{4.29}$$

where

$$[\Delta \dot{X}_{FSIG}] = \begin{bmatrix} \Delta \dot{i}_{Ld} & \Delta \dot{i}_{Lq} & \Delta \dot{v}_{ds} & \Delta \dot{v}_{qs} \end{bmatrix}^T$$

$$[At_{stl}] = \begin{bmatrix} -\frac{\omega_b R_{s2}}{x_{s2}} & \omega_b & \frac{\omega_b}{x_{s2}} & 0 \\ -\omega_b & -\frac{\omega_b R_{s2}}{x_{s2}} & 0 & \frac{\omega_b}{x_{s2}} \\ -\omega_b x_{sc} & 0 & 0 & \omega_b \\ 0 & -\omega_b x_{sc} & -\omega_b & 0 \end{bmatrix}$$

$$[Bt_{stl}] = \begin{bmatrix} -\omega_b / x_{s2} & 0 & 0 & 0 \\ 0 & -\omega_b / x_{s2} & 0 & 0 \\ 0 & 0 & \omega_b x_{sc} & 0 \\ 0 & 0 & 0 & \omega_b x_{sc} \end{bmatrix}$$

4.3.5 The dynamic model of the overall system

Figure 4.6 shows the connection of FSIG-WTs with the FBM. The Park transformation matrix and its inverse are used for the connection of the synchronous generator with the rest of the system as depicted in Figure 4.6. As the multi-mass synchronous generator is represented in D-Q rotor reference frame while the rest of the model is represented in d-q synchronous reference frame. The Park transformation matrix is used to convert the D-Q output current components of the synchronous generator from the rotor reference frame to d-q synchronous reference frame current components and vice versa. The overall mathematical analysis of the system has been derived by performing some additional mathematical operations. As the connecting the FSIG-WF with the FBM demands that the equations of the series compensated transmission line, Equation (3.15) to Equation (3.17), to be changed. With relation to Figures 4-1 and 4-2, the state space equations for the series capacitor compensated transmission line at the FBM are modified as follows:

$$\left[\frac{dX_{TL}}{dt}\right] = [At_{TL}][X_{TL}] + [Bt1_{TL}]\begin{bmatrix} v_d \\ v_q \end{bmatrix} + [Bt_{2TL}][V_b] \tag{4.30}$$

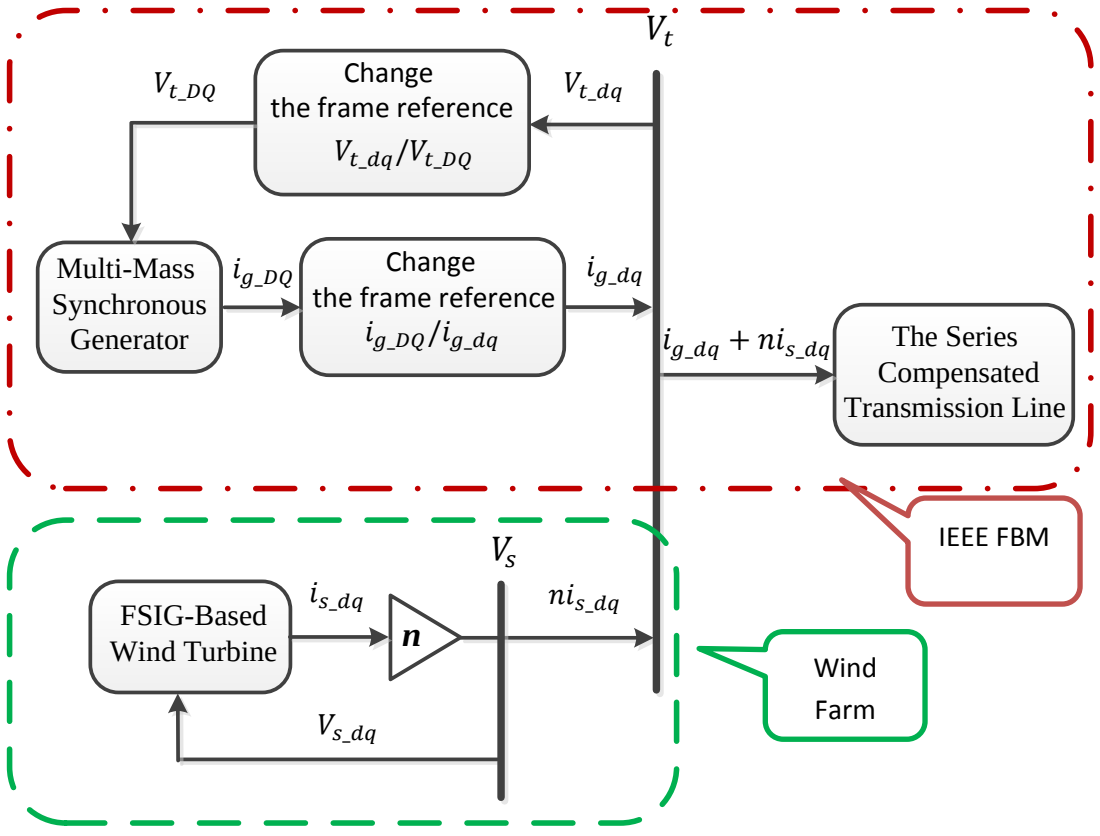

Fig. 4.6 Sub-System interactions for the FBM featuring FSIG-WTs.

where

$$[X_{TL}] = [e_{cd} \quad e_{cq} \quad i_{dTL} \quad i_{qTL}]^T$$

$$[At_{TL}] = \begin{bmatrix} 0 & \omega_s & \omega_s x_C & 0 \\ -\omega_s & 0 & 0 & \omega_s x_C \\ -\omega_s/x_L & 0 & -\omega_s(R_L/x_L) & \omega_s \\ 0 & -\omega_s/x_L & -\omega_s & -\omega_s(R_L/x_L) \end{bmatrix}$$

$$[Bt1_{TL}] = \begin{bmatrix} 0 & 0 \\ 0 & 0 \\ \omega_s/x_L & 0 \\ 0 & \omega_s/x_L \end{bmatrix}, \quad [Bt2_{TL}] = \begin{bmatrix} 0 \\ 0 \\ \frac{-\omega_s \sin(\delta)}{\overline{x}_L} \\ \frac{-\omega_s \cos(\delta)}{x_L} \end{bmatrix}$$

where i_{dTL} and i_{qTL} represent the d-q components of the current in the series compensated transmission line which are the summation of output currents of the synchronous and induction generators while V_b and δ are the infinite bus voltage and the load angle between a two reference frame.

To obtain the eigenvalues for the model the nonlinear equation (4.30) is linearized around the operating point, so the following equation can be written in terms of the output currents of synchronous and wind farm generators as follows:

$$\begin{bmatrix} \Delta\dot{e}_{cd} \\ \Delta\dot{e}_{cd} \\ \Delta v_d \\ \Delta v_q \end{bmatrix} = [Att_{TL}] \begin{bmatrix} \Delta e_{cd} \\ \Delta e_{cd} \end{bmatrix} + [At11_{TL}] \begin{bmatrix} \Delta\dot{i}_d \\ \Delta\dot{i}_q \end{bmatrix} + [At12_{TL}] \begin{bmatrix} \Delta\dot{i}_{Ld} \\ \Delta\dot{i}_{Lq} \end{bmatrix} + [At21_{TL}] \begin{bmatrix} \Delta i_d \\ \Delta i_q \end{bmatrix}$$

$$+ \ [At22_{TL}] \begin{bmatrix} \Delta i_{Ld} \\ \Delta i_{Lq} \end{bmatrix} + [Btt_{TL}][\Delta\delta] \qquad (4.31)$$

where

$$[Att_{TL}] = \begin{bmatrix} 0 & \omega_s \\ -\omega_s & 0 \\ 0 & 0 \\ 0 & 0 \end{bmatrix}, \qquad [Btt_{TL}] = \begin{bmatrix} 0 \\ 0 \\ V_b \cos(\delta_0) \\ -V_b \sin(\delta_0) \end{bmatrix}$$

$$[At11_{TL}] = \begin{bmatrix} 0 & 0 \\ 0 & 0 \\ (x_L/\omega_s) & 0 \\ 0 & (x_L/\omega_s) \end{bmatrix}, \qquad [At12_{TL}] = \begin{bmatrix} 0 & 0 \\ 0 & 0 \\ (x_L/\omega_s) & 0 \\ 0 & (x_L/\omega_s) \end{bmatrix}$$

$$[At21_{TL}] = \begin{bmatrix} (\omega_b x_C) & 0 \\ 0 & (\omega_b x_C) \\ R_L & -x_L \\ x_L & R_L \end{bmatrix}, \qquad [At22_{TL}] = \begin{bmatrix} (\omega_b x_c) & 0 \\ 0 & (\omega_b x_C) \\ R_L & -x_L \\ x_L & R_L \end{bmatrix}$$

Combining Equations (4.19), (4.24), (4.31) and Equations related to the turbine-generator shaft and excitation system of the synchronous generator in 'Chapter 3', the overall linearized equations of the system under study are given by:

$$[\Delta \dot{X}_{sys}] = [At_{sys}][\Delta X_{sys}] \tag{4.32}$$

where

$$[\Delta X_{sys}] = [\Delta\omega_H\ \Delta\theta_H\ \Delta\omega_I\ \Delta\theta_I\ \Delta\omega_{LPA}\ \Delta\theta_{LPA}\ \Delta\omega_{LPB}\ \Delta\theta_{LPB}\ \Delta\omega\ \Delta\delta\ \Delta\omega_{EXC}\ \Delta\theta_{EXC}\ \ldots\ldots$$
$$\Delta T_H\ \Delta T_i\ \Delta T_A\ \Delta a\ \Delta g\ \Delta e_{cd}\ \Delta e_{cq}\ \Delta i_d\ \Delta i_q\ \ \Delta i_F\ \Delta i_D\ \Delta i_Q\ \Delta i_S\ \ \Delta V_R\ \Delta E_{ED}\ \ldots\ldots$$
$$\Delta i_{ds}\ \Delta i_{qs}\ \ \Delta i_{dr}\ \Delta i_{qr}\ \ \Delta\omega_r\ \Delta i_{Ld}\ \Delta i_{Lq}\ \ \Delta v_{ds}\ \Delta v_{qs}]$$

The complete linearized model of the system under study consists of 36 state variables.

4.4 Simulation Results

Using the complete state space mode described in section 4.4, the effect of the FSIG-WTs on SSR has been studied through eigenvalue analysis and time domain simulations over a wide range of series compensation percentages and different ratings of FSIG-WTs.

4.4.1 Eigenvalue analysis

As mentioned in Chapter 3 eigenvalue analysis was used to study the stability of the system. The real parts of the eigenvalues indicate the stability of the system and provide information on system damping factors [8]. When the real parts of all the eigenvalues are negative, the system is stable. If there is at least one eigenvalue with positive real part the system is unstable.

a- The effect of series compensation

To investigate the influence of FSIG-WTs on SSR at various levels of series compensation, 100 FSIG-WT units with a power rating of 200 MW are connected with the FBM. Table 4.2 shows the comparison between the eigenvalues of the FBM alone and those for the FBM connected to the FSIG-WTs at 15%, 40% and 50% series compensation. The five torsional oscillation modes in addition to mode zero, corresponding to the rotor angle and the rotor angular speed of the synchronous generator, are provided in Table 4.2. The information contained in this table is summarised as follows:

- At 15% series compensation level, the FBM system is unstable as the real part of mode zero is positive. Connecting FSIG-WTs with the FBM makes the system stable as FSIG-WTs increase dynamic stability [10].
- At 40% series compensation level, the two systems become unstable due to the instability of torsional mode 4. This happens since the frequency of the subsynchronous mode (SUB), the complementary of the electrical transmission mode, is close to the frequency of the torsional mode 4, exciting it, and thus the system becomes unstable.
- When the series compensation level is increased to 50%, the 3rd mode in addition to 4th mode becomes unstable for the both systems. The frequency

of the subsynchronous mode is closer to the natural frequency of the mode 3, i.e. 25.7 Hz.

- It is noticeable from Table 4.2 that the frequency of the mode SUB for the system of FBM connected to FSIG-WTs is reduced compared to the value for the FBM alone at the same series compensated percentage. By comparing the real parts of the unstable torsional modes for the two systems, it can be seen that, connecting FSIG-WTs with the FBM attenuates the amplitude of the torsional oscillations, but these are not fully damped.

Table 4-2 Comparison between eigenvalues at different series compensation levels.

Modes	15% Series Compensation		40% series compensation	
	FBM only	FBM with WT	FBM only	FBM with WT
5	-0.1818 ±j 298.18	-0.1818 ±j 298.18	-0.1818 ±j298.18	-0.1818 ±j 298.18
4	-0.2778 ±j 203.49	-0.3092 ±j 203.51	+0.905 ***±j 201.68***	+0.3375 ***±j 202.6***
3	-0.2607 ±j 160.82	-0.277 ±j 160.85	-0.37622 ±j 161.5	-0.3676 ±j 161.6
2	-0.6738 ±j 127.07	-0.6778 ±j 127.08	-0.6849 ±j127.14	-0.6874 ±j 127.14
1	-0.3499 ±j 99.681	-0.4023 ±j 99.827	-0.4409 ±j 100.19	-0.4717 ±j 100.27
zero	**+ 0.0537±j 12.11**	**-0.7487 ±j 10.158**	**-0.2921 ±j 13.824**	**-1.7332 ±j 11.8**
SUB	-3.8453 ±j 258.69	-4.503 ±j 254.21	-4.3165 ***±j 184.98***	-4.416 ***±j 176.52***

Modes	50% Series Compensation	
	FBM only	FBM with WT
5	-0.1818 ±j298.18	-0.1818 ±j298.18
4	+0.2501 ±j202.36	+0.0899 ±j202.86
3	+2.9614±***j161.88***	+1.2589 ±***j 159.94***
2	-0.6945 ±j127.22	-0.69618 ±j127.23
1	-0.5045±j100.59	-0.5268 ±j100.63
zero	**-0.44719±j14.625**	**-2.356 ±j14.448**
SUB	-6.705 ±***j160.79***	-5.4588 ±***j153.89***

Figure 4.7 gives an clear example for the effect of connecting FSIG-WTs with FBM on the SSR over a wide range of series compensation. Figure 4.7 shows comparison between the eigenvalues for the FBM alone and FBM including FSIG-WTs.

Figure 4.7a presents the comparison between the real parts of 4^{th} mode for FBM alone represented by solid brown curve and FBM including FSIG-WTs which is represented by dashed brown line. Figure 4.7b shows the comparison between the imaginary parts of SUB mode for FBM alone and for FBM including FSIG-WTs.

Regarding Figure 4.7b, the black line represents the frequency of SUB mode of FBM including FSIG-WTs while the red line represents the frequency of SUB mode of FBM alone. The black line crosses the straight brown line, which represents the frequency of 4^{th} mode at lower series compensation level than that for the red line. As a result, 4^{th} mode of FBM including FSIG-WTs starts to oscillate and be unstable at lower series compensation percentage than that for FBM alone. That is noticeable through Figure 4.7a as the dashed curve crosses the zero line (straight black line) at lower series compensation level than that when solid line crosses the zero line.

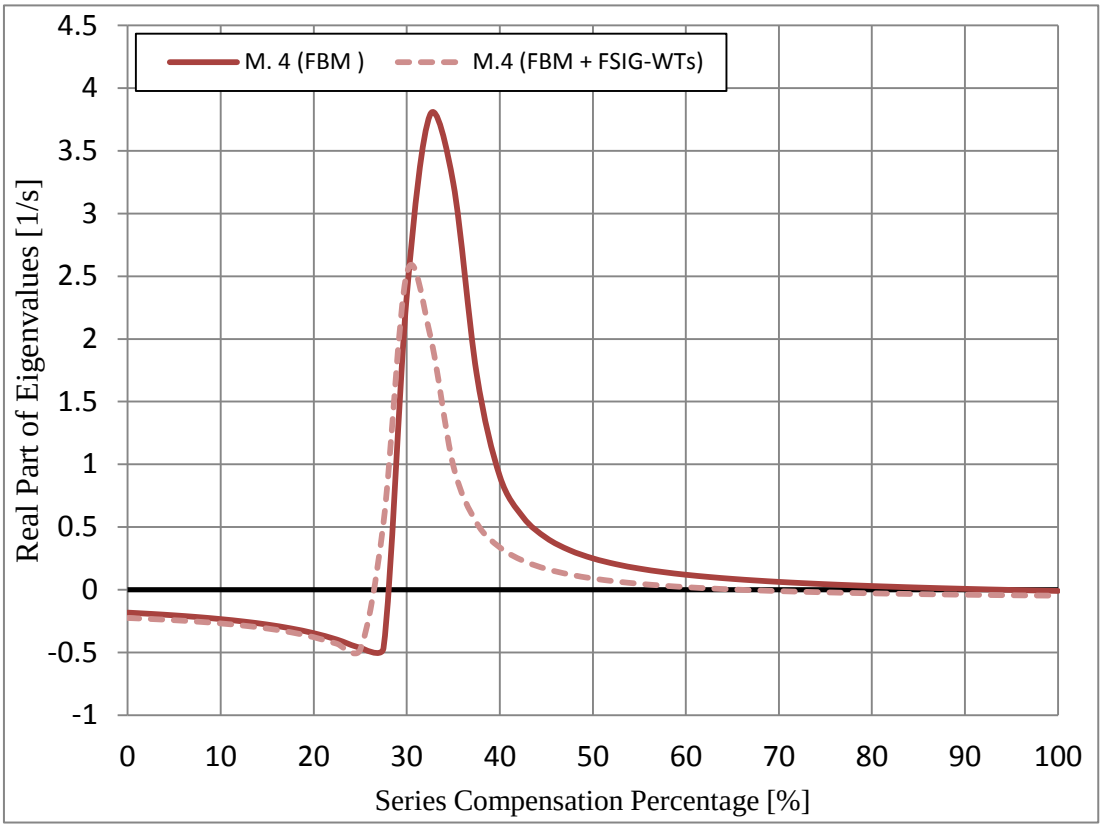

(a)

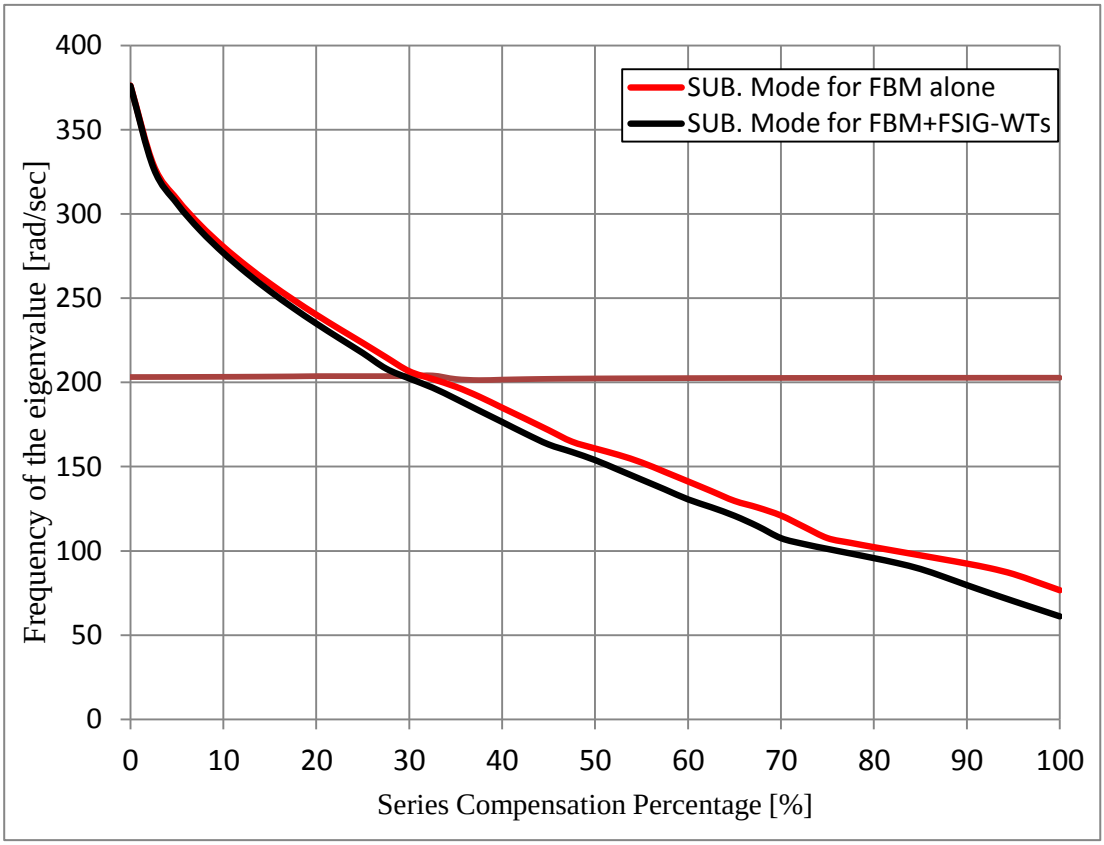

(b)

Fig. 4.7 Stability of the torsional modes in terms of series compensation level for FBM and for FBM with FSIG-WTs: (a) Real Part of 4th mode (b) Frequency of SUB mode.

The data mentioned in table 4.2 is indicated by vertical dashed lines in Figure 4.8. Figure 4.8 presents a comparison between the torsional modes in addition to mode zero for the FBM alone and for the FSIG connected with the FBM over a wide range of series compensation levels (0-100%). Figure 4.9 shows the range of series compensation levels between 10-55% for the two systems.

Until 20% series compensation, the instability within the FBM system is due to mode zero as its real part is positive. On the other hand, the mode zero of the FBM system with FSIG-WTs is stable over these compensation levels, as shown in Figure 4.8a and Figure 4.9a.

Until 25% series compensation, there is no effect for the torsional oscillations due to SSR for the two systems as the frequency of the mode SUB is far away from any natural frequency of the torsional modes.

By increasing the series compensation percentage, the two systems are unstable because of the occurrence of SSR, as the frequency of the SUB mode becomes close to the natural frequency of one of the torsional modes. It is noticeable from Figure 4.8a that the excitation of the torsional modes leading to instability and oscillation for the FBM system with FSIG-WTs occurs at a lower series compensation percentage than that for the FBM alone. This shifting is due to the reduction of the frequency of the SUB mode for the FBM with FSIG-WTs, as shown in Figure 4.8b.

Although connecting FSIG-WTs with the FBM attenuates the amplitude of the torsional oscillations, it increases the range of series compensation percentage over which SSR will occur.

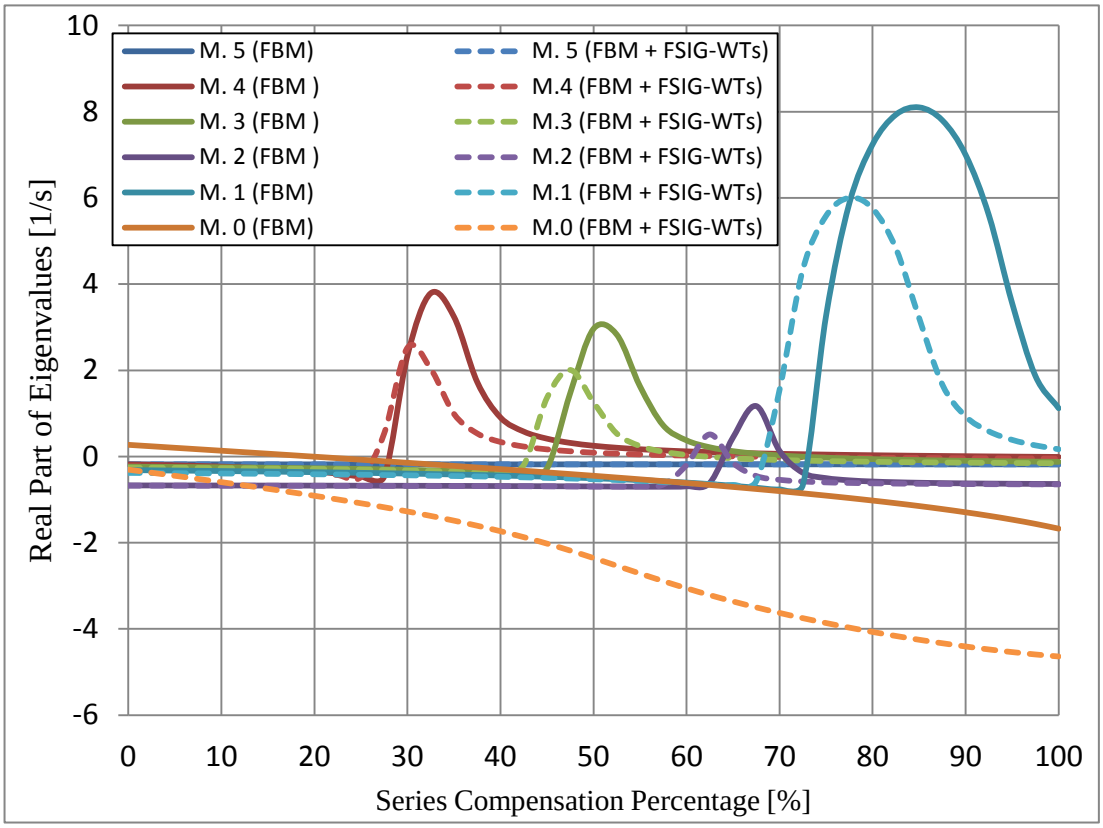

(a)

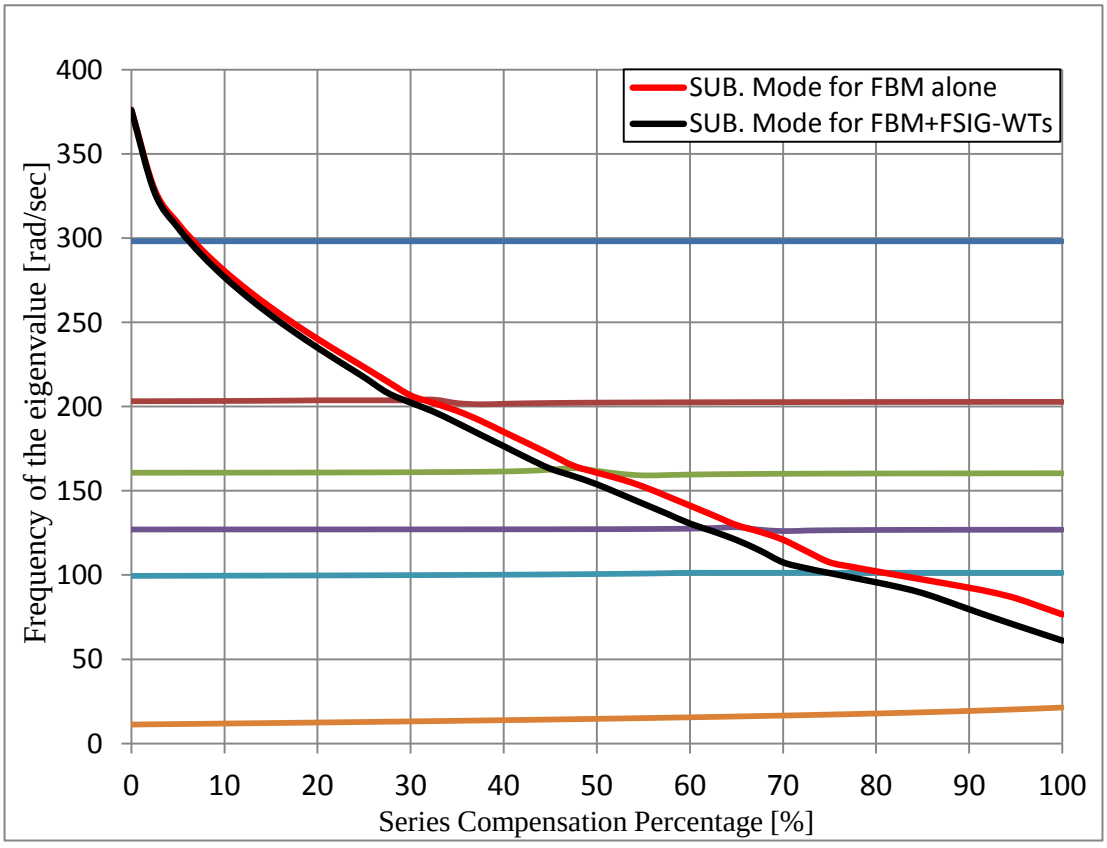

(b)

Fig. 4.8 Stability of the torsional modes in terms of series compensation level for FBM and for FBM with FSIG-WTs: (a) Real Parts of modes (b) Frequency of modes.

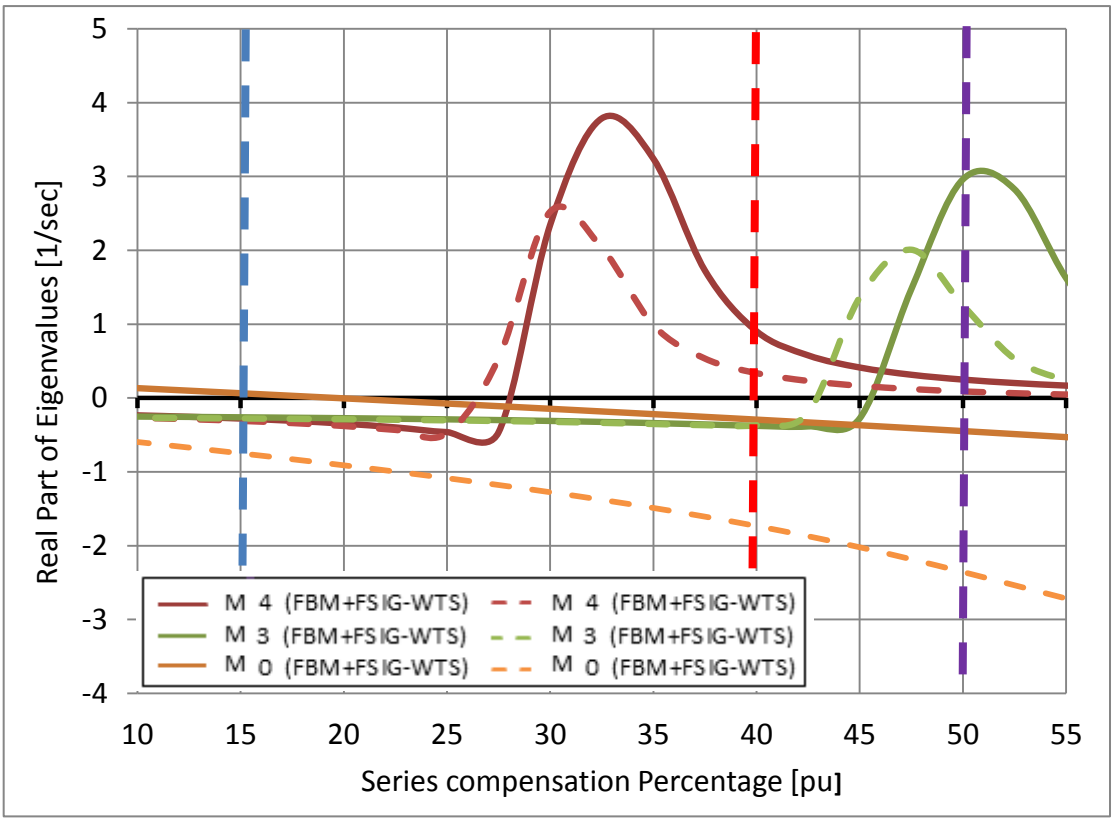

(a)

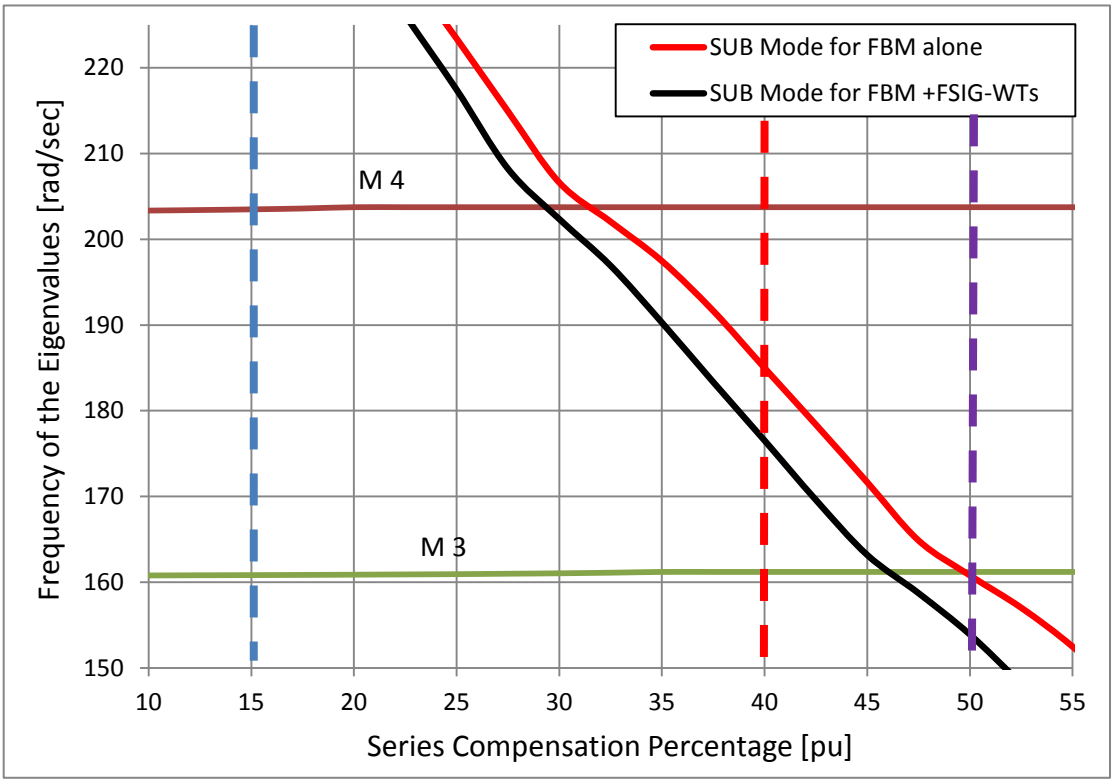

(b)

Fig. 4.9 Stability of the torsional modes in terms of series compensation level (10% to 55%) for FBM and for FBM with FSIG-WT.

b- Effect of varying the power rating of FSIG-WF on SSR

In order to investigate the effect of the wind farm power rating on SSR, the installed capacity was set to 200 MW, 500 MW and 750 MW and the analysis of section (a) repeated. Figure 4.10 shows the comparison between the frequencies of the SUB modes for the FBM alone and for the FBM with FSIG-WF for different power ratings. It is noticeable that the frequency of SUB mode decreases with the increase in the power rating of FSIG-WF. Thereby, SSR occurs at a lower value of series compensation level than before as shown in Figure 4.11.

Figure 4-11 shows the effect of increasing the power rating of the FSIG-WF on different modes. This happens since the torsional modes become unstable at lower series compensation level as a result of increasing the power rating of the FSIG-WF.

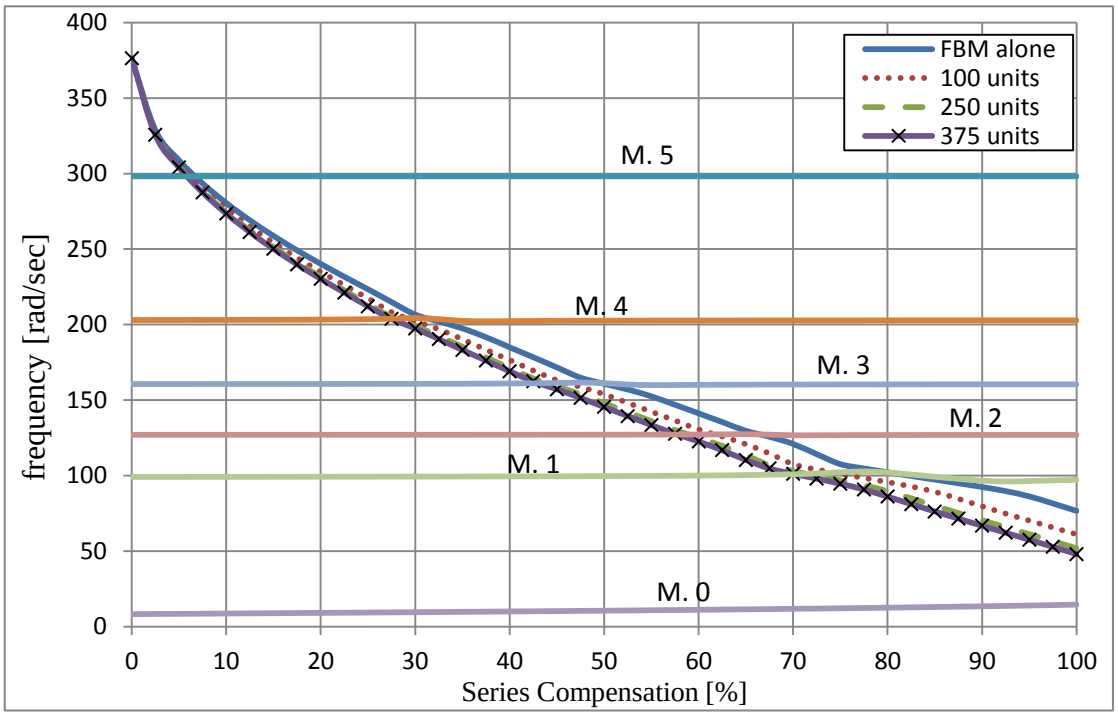

Fig. 4.10 The Frequency of the Subsynchronous mode in terms of series compensation level for FBM and FBM with different ratings of FSIG-WTs.

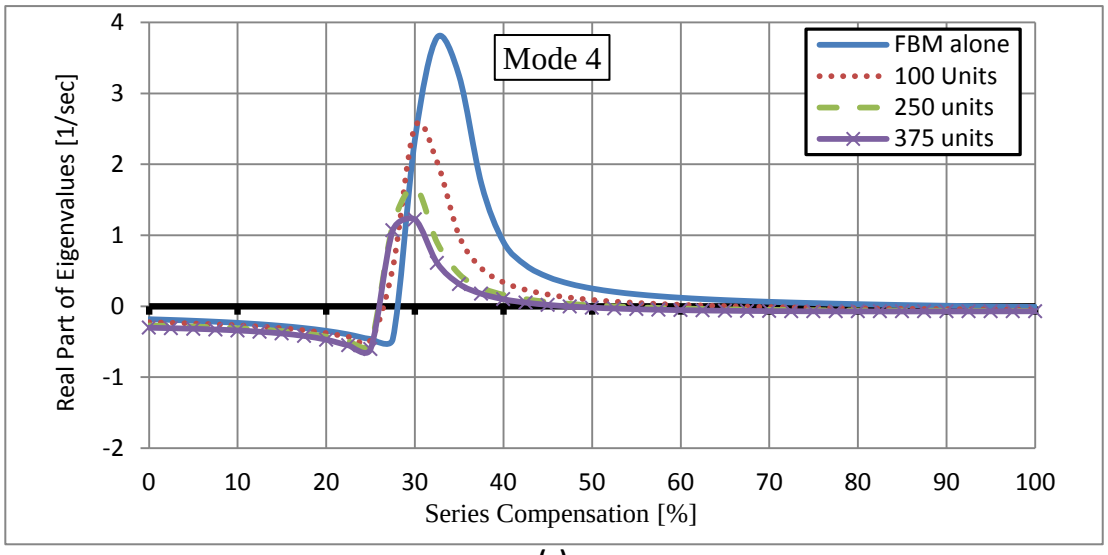
Mode 4
FBM alone
100 Units
250 units
375 units
Real Part of Eigenvalues [1/sec]
Series Compensation [%]
4
3
2
1
0
-1
-2
0
10
20
30
40
50
60
70
80
90
100

(a)

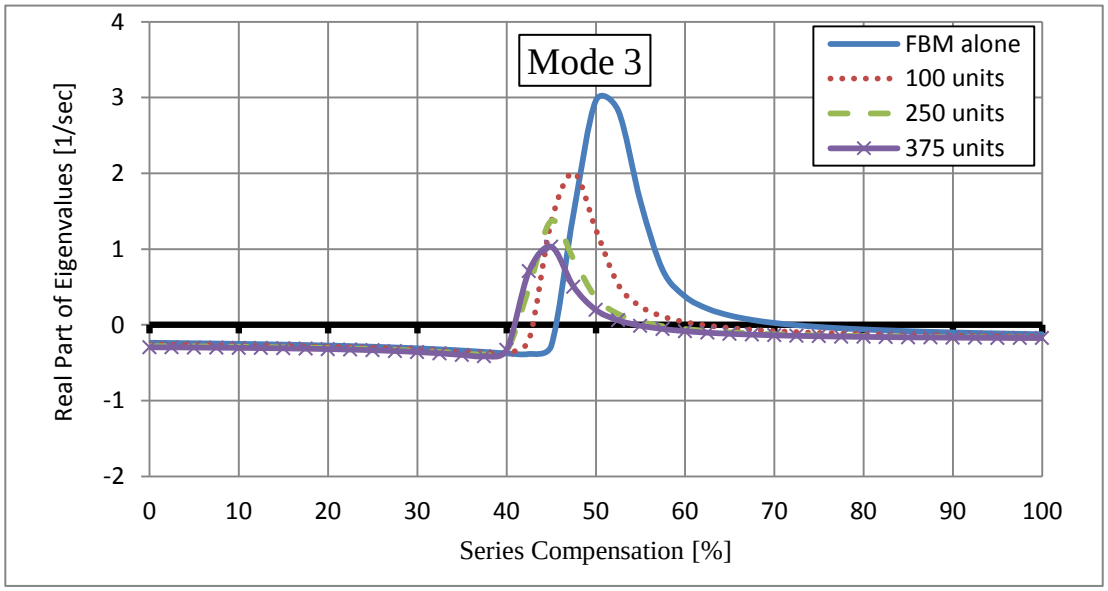
Mode 3
FBM alone
100 units
250 units
375 units
Real Part of Eigenvalues [1/sec]
Series Compensation [%]
4
3
2
1
0
-1
-2
0
10
20
30
40
50
60
70
80
90
100

(b)

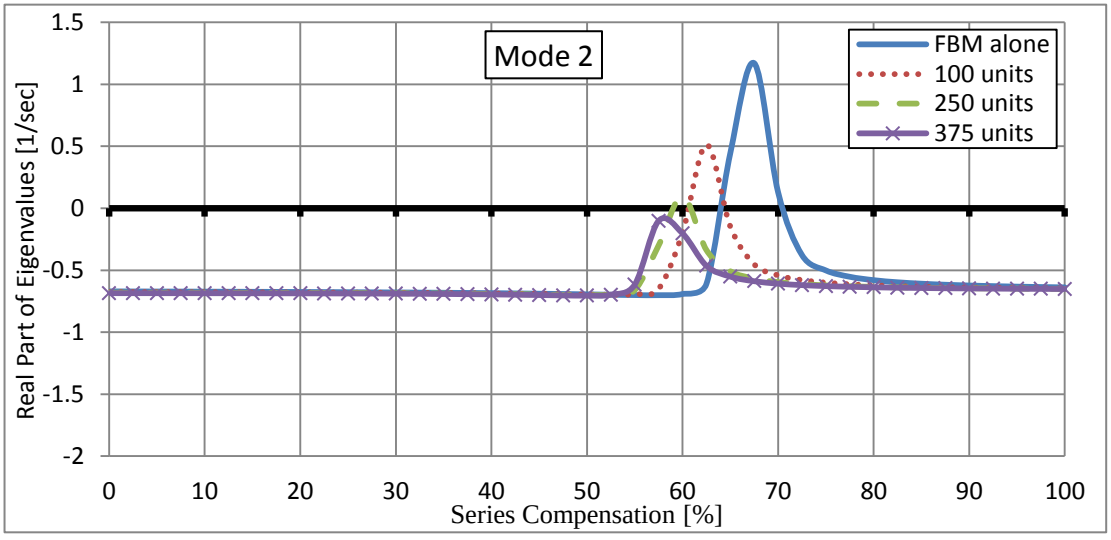
Mode 2
FBM alone
100 units
250 units
375 units
Real Part of Eigenvalues [1/sec]
Series Compensation [%]
1.5
1
0.5
0
-0.5
-1
-1.5
-2
0
10
20
30
40
50
60
70
80
90
100

(c)

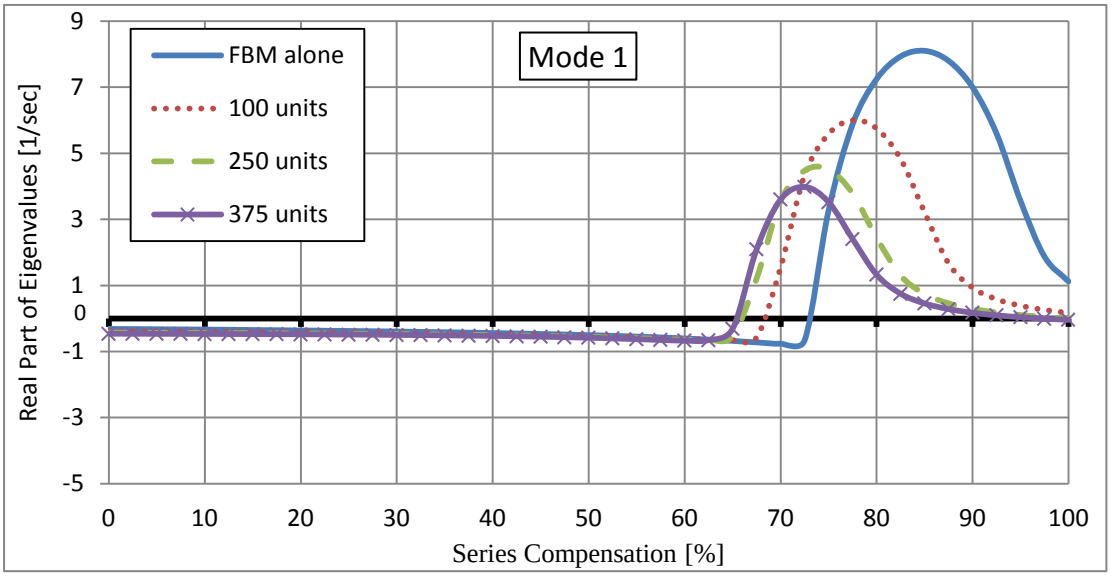

(d)

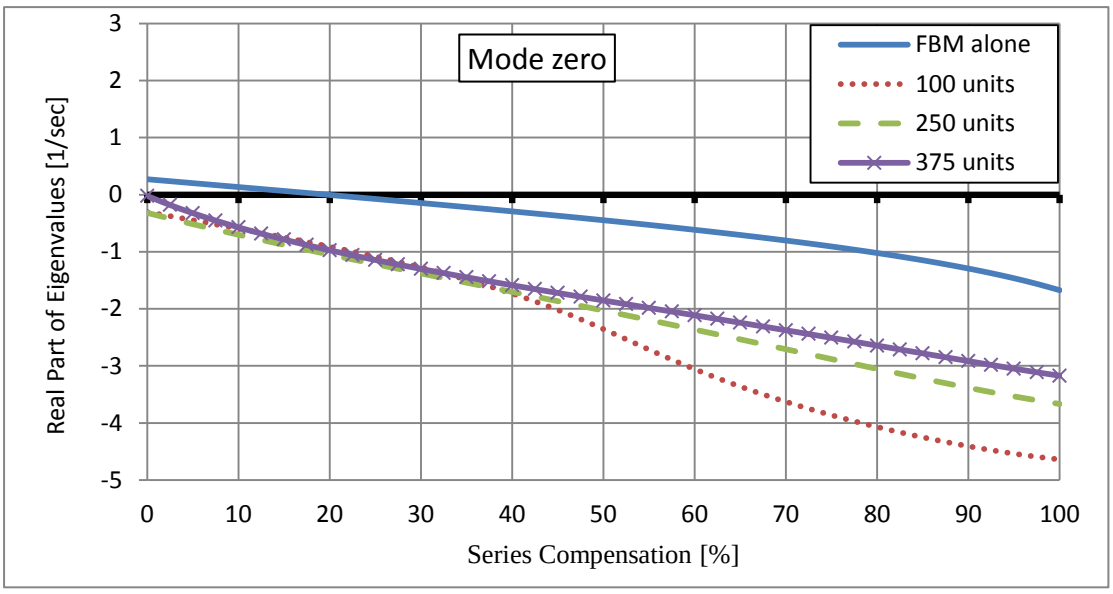

(e)

Fig. 4.11 Stability of the torsional modes in terms of series compensation level for FBM and for FBM with FSIG-WTs at different ratings: (a) Mode 4, (b) Mode 3, (c) Mode 2, (d) Mode 1 and (e) Mode 0

4.4.2 The effect of FSIG-WTs on SSR

There are two frequencies over the series compensated transmission line in the FBM system during SSR condition; system frequency and the subsynchronous frequency. These frequencies create two different values of slip: the rated slip (s_R) which depends on the system frequency as shown in equation (4.2) and the subsynchronous slip (s_{SSR}) which depends on the subsynchronous frequency, and defined by:

$$s_{SSR} = \frac{\omega_{SSR} - \omega_r}{\omega_{SSR}} \quad (4.33)$$

where ω_{SSR} is the angular frequency of subsynchronous currents in the series compensated transmission line.

When a resonance occurs in the network, the rated slip and the subsynchronous slip can be considered to exist simultaneously. To study the effects of the rated and subsynchronous slips on SSR, they are considered separately.

At the resonance frequency, the synchronous generator and the infinite bus are considered to be short circuited. Therefore, the buses D and B are connected to the ground as shown in Figure 4.12(b). The total impedance of FSIG-WTs is included within the impedance z_2, consisting of the total resistance (R_2) and the total inductance (L_2), to investigate the effect of the equivalent rotor resistance of FSIG-WTs ($\frac{r_r}{slip}$) on the resonance frequency.

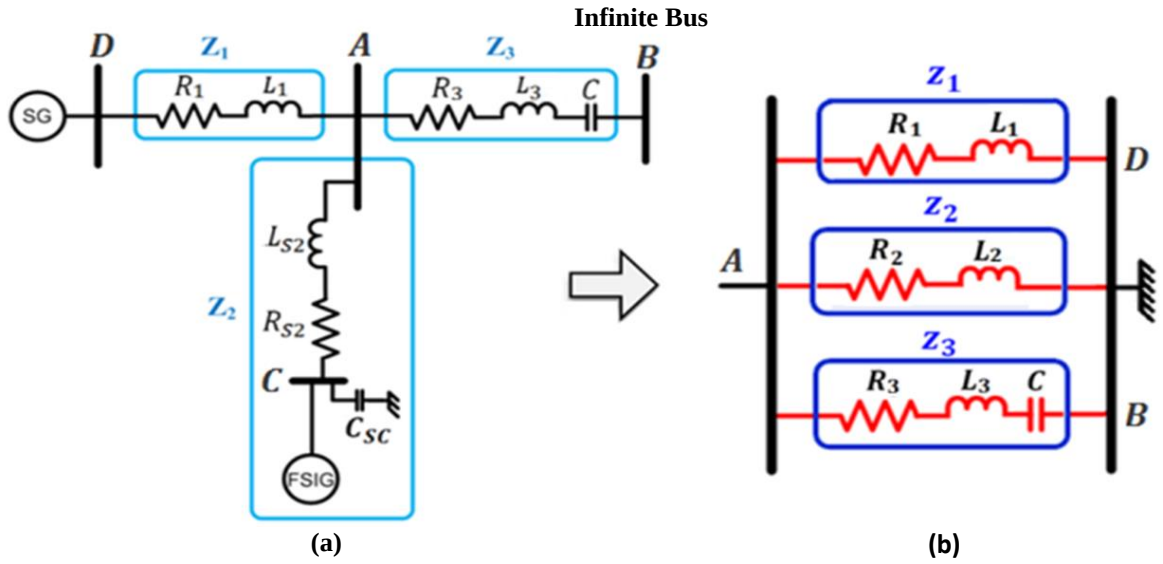

Fig. 4.12 FSIG-WTs connecting with FBM: (a) connection of FSIG-WTs with FBM, (b) parallel connection

z_1, z_2 and z_3 are the equivalent impedance of the transformer connecting the synchronous generator with bus D, the equivalent impedance representing the summation of the impedances of the second transmission line (AC) and the FSIG-WTs and the equivalent impedance of the series compensated transmission line (AB) respectively.

From Figure 4.12(b); Impedance of the transformer connecting the synchronous generator with network is:

$$z_1 = R_1 + j\omega_{\mathrm{SSR}} L_1 \tag{4.34}$$

Impedance of the line AC and FSIG-WTs is:

$$z_2 = R_2 + j\omega_{\mathrm{SSR}} L_2 \tag{4.35}$$

where $R_2 = R_{s2} + Re(z_{FSIG-WTs})$

$L_2 = L_{s2} + Im(z_{FSIG-WTs})/\omega_{\mathrm{SSR}}$

Impedance of series compensated transmission line is:

$$z_3 = R_3 + j\omega_{\mathrm{SSR}} L_3 + \frac{1}{j\omega_{\mathrm{SSR}} C} \tag{4.36}$$

$z_{\mathrm{FSIG-WTs}}$ can be found using the parameters defined in Figure 4-3 as:

$$z_r = \frac{r_r}{s_{SSR}} + \mathrm{j}x_{\mathrm{r}} \tag{4.37}$$

$$z_s = r_s + jx_s \tag{4.38}$$

$$z_{\mathrm{R1}} = z_{\mathrm{r}} // \mathrm{j}x_{\mathrm{m}} = \frac{(\frac{r_{\mathrm{r}}}{s_{\mathrm{SSR}}} + \mathrm{j}x_{\mathrm{r}})\mathrm{j}x_{\mathrm{m}}}{\frac{r_{\mathrm{r}}}{s_{\mathrm{SSR}}} + \mathrm{j}(x_{\mathrm{r}} + x_{\mathrm{m}})} \tag{4.39a}$$

$$z_{R2} = z_{R1} + z_s = \frac{(\frac{r_r}{s_{SSR}} + jx_r)jx_m}{\frac{r_r}{s_{SSR}} + j(x_r + x_m)} + (r_s + jx_s) = \frac{\left(\frac{r_r}{s_{SSR}} + jx_r\right)jx_m + (\frac{r_r}{s_{SSR}} + j(x_r + x_m))(r_s + jx_s)}{\frac{r_r}{s_{SSR}} + j(x_r + x_m)} \tag{4.39b}$$

$$z_{FSIG-WTs} = (z_{R2} // jx_{sc})/n = \frac{(z_{R2})jx_{sc}}{(z_{R2} + jx_{sc})n}$$

$$= \frac{(\left(\frac{r_r}{s_{SSR}} + jx_r\right)jx_m + (\frac{r_r}{s_{SSR}} + j(x_r + x_m))(r_s + jx_s))(jx_{sc})}{((\left(\frac{r_r}{s_{SSR}} + jx_r\right)jx_m + (\frac{r_r}{s_{SSR}} + j(x_r + x_m))(r_s + jx_s))(jx_{sc}) + (\frac{r_r}{s_{SSR}} + j(x_r + x_m)))n} \tag{4.39}$$

where z_r and z_s are the rotor and stator impedances of the FSIG-WTs. x_m and x_{sc} are the magnetising reactance and the reactance of the power factor correction capacitor of the FSIG-WTs. Double slash '//' represents parallel connection. n is the number of FSIG-WTs connected in the wind farm. R_{s2} and x_{s2} are the resistance and reactance of the second transmission line (AC).

By taking the Laplace Transform of equations (4.34) to (4.36) as:

$$z_1(s) = sL_1 + R_1 \tag{4.40}$$

$$z_2(s) = sL_2 + R_2 \tag{4.41}$$

$$z_3(s) = \frac{s^2 L_3 C + sR_3 C + 1}{sC} \tag{4.42}$$

where s is the Laplace operator.

The total impedance of the parallel arrangement shown in Figure 4.12(b) is written in the frequency domain as:

$$z_A(s) = \frac{1}{z_1(s)} + \frac{1}{z_2(s)} + \frac{1}{z_3(s)}$$

$$= \frac{z_1(s)z_2(s) + z_2(s)z_3(s) + z_3(s)z_1(s)}{z_1(s)z_2(s)z_3(s)} = \frac{z_1(s) + z_3(s) + \frac{z_1(s)z_3(s)}{z_2(s)}}{z_1(s)z_3(s)} \tag{4.43}$$

At resonance, $z_A(s)$ equals zero. Therefore, the numerator of the $z_A(s)$ equals zero:

$$z_1(s) + z_3(s) + \frac{z_1(s)z_3(s)}{z_2(s)} = 0 \tag{4.44}$$

The values of s were determined using a MATLAB script. The imaginary part of the conjugate pair of s represents the value of the resonance frequency (ω_{SSR}) of z_A in (rad/sec). The frequency of the subsynchronous currents over the series compensated transmission line in the FBM alone is used as an initial value to determine the equivalent rotor resistance of the FSIG-WTs. Then the resistance and inductance of the equivalent impedances z_2 and z_A are determined to calculate the new value of ω_{SSR}. The iteration continues until the difference between the new value and the initial value of ω_{SSR} ($\Delta\omega_{SSR}$) becomes equal or less than tolerance value (0.1 rad/s). Table 4.3 shows this iterative process with 50% series compensation as an example to demonstrate how ω_{SSRF} was at the rated and the subsynchronous slips for 100 units of FSIG-WTs.

Table 4.3 The iteration process to determine the final value of the resonance frequency ($\boldsymbol{\omega_{SSR}}$) at 50% series compensation.

steps	Process	Subsynchronous slip (s_{SSR})	Rated slip (s_R)
1	Set ω_{SSR} of the FBM alone as the initial value ω_{SSR0}	$\omega_{SSR0} = 215.14$ rad/s	$\omega_{SSR0} = 215.14$ rad/s
2	Calculate slip at ω_{SSR0}	$s_{SSR} = \frac{\omega_{SSR0} - \omega_r}{\omega_{SSR0}} = -0.76$	$s_R = \frac{\omega_s - \omega_r}{\omega_s} = -0.0057$
3	Calculate the equivalent rotor resistance of one FSIG-WT	$\frac{r_r}{s_{SSR}}$ =-900.27 Ω	$\frac{r_r}{s_R} = -1.204 \times 10^5$ Ω
5	Calculate the total impedance of 100 FSIG-WTs (see equations (4.34) to (4.36))	$z_t = -2.720 + J\,85.84$	$z_t = -12574.1 + J2447.1$
6	Calculate the equivalent impedance of each branch in the parallel arrangement shown in Figure 4-11b (see equations (4.38) to (4.40))	$z_1 = 0.104\,s + 2.801$ $z_2 = 0.8309\,s + 4.227$ $z_3 = 0.41603s + 5.6032 + \frac{1}{3.382e-005\ s}$	$z_1 = 0.104\,s + 2.801$ $z_2 = 0.82\,s - 1255$ $z_3 = 0.41603s + 5.6032 + \frac{1}{3.382e-005\ s}$
7	Calculate the total impedance of parallel arrangement shown in Figure 4-11 (see equation (4-41))		
8	Calculate the value of Laplace operator(s) (see equation (4.42))	s= -7.7343 ±J 240.99	s= -6.6132 ±J 215.14
9	Set the new value of ω_{SSR}	$\omega_{SSR} = 240.99$ rad/s	$\omega_{SSR} = 215.14$ rad/s
10	Calculate the tolerance $\Delta\omega_{SSR}$ as $\Delta\omega_{SSR} = \omega_{SSR} - \omega_{SSR0}$	$\Delta\omega_{SSR} = 25.85$ rad/s	$\Delta\omega_{SSR} = 0$ rad/s
11	If $\Delta\omega_{SSR} \leq 0.1$ rad/s, Finish and $\omega_{SSRF} = \omega_{SSR}$ Else, $\omega_{SSR0} = \omega_{SSR}$ and return to step 2	$\omega_{SSR0} = 240.99$ rad/s and return to step 2	Finish and $\omega_{SSRF} = 215.14$ rad/s

ω_{SSRF} and its complementary (ω_{ER}) are calculated for the s_{SSR} and the rated slip over a wide range of series compensation levels and a various numbers of FSIG-WTs as shown in Figures 4.13 and 4.14. The complementary frequency (ω_{ER}) of the resonant frequency is the difference between the system frequency (ω_0) and the resonant frequency ($\omega_{ER} = \omega_0 - \omega_{SSRF}$).

Figure 4.13 shows the effect of s_{SSR} on ω_{SSRF} and its complementary frequency (ω_{ER}). The connection of the FSIG-WTs with FBM increases the value of ω_{SSRF} to be higher than that for FBM alone. As shown in Figure 4.13a, the value of ω_{SSRF} increases by increasing the number of FSIG-WTs due to the reduction in the total impedance of FSIG-WTs. Consequently, the value of ω_{ER} decreases when the number of FSIG-WTs is increased, see Figure 4-13b. The similarity between Figure 4-10 and Figure 4-13b emphasizes that the reduction of the frequency of the SUB mode is due to the influence of subsynchronous slip.

Figure 4.14 shows the effect of rated slip on ω_{SSRF} and ω_{ER}. As shown in Figure 4.14a, the values of ω_{SSRF} for the various numbers of FSIG-WTs are the same and equal to the frequency of the subsynchronous currents of FBM alone. As a consequence, the curves of the ω_{ER} for the various numbers of FSIG-WTs are coincide with the curve of the SUB mode of FBM alone as shown in Figure 4.14b.

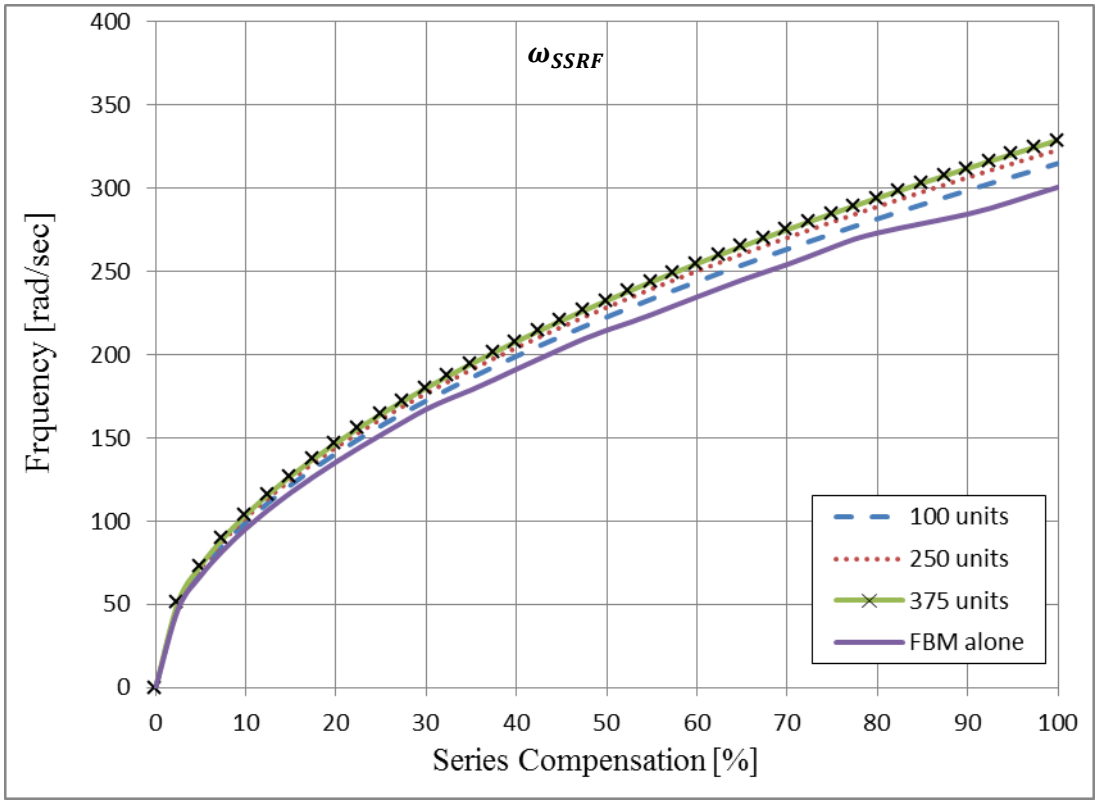

(a)

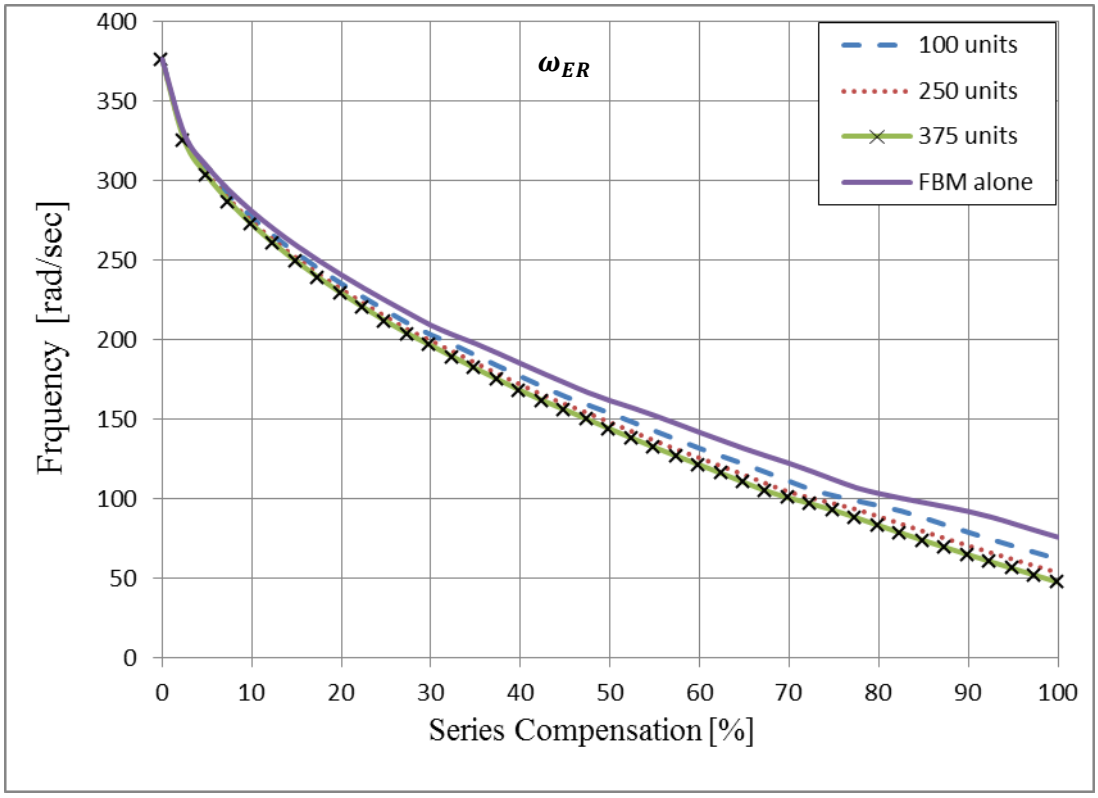

(b)

Fig. 4.13 The effect of FSIG-WTs on SSR because of subsynchronous slip: (a) the resonant frequencies of f_R and (b) the frequencies of f_{ER} for the different numbers of FSIG-WTs.

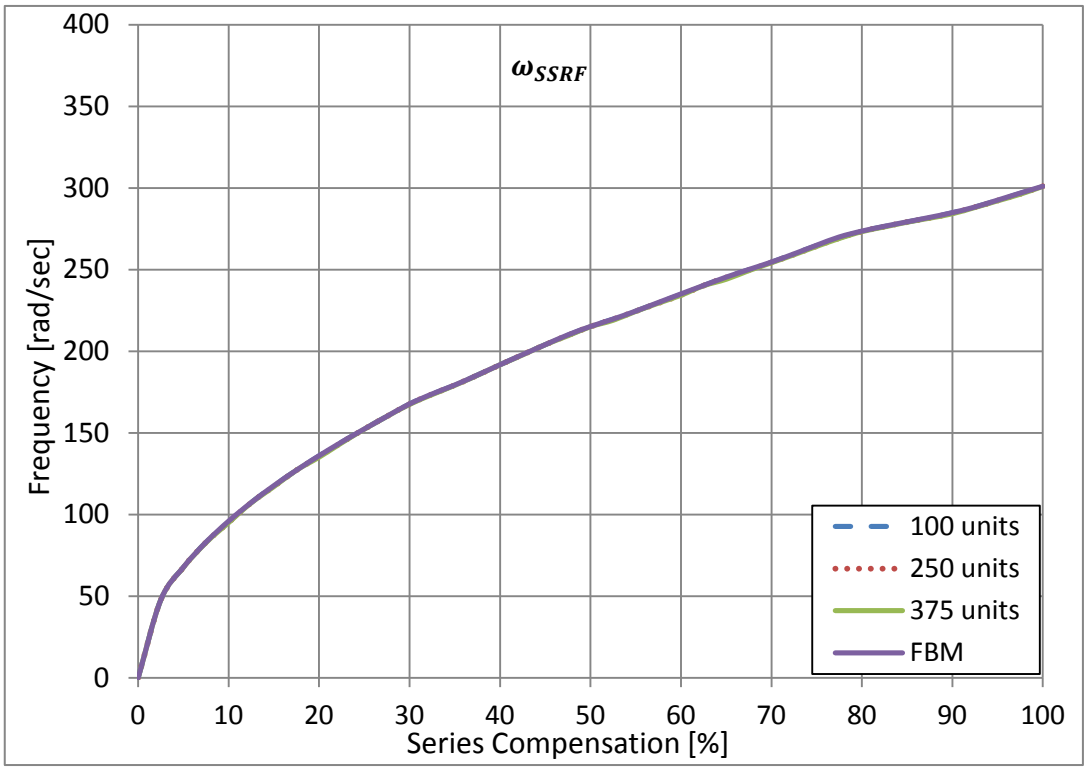

(a)

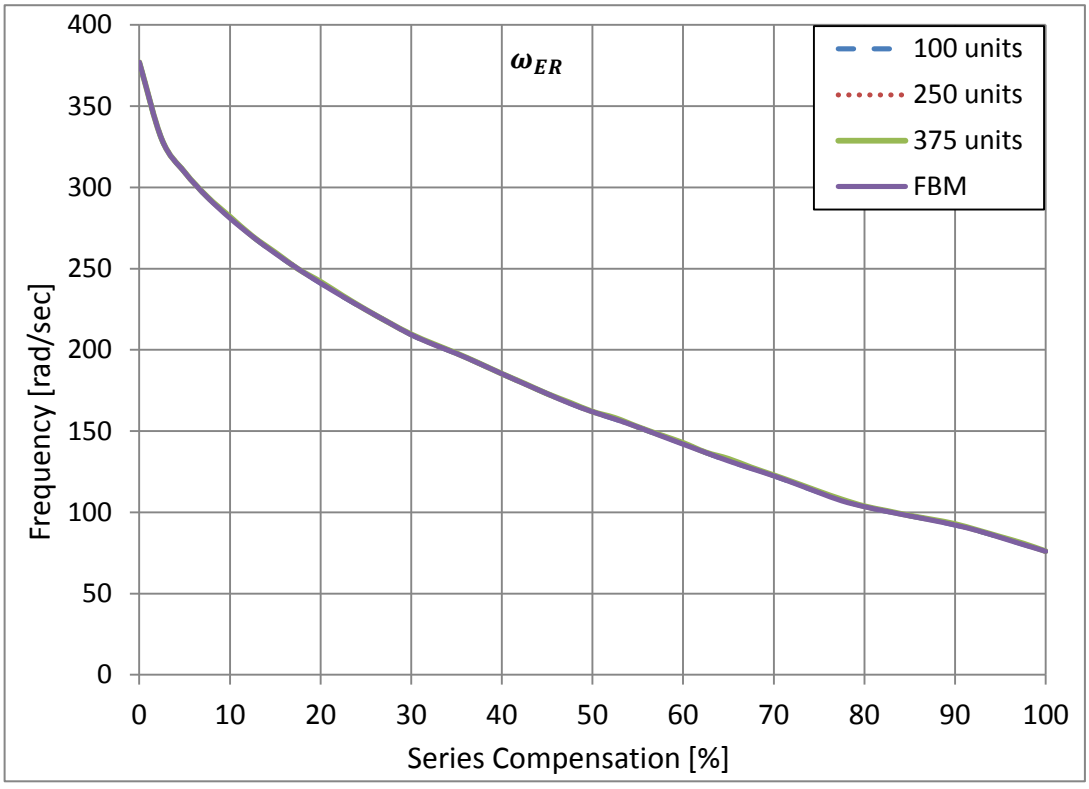

(b)

Fig. 4.14 The effect of FSIG-WTs on SSR because of rated slip: (a) the resonant frequencies of f_R and (b) the frequencies of f_{ER} for the different numbers of FSIG-WTs.

4.4.3 Time domain simulation

A time domain simulation of the FSIG-WTs connected to the FBM was carried out in PSCAD/EMTDC. To investigate the dynamic performance of the system model under disturbance, a three-phase fault is initiated at time=1.5*s* and is released after 75 *msec*. From the results of the eigenvalue analysis, it would be expected that connecting FSIG-WTs with FBM shifts the occurrence of SSR to a lower series compensation level than that for FBM alone and the amplitude of oscillation is attenuated by increasing the power rating of FSIG-WTs.

Comparisons between the time domain simulations results are made first between FBM alone and FBM with a 200 MW FSIG-WF at 27% series compensation. Figure 4.15 shows a comparison between the frequency at Bus A of the Transmission line network for the two systems, FBM alone and connecting with FSIG-WF. It is noticed that, the oscillating frequency of the current over the transmission line for system of FBM alone settle down after clearing the fault. On the other side, the increasing frequency of the system of FSIG-WF connecting with FBM after the fault shows that this system becomes unstable due to SSR. Figure 4.16 shows a comparison of the frequency spectrum for phase a current at the series compensated transmission line of the FBM alone and FBM featuring FSIG-WTs. It can be noticed that connecting FSIG-WTs with FBM increases the frequency of electrical resonant mode. Therefore, SUB mode, the complementary of the electrical resonant mode, becomes smaller than that for FBM alone and equals 32.5 Hz, which equals the frequency of 4^{th} mode. As a results, 4^{th} mode is excited and oscillates and the system becomes unstable.

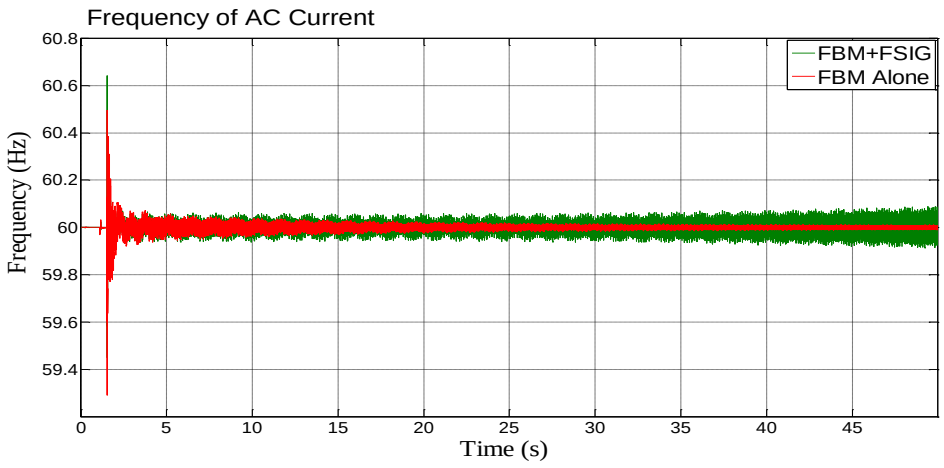

Fig. 4.15 Comparisons between frequencies of phase *a* current over the transmission line in the multi-mass rotor shaft of FBM alone and including FSIG-WTs at 27% series compensation

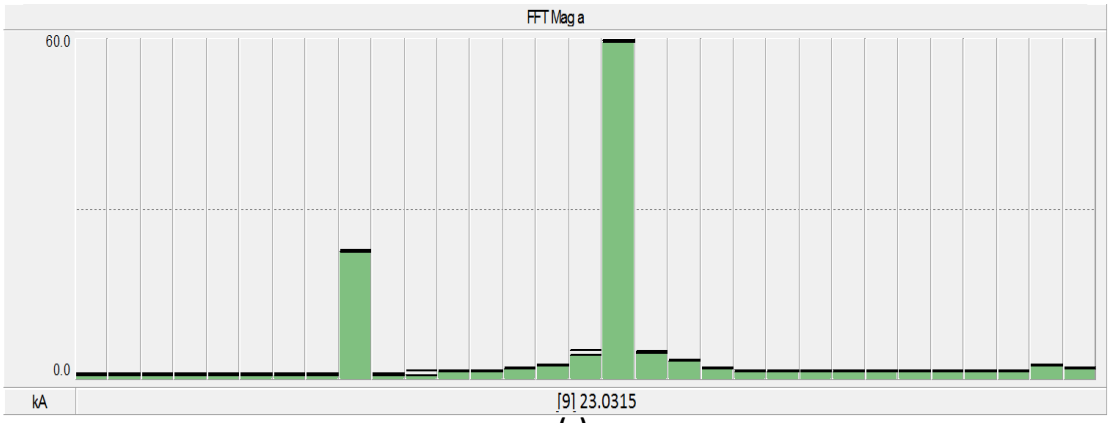

(a)

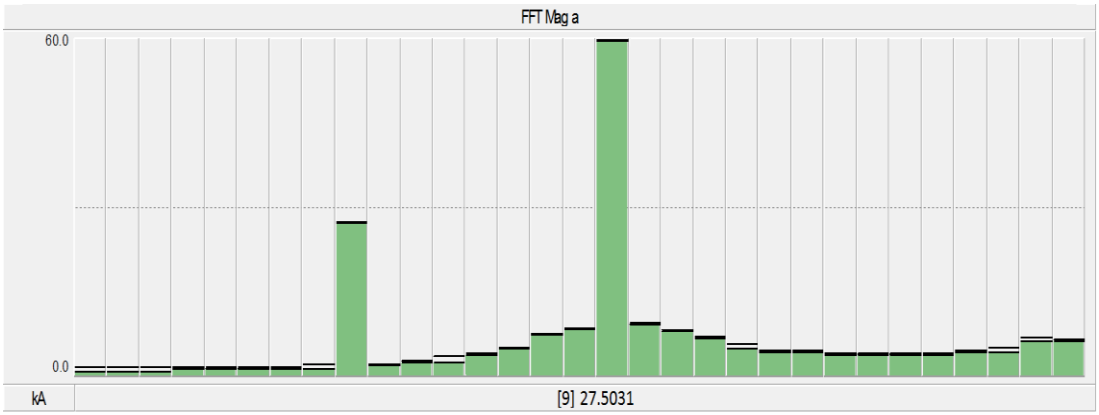

(b)

Fig. 4.16 Frequency spectrum of phase a current: (a) of FBM alone; (b) FBM including FSIG-WTS at 27% series compensation

The graphs of Figure 4.17 present the comparison between the torque interactions between the individual shafts on the multi-mass synchronous generator for the two systems at 27% series compensation. Figure 4.17 illustrates that the system of FBM alone is stable and the FSIG-WTs connecting with FBM system is unstable because of SSR. The dominant frequency of the torsional oscillations related to FBM connected with FSIG-WTs is around 32.5 *Hz*, which represents the frequency of the 4^{th} mode.

Figure 4.18 shows the comparison between the torque responses in the multi-mass rotor shaft of the synchronous generator for the FBM connected with various power ratings of FSIG-WTs (200, 500 and 750 MW) at 50 % series compensation. All the modes are unstable because of SSR and the dominant frequency of the oscillations is around 25.6 *Hz*, the frequency of the torsional mode three.

It is noticeable from Figure 4.18 that the amount of oscillation on the torque responses in the multi-mass rotor shaft decreases when the power rating of the FSIG-WTs is increased.

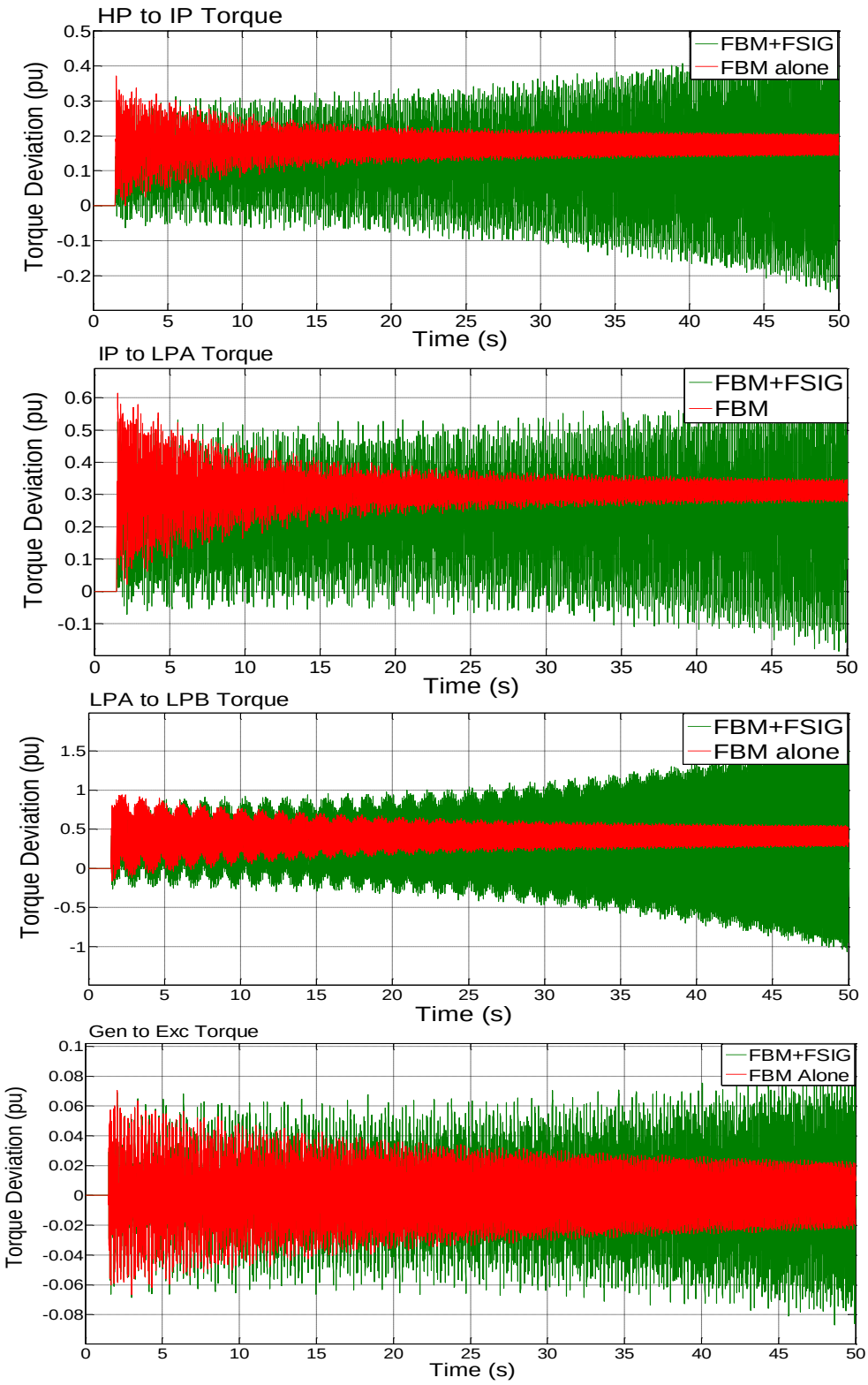

Fig. 4.17 Comparisons between torque responses in the multi-mass rotor shaft of IEEE FBM alone and including FSIG-WTs at 27% series compensation

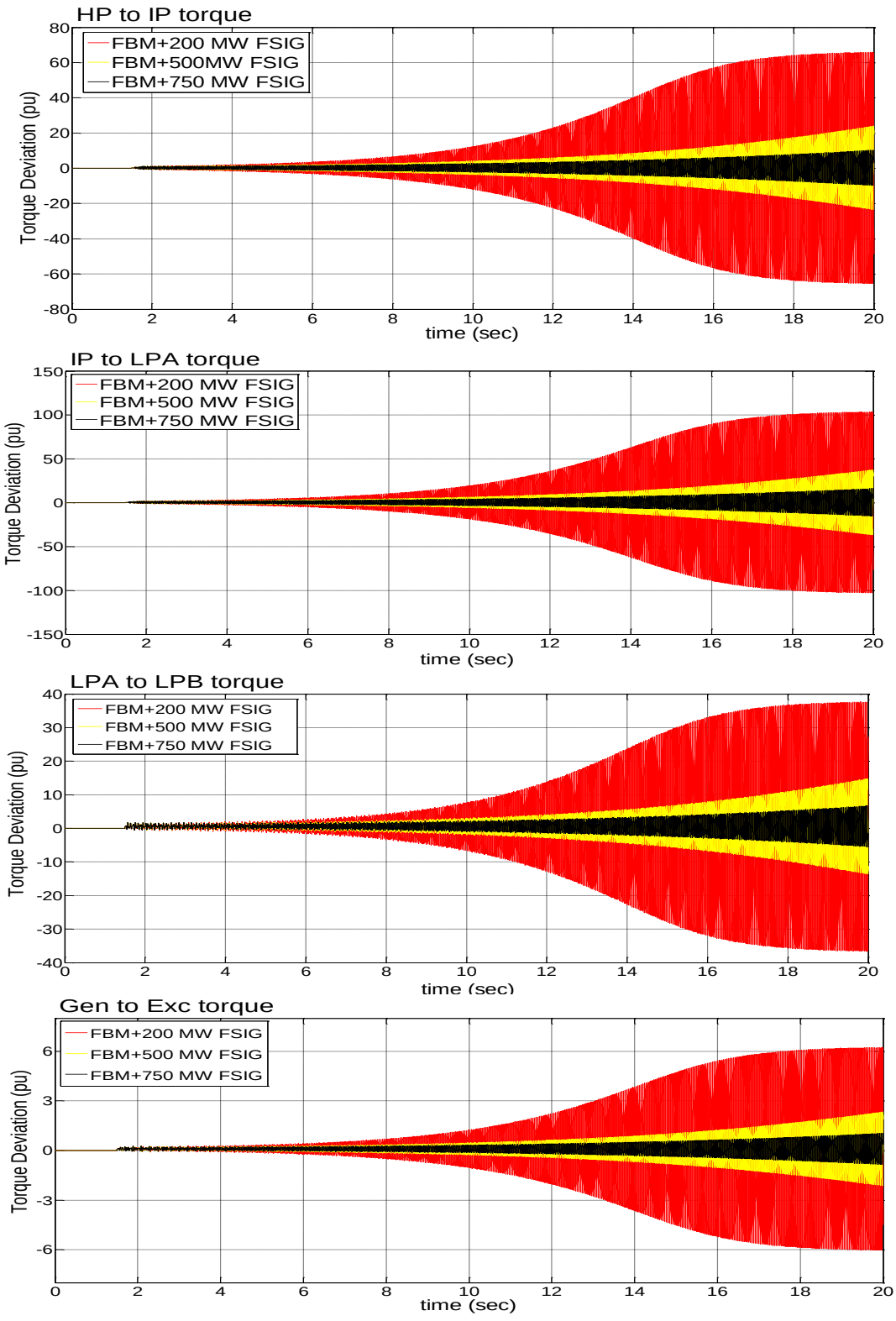

Fig. 4.18 Comparisons between torque responses in the multi-mass rotor shaft of IEEE FBM including different power ratings of FSIG-WTs at 50% series compensation

4.5 Conclusion

The influence of FSIG-WTs on SSR in a series compensated transmission line has been studied. Eigenvalue analyses in MATLAB and time domain simulations in the PSCAD environment have been carried out at a wide range of series compensation levels and different power ratings of FSIG-WTs.

The results reveal that connecting FSIG-WTs to FBM causes the SSR to occur at a lower series compensation level than that for FBM alone. That means it increases the range of series compensation level at which SSR can occur. Therefore, FSIG-WTs have an adverse effect on the SSR occurring at the multi-mass synchronous generator.

FSIG-WTs are affected by the frequency of the subsynchronous currents over the series compensated transmission line. Therefore, another slip called subsynchronous slip in addition to the rated slip of the FSIG is created. The subsynchronous slip changes the equivalent impedance of the FSIG-WTs which, in turn, causes a reduction of the natural frequency of the series compensated transmission line by changing the value of the equivalent impedance causing it. Therefore, SSR occurs at lower series compensation level than that for the FBM alone.

Chapter 5-

An LQR-Based SSR Damping Controller For FRC-WTs

5.1- Introduction

The new generation of Flexible AC transmission system (FACTS) controllers based on Voltage Source Converters (VSC), such as Static Synchronous Compensator (STATCOM), can play a major role in the mitigation of SSR torsional oscillations induced in the turbine shaft system. However, it is uneconomical to install such a controller in the power system primarily for the purpose of damping SSR.

The grid side converters of the Fully Rated Converter-Based Wind Turbines (FRC-WTs) have similar dynamic response of STATCOM. Therefore, the grid side converters of FRC-WTs can be used to damp SSR in the steam turbine because of fixed series compensation.

The objective of this chapter is to investigate the effectiveness of disgning an auxilary damping controller for the grid-side converters used in FRC-WTs to mitigate SSR. SSR damping controller is designing using optimal control technique within the grid-side converters of the FRC-WTs to damp SSR occrrence in the steam turbine shafts. A Linear Quadratic Regulator (LQR) is used as a kind of optimal control to damp SSR oscillations occurred at the shafts of the steam turbine. For this study, Eigenvalue analysis and digital time-domain simulations have been employed.

5.2- System under Study

Figure 5.1 shows the single line diagram of FRC-WTs system connected to IEEE First Benchmark Model (FBM). System *I* represents the FBM which is a turbine-generator connected via a transformer to a large AC network (infinite bus) through a series compensated transmission line (Line I) [72]. System *II* represents the FRC-WTs connected to the main transmission line (I) through a transmission line (Line II) [10]. The data of the system I was given in Chapter '3' while the data of the system II is given by the end of this chapter.

In order to develop the mathematical model for FBM featuring FRC-WTs, the differential equations of the turbine-generator, the turbine-generator mechanical system and the series capacitor compensated transmission line given in Chapter '3' are used here. The FRC-WTs and its controllers are modelled as described in the next two sections.

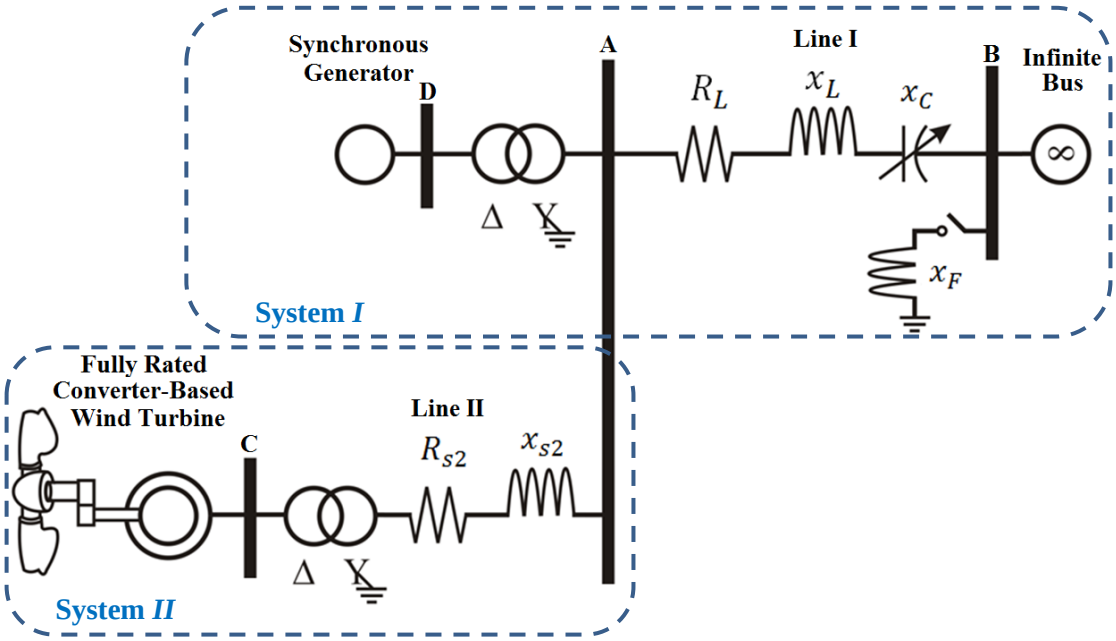

Fig. 5.1 Schematic diagram of FRC-WTs connected to FBM.

5.3 Fully Rated Converter-Based Wind Turbine

The schematic diagram of FRC-WT is shown in Figure 5.2. The FRC-WT is advantaged by employing a wide range of electrical generator types such as induction generator and synchronous generator [10].

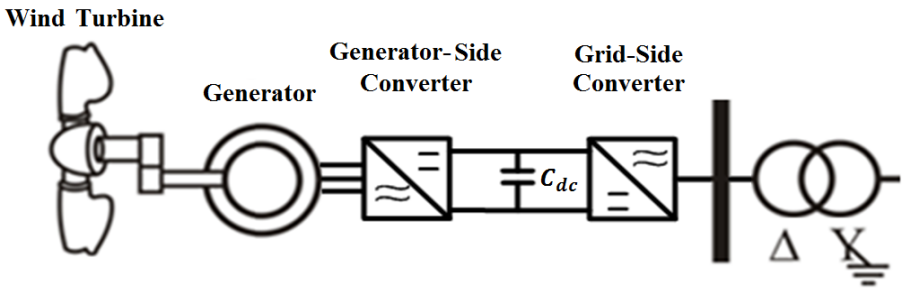

Fig. 5.2 Typical configuration of a Fully Rated Converter-Based Wind Turbine [10].

The power converter system of the FRC-WTs consists of the generator-side and the grid-side converters connected back-to-back through a DC link. The grid side converter is a pulse width modulated-VSC (PWM-VSC). The generator-side converter can be a diode-based rectifier or a PWM-VSC [10], [77]. The rated power of the generator decides the rating of power converters in this type of wind turbine.

For FRC-WTs, the presence of the back-to-back converter provides a decoupling between the grid and the turbine. Therefore, if an oscillation is triggered on the grid side of the converter it will not be reflected on the wind turbine side. As a result, this type of turbine is not affected by SSR problems [33]. Thereby, wind turbine side VSC of FRC-WT is modelled as a current source to stand with the grid side converter as shown, in Figure 5.3.

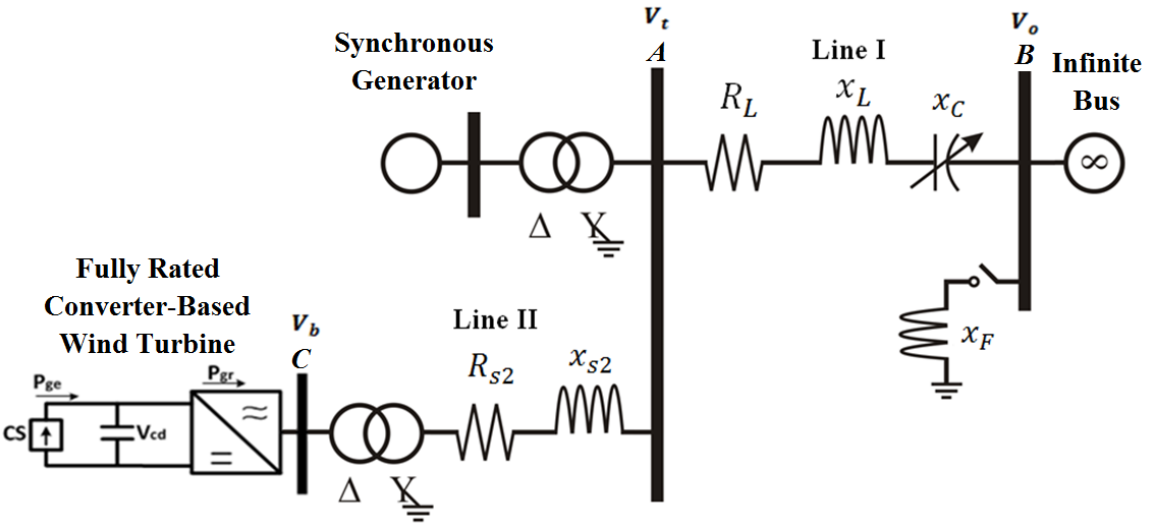

Fig. 5.3 Schematic diagram of FRC-WTs connecting to FBM.

5.3.1 FRC-WT system dynamic model.

Replacing wind turbine, generator and generator side converter with current source has simplified the mathematical model of the whole system under study as shown in Figure 5.3. The voltage magnitude at bus *A* is defined in d-q axes as:

$$v_t = v_{td} + jv_{tq} \tag{5.1}$$

$$\begin{bmatrix} v_{td} \\ v_{tq} \end{bmatrix} = \begin{bmatrix} R_L & -x_L \\ x_L & R_L \end{bmatrix} \begin{bmatrix} i_{td} \\ i_{tq} \end{bmatrix} + \frac{x_L}{\omega_b} \begin{bmatrix} \frac{di_{td}}{dt} \\ \frac{di_{tq}}{dt} \end{bmatrix} + \begin{bmatrix} e_{cd} \\ e_{cq} \end{bmatrix} + \begin{bmatrix} V_{od} \\ V_{oq} \end{bmatrix} \tag{5.2}$$

where V_{od} and V_{oq} are the *d-q* components of the voltage at the infinite bus (V_o). e_{cd} and e_{cq} are the *d-q* voltage components across the series compensated capacitor. R_L and x_L are the equivalent resistance and the inductance of the transmission line (line *I*) in Figure 5.3. i_{td} and i_{tq} are the *d-q* components of current flowing through the series compensated transmission line as shown in Figure 5.4.

Regarding Figure 5.4, equation 5.2 can be rewritten as:

$$\begin{bmatrix} v_{td} \\ v_{tq} \end{bmatrix} = \begin{bmatrix} R_L & -x_L \\ x_L & R_L \end{bmatrix} \begin{bmatrix} i_d \\ i_q \end{bmatrix} + \begin{bmatrix} R_L & -x_L \\ x_L & R_L \end{bmatrix} \begin{bmatrix} i_{sd} \\ i_{sq} \end{bmatrix} + \frac{x_L}{\omega_b} \begin{bmatrix} \frac{di_d}{dt} \\ \frac{di_q}{dt} \end{bmatrix} + \frac{x_L}{\omega_b} \begin{bmatrix} \frac{di_{sd}}{dt} \\ \frac{di_{sq}}{dt} \end{bmatrix} + \begin{bmatrix} e_{cd} \\ e_{cq} \end{bmatrix} + \begin{bmatrix} V_{od} \\ V_{oq} \end{bmatrix} \tag{5.3}$$

where i_{sd} and i_{sq} are the *d-q* components of output current of the FRC-WTs. i_d and i_q are the *d-q* components of output current of the synchronous generator as shown in Figure 5.4.

Fig. 5.4 The d-q current components in the transmission line (Line I).

The equivalent circuit per phase of FRC-WTs model is shown in Figure 5.5. Based on the principle of VSC operation, the voltage source v_b is defined as:

$$v_b = mkV_{dc}\angle\psi \tag{5.4}$$

where *k*, *m* and ψ are the ratio between AC and DC voltage, the modulation ratio defined by PWM and the phase angle which is defined by PWM [10], [36], [78].

Adopting the time *t* in seconds, the based angular speed (ω_b) in rad/s and the other quantities in per unit, the dynamic equations for grid side converter are expressed as:

$$\begin{bmatrix} v_{bd} \\ v_{bq} \end{bmatrix} = \begin{bmatrix} v_{td} \\ v_{tq} \end{bmatrix} + \frac{x_{s2}}{\omega_b}\begin{bmatrix} \frac{di_{sd}}{dt} \\ \frac{di_{sq}}{dt} \end{bmatrix} + \begin{bmatrix} R_{s2} & -x_{s2} \\ x_{s2} & R_{s2} \end{bmatrix}\begin{bmatrix} i_{sd} \\ i_{sq} \end{bmatrix} \tag{5.5}$$

$$\begin{bmatrix} v_{bd} \\ v_{bq} \end{bmatrix} = mkV_{dc}\begin{bmatrix} \sin(\delta-\psi) \\ \cos(\delta-\psi) \end{bmatrix} \tag{5.6}$$

where v_{bd} and v_{bq} are the terminal voltage of grid side converter. i_{sd} and i_{sq} are the *d-q* components of current injected from the FRC-WTs. R_{s2} and x_{s2} are the equivalent resistance and inductance of the transmission line (Line II). δ is the load angle separated between the two frame references.

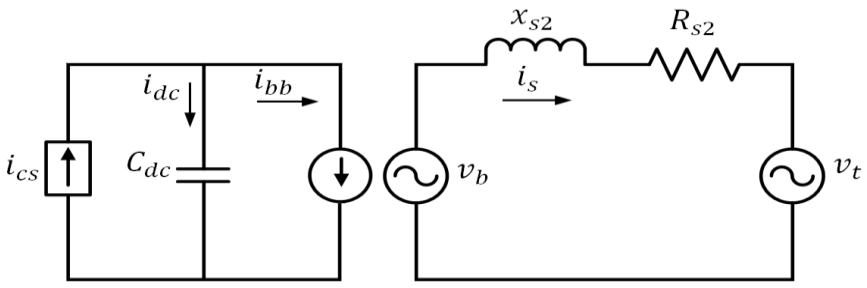

Fig. 5.5 FRC-WT back-to-back system equivalent circuit for dynamic analysis [36].

By substituting equation (5.6) into equation (5.5) as follows:

$$\begin{bmatrix} v_{td} \\ \\ v_{tq} \end{bmatrix} = mkV_{dc} \begin{bmatrix} \sin(\delta - \psi) \\ \\ \cos(\delta - \psi) \end{bmatrix} - \frac{x_{s2}}{\omega_b} \begin{bmatrix} \frac{di_{sd}}{dt} \\ \\ \frac{di_{sq}}{dt} \end{bmatrix} - \begin{bmatrix} R_{s2} & -x_{s2} \\ \\ x_{s2} & R_{s2} \end{bmatrix} \begin{bmatrix} i_{sd} \\ \\ i_{sq} \end{bmatrix} \tag{5.7}$$

By substituting equation (5.7) in equation (5.3) and making linearization, the state space equations of the d-q current components in the line *II* are given as:

$$[\Delta \dot{x}_{stl}] = [At_2][\Delta x_{stl}] + [Bt_2] \begin{bmatrix} \Delta\delta \\ \Delta e_{cd} \\ \Delta e_{cq} \\ \Delta i_d \\ \Delta i_q \\ \Delta \dot{i}_d \\ \Delta \dot{i}_q \\ \Delta m \\ \Delta\psi \\ \Delta V_{dc} \end{bmatrix} \tag{5.8}$$

where

$$[\Delta \dot{x}_{stl}] = \begin{bmatrix} \Delta \dot{i}_{sd} & \Delta \dot{i}_{sq} \end{bmatrix}^T$$

$$[At_2] = \frac{\omega_b}{(x_L + x_{s2})} \begin{bmatrix} -(R_{s2} + R_L) & (x_L + x_{s2}) \\ \\ -(x_{s2} + x_L) & -(R_{s2} + R_L) \end{bmatrix}$$

$$[Bt_2] = \frac{\omega_b}{(x_L + x_{s2})} \begin{bmatrix} (\cos(\delta_0 - \psi_0) - V_o \cos(\delta_0)) & (V_o \sin(\delta_0) - \sin(\delta_0 - \psi_0)) \\ -1 & 0 \\ 0 & -1 \\ -R_L & -x_L \\ x_L & -R_L \\ -x_L & 0 \\ 0 & -x_L \\ kV_{dc0}\sin(\delta_0 - \psi_0) & kV_{dc0}\cos(\delta_0 - \psi_0) \\ km_0 V_{dc0}\cos(\delta_0 - \psi_0) & -km_0 V_{dc0}\sin(\delta_0 - \psi_0) \\ km_0 \sin(\delta_0 - \psi_0) & km_0 \cos(\delta_0 - \psi_0) \end{bmatrix}^T$$

where δ_0, V_{dc0}, m_0 and ψ_0 are the initial values of load angle, the DC voltage, PWM amplitude modulation ratio and phase angle of the grid side converter.

As shown in Figure 5.5, the DC voltage state variable is derived as:

$$i_{dc} = C_{dc}\frac{dV_{dc}}{dt} = i_{cs} - i_{bb} \tag{5.9}$$

where i_{dc}, i_{cs} and i_{bb} are the current in the DC capacitor, current outputs from the current source and the current inputs to the grid side converter-based wind turbine.

By multiplying equation (5.9) by V_{dc} as follows:

$$C_{dc}V_{dc}\frac{dV_{dc}}{dt} = V_{dc}i_{cs} - V_{dc}i_{bb} = P_{ge} - P_{gr} \tag{5.10}$$

where P_{ge} and P_{gr} are the active power of the generator side converter and the grid side converter.

The apparent power output from the grid side converter of FRC-WTs is given as:

$$S_{gr} = P_{gr} + JQ_{gr} = v_b i_s^* = kmV_{dc}[\sin(\delta - \psi) + j\cos(\delta - \psi)](i_{sd} + j\, i_{sq})^*$$
$$= kmV_{dc}[\sin(\delta - \psi) + j\cos(\delta - \psi)](i_{sd} - j\, i_{sq}) \tag{5.11}$$

where

$$P_{gr} = kmV_{dc}i_{sd}\sin(\delta - \psi) + kmV_{dc}i_{sq}cos(\delta - \psi) \tag{5.12}$$

$$Q_{gr} = kmV_{dc}i_{sd}\cos(\delta - \psi) - kmV_{dc}i_{sq}sin(\delta - \psi) \tag{5.13}$$

By substituting equation (5.12) in equation (5.10) as follows:

$$C_{dc}V_{dc}\frac{dV_{dc}}{dt} = P_{ge} - mkV_{dc}(sin(\delta - \psi)\, i_{sd} + cos(\delta - \psi)\, i_{sq}) \tag{5.14}$$

$$\frac{dV_{dc}}{dt} = \frac{P_{ge}}{C_{dc}V_{dc}} - \frac{mk}{C_{dc}}(sin(\delta - \psi)\, i_{sd} + cos(\delta - \psi)\, i_{sq}) \tag{5.15}$$

By making linearization to equation (5.15), the state variable of the DC voltage is given as:

$$\Delta\dot{V}_{dc} = \frac{km_0}{C_{dc}}\left[sin(\delta_0 - \psi_0)\, i_{sq0} - cos(\delta_0 - \psi_0)\, i_{sd0}\right]\Delta\delta - \frac{km_0}{C_{dc}}sin(\delta_0 - \psi_0)\,\Delta i_{sd} -$$
$$\frac{km_0}{C_{dc}}cos(\delta_0 - \psi_0)\,\Delta i_{sq} - \frac{k}{C_{dc}}[sin(\delta_0 - \psi_0)\, i_{sd0} + cos(\delta_0 - \psi_0)\, i_{sq0}]\Delta m +$$
$$\frac{km_0}{C_{dc}}[sin(\delta_0 - \psi_0)\, i_{sq0} - cos(\delta_0 - \psi_0)\, i_{sd0}]\Delta\psi - \frac{p_{ge}}{C_{dc}V_{dco}^2}\Delta V_{dc} \tag{5.16}$$

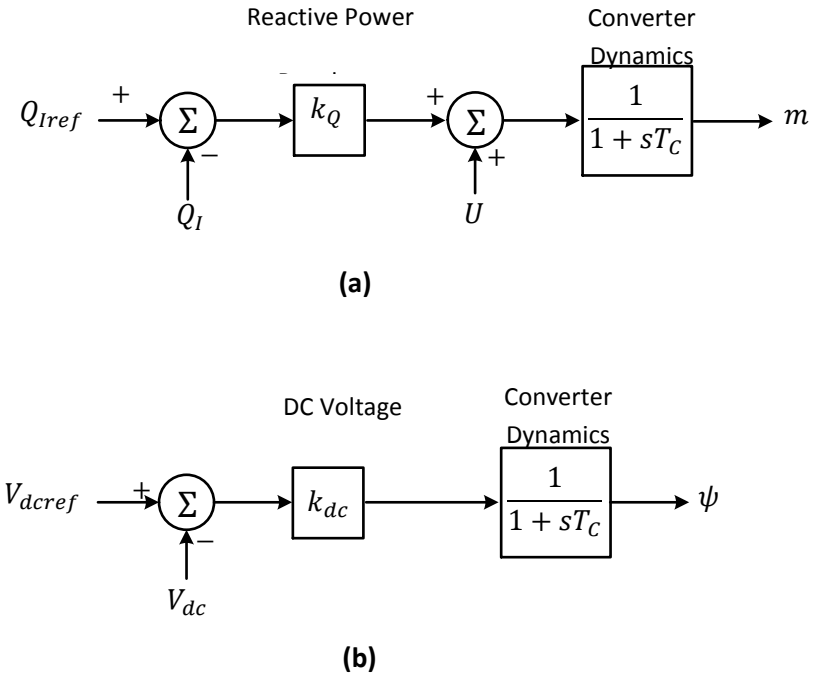

Fig. 5.6 The multiple functional of FRC-WT grid side converter:
(a) Reactive power regulator and the SSR damping signal controller; (b) DC voltage regulator.

5.3.2 The regulators of FRC-WTs grid side converter

Figure 5.6 shows a schematic diagram of VSC controllers which comprise two main controllers of VSC of FRC-WTs. The state variables Δm and $\Delta\psi$ are derived as:

$$\Delta\dot{m} = \frac{k_Q}{T_C}\Delta Q + \frac{1}{T_C}\Delta U - \frac{1}{T_C}\Delta m \tag{5.17}$$

where k_Q and T_C are the gain and the time constant of the reactive power regulator. ΔU represents the signal of the auxiliary controller used to damp SSR.

ΔQ represents the change in reactive power of the grid side converter which is given by linearizing equation (5.13) as:

$$\begin{aligned}\Delta Q_{gr} = {} & km_0V_{dc0}\cos(\delta_0-\psi_0)\Delta i_{sd} - km_0V_{dc0}\sin(\delta_0-\psi_0)\,\Delta i_{sq} + \\ & kV_{dc0}\left[i_{sd0}\cos(\delta_0-\psi_0) - i_{sq0}\sin(\delta_0-\psi_0)\right]\Delta m - km_0V_{dc0}\left[i_{sd0}\sin(\delta_0-\psi_0) - \right. \\ & \left. i_{sq0}\cos(\delta_0-\psi_0)\right]\Delta\psi - km_0V_{dc0}\left[i_{sd0}\sin(\delta_0-\psi_0) - i_{sq0}\cos(\delta_0-\psi_0)\right]\Delta\delta + \\ & km_0\left[i_{sd0}\cos(\delta_0-\psi_0) - i_{sq0}\sin(\delta_0-\psi_0)\right]\Delta V_{dc}\end{aligned} \tag{5.18}$$

By substituting equation (5.18) into equation (5.17), the PWM amplitude modulation ratio state variable is given as:

$$\Delta\dot{m} = \frac{k_Q}{T_C}\Delta Q + \frac{1}{T_C}\Delta U - \frac{1}{T_C}\Delta m$$
$$= \frac{k_Q k m_0 V_{dc0}}{T_C}\left[i_{sq0}\cos(\delta_0 - \psi_0) - i_{sd0}\sin(\delta_0 - \psi_0)\right]\Delta\delta + \frac{k_Q k m_0 V_{dc0}}{T_C}\cos(\delta_0 - \psi_0)\Delta i_{sd} - \frac{k_Q k m_0 V_{dc0}}{T_C}\sin(\delta_0 - \psi_0)\Delta i_{sq} +$$
$$\frac{1}{T_C}\left(k_Q k V_{dc0}\left[i_{sd0}\cos(\delta_0 - \psi_0) - i_{sq0}\sin(\delta_0 - \psi_0)\right] - 1\right)\Delta m - \frac{k_Q k m_0 V_{dc0}}{T_C}\left[i_{sd0}\sin(\delta_0 - \psi_0) - i_{sq0}\cos(\delta_0 - \psi_0)\right]\Delta\psi +$$
$$\frac{k_Q k m_0}{T_C}\left[i_{sd0}\cos(\delta_0 - \psi_0) - i_{sq0}\sin(\delta_0 - \psi_0)\right]\Delta V_{dc} + \frac{1}{T_C}\Delta U \quad (5.19)$$

The state space variable of the angle ψ is given as:

$$\Delta\dot{\psi} = \frac{k_{dc}}{T_C}\Delta V_{dc} - \frac{1}{T_C}\Delta\psi \quad (5.20)$$

where k_{dc} and T_C are the gain and the time constant of the DC voltage regulator.

The state space equations for the FRC-WTs are given as:

$$[\Delta\dot{x}_{FRC}] = [At_3][\Delta x_{FRC}] + [Bt_3]\begin{bmatrix}\Delta\delta\\ \Delta i_{sd}\\ \Delta i_{sq}\end{bmatrix} + \begin{bmatrix}\frac{1}{T_C}\\ 0\\ 0\end{bmatrix}[\Delta U] \quad (5.21)$$

where

$$[\Delta\dot{x}_{FRC}] = [\Delta\dot{m} \quad \Delta\dot{\psi} \quad \Delta\dot{V}_{dc}]^T \quad (5.22)$$

$$[At_3] = \begin{bmatrix}a_{11} & a_{12} & a_{13}\\ a_{21} & a_{22} & a_{23}\\ a_{31} & a_{32} & a_{33}\end{bmatrix}$$

$$[Bt_3] = \begin{bmatrix}b_{11} & b_{12} & b_{13}\\ b_{21} & b_{22} & b_{23}\\ b_{31} & b_{32} & b_{33}\end{bmatrix}$$

The elements of At_3 are given as:

$$a_{11} = \left(\frac{k_Q k V_{dc0}}{T_C}\left[i_{sd0}\cos(\delta_0 - \psi_0) - i_{sq0}\sin(\delta_0 - \psi_0)\right] - \frac{1}{T_C}\right)$$

$$a_{12} = -\frac{k_Q k m_0 V_{dc0}}{T_C}\left[i_{sd0}\sin(\delta_0 - \psi_0) - i_{sq0}\cos(\delta_0 - \psi_0)\right]$$

$$a_{13} = \frac{k_Q k m_0}{T_C}\left[i_{sd0}\cos(\delta_0 - \psi_0) - i_{sq0}\sin(\delta_0 - \psi_0)\right]$$

$$a_{21} = 0$$

$$a_{22} = \frac{k_{dc}}{T_C}$$

$$a_{23} = -\frac{1}{T_C}$$

$$a_{31} = \frac{k}{C_{dc}}\left[sin(\delta_0 - \psi_0)\, i_{sd0} + cos(\delta_0 - \psi_0)\, i_{sq0}\right]$$

$$a_{32} = \frac{k m_0}{C_{dc}}\left[sin(\delta_0 - \psi_0)\, i_{sq0} - cos(\delta_0 - \psi_0)\, i_{sd0}\right]$$

$$a_{33} = -\frac{p_{ge}}{C_{dc} V_{dco}^2}$$

The elements of Bt_3 are given as:

$$b_{11} = \frac{k_Q k m_0 V_{dc0}}{T_C}\left[i_{sq0}\cos(\delta_0 - \psi_0) - i_{sd0}\sin(\delta_0 - \psi_0)\right]$$

$$b_{12} = \frac{k_Q k m_0 V_{dc0}}{T_C}\cos(\delta_0 - \psi_0)$$

$$b_{13} = -\frac{k_Q k m_0 V_{dc0}}{T_C}\sin(\delta_0 - \psi_0)$$

$$b_{21} = 0$$

$$b_{22} = 0$$

$$b_{23} = 0$$

$$b_{31} = \frac{k m_0}{C_{dc}}\left[sin(\delta_0 - \psi_0)\, i_{sq0} - cos(\delta_0 - \psi_0)\, i_{sd0}\right]$$

$$b_{32} = -\frac{k m_0}{C_{dc}} sin(\delta_0 - \psi_0)$$

$$b_{33} = -\frac{k m_0}{C_{dc}} cos(\delta_0 - \psi_0)$$

5.4 The Dynamic Model of the Overall System

Figure 5.7 shows the connection of FRC-WTs with the FBM. The Park transformation matrix and its inverse are used for the connection of the synchronous generator with the rest of the system as depicted in Figure 5.7. As the multi-mass synchronous generator is represented in D-Q rotor reference frame while the rest of the model is represented in d-q synchronous reference frame.

The overall mathematical analysis of the system has been derived by performing some additional mathematical operations. As connecting the FRC-WF with the FBM demands that the equations of the series compensated transmission line, equation (3.15) to equation (3.17) in Chapter 3, to be changed.

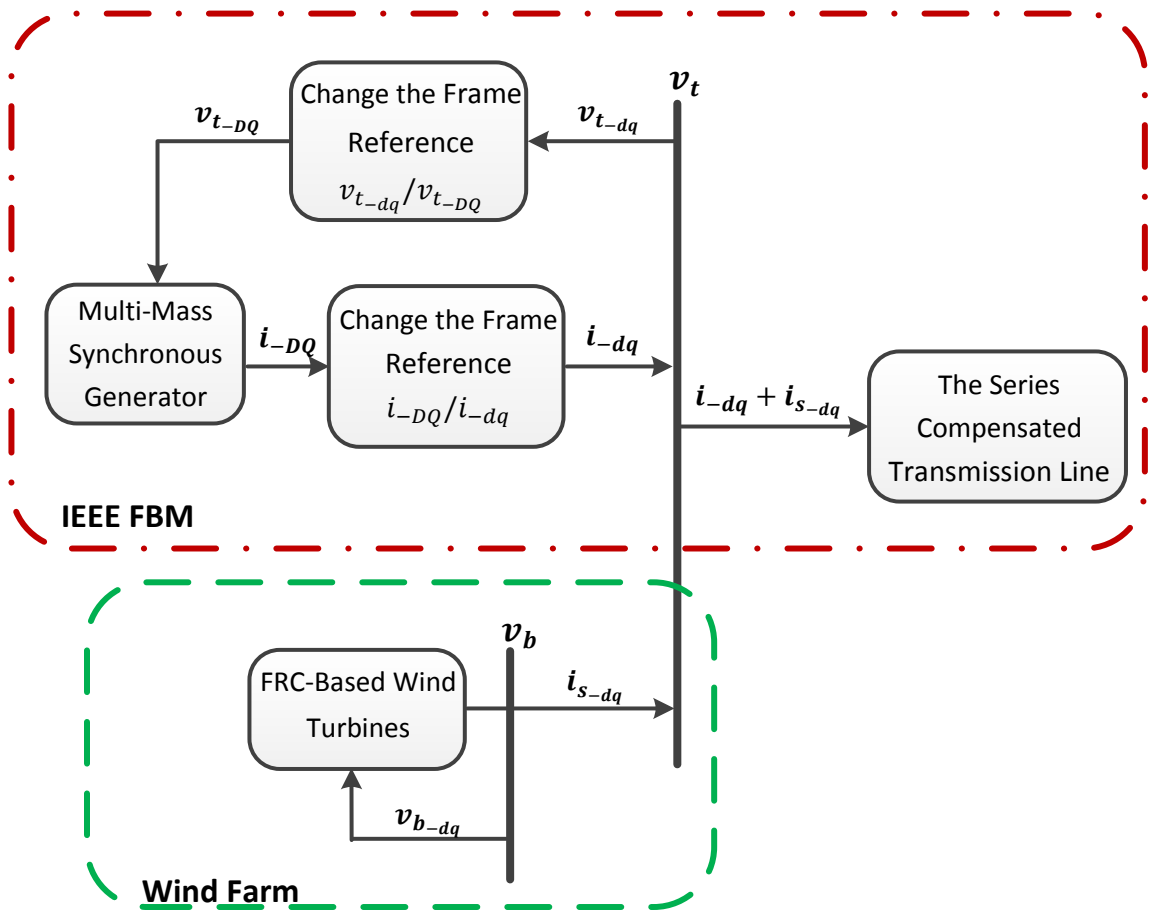

Fig. 5.7 Sub-System interactions for the IEEE FBM featuring FRC-WTs.

With relation to Figures 5.1 and 5.3, the state space equations for the series capacitor compensated transmission line (Line I) are modified as follows:

$$\left[\frac{dX_{TL}}{dt}\right] = [At_{TL}][X_{TL}] + [Bt1_{TL}]\begin{bmatrix} v_{td} \\ v_{tq} \end{bmatrix} + [Bt_{2TL}][V_o] \tag{5.23}$$

where

$$[X_{TL}] = [e_{cd} \quad e_{cq} \quad i_{td} \quad i_{tq}]^T$$

$$[At_{TL}] = \begin{bmatrix} 0 & \omega_s & \omega_s x_C & 0 \\ -\omega_s & 0 & 0 & \omega_s x_C \\ \frac{-\omega_s}{x_L} & 0 & (\frac{-\omega_s R_L}{x_L}) & \omega_s \\ 0 & \frac{-\omega_s}{x_L} & -\omega_s & (\frac{-\omega_s R_L}{x_L}) \end{bmatrix}$$

$$[Bt1_{TL}] = \begin{bmatrix} 0 & 0 \\ 0 & 0 \\ \frac{\omega_s}{x_L} & 0 \\ 0 & \frac{\omega_s}{x_L} \end{bmatrix}, \quad [Bt2_{TL}] = \begin{bmatrix} 0 \\ 0 \\ \frac{-\omega_s \sin(\delta)}{x_L} \\ \frac{-\omega_s \cos(\delta)}{x_L} \end{bmatrix}$$

By linearizing Equation (5.23), the following equation can be written in terms of the output currents of synchronous and wind farm generators as follows:

$$\begin{bmatrix} \Delta\dot{e}_{cd} \\ \Delta\dot{e}_{cq} \\ \Delta v_{td} \\ \Delta v_{tq} \end{bmatrix} = [Att_{TL}]\begin{bmatrix} \Delta e_{cd} \\ \Delta e_{cd} \end{bmatrix} + [At11_{TL}]\begin{bmatrix} \Delta\dot{i}_d \\ \Delta\dot{i}_q \end{bmatrix} + [At12_{TL}]\begin{bmatrix} \Delta\dot{i}_{sd} \\ \Delta\dot{i}_{sq} \end{bmatrix} + [At21_{TL}]\begin{bmatrix} \Delta i_d \\ \Delta i_q \end{bmatrix}$$

$$+ \ [At22_{TL}]\begin{bmatrix} \Delta i_{sd} \\ \Delta \boldsymbol{i}_{sq} \end{bmatrix} + [Btt_{TL}][\Delta\delta] \tag{5.24}$$

where

$$[Att_{TL}] = \begin{bmatrix} 0 & \omega_s \\ -\omega_s & 0 \\ 0 & 0 \\ 0 & 0 \end{bmatrix}, \qquad [Btt_{TL}] = \begin{bmatrix} 0 \\ 0 \\ V_o \cos(\delta_0) \\ -V_o \sin(\delta_0) \end{bmatrix}$$

$$[At11_{TL}] = \begin{bmatrix} 0 & 0 \\ 0 & 0 \\ \frac{\omega_s}{x_L} & 0 \\ 0 & \frac{\omega_s}{x_L} \end{bmatrix}, \qquad [At12_{TL}] = \begin{bmatrix} 0 & 0 \\ 0 & 0 \\ \frac{\omega_s}{x_L} & 0 \\ 0 & \frac{\omega_s}{x_L} \end{bmatrix}$$

$$[At21_{TL}] = \begin{bmatrix} (\omega_b x_C) & 0 \\ 0 & (\omega_b x_C) \\ R_L & -x_L \\ x_L & R_L \end{bmatrix}, \qquad [At22_{TL}] = \begin{bmatrix} (\omega_b x_c) & 0 \\ 0 & (\omega_b x_C) \\ R_L & -x_L \\ x_L & R_L \end{bmatrix}$$

Combining equations (5.8), (5.21), (5.24) and equations related to the turbine- generator shaft and excitation system of the synchronous generator in Chapter '3', the overall linearized equations of the system under study are given by:

$$[\Delta \dot{X}_{sys}] = [At_{sys2}][\Delta X_{sys}] + [Bt_{sys2}][\Delta U_{sys}] \tag{5.25}$$

$$[\Delta y_{sys}] = [Ct_{sys2}][\Delta X_{sys}] \tag{5.26}$$

where

$$[\Delta X_{sys}] = [\Delta\omega_H\ \Delta\theta_H\ \Delta\omega_I\ \Delta\theta_I\ \Delta\omega_{LPA}\ \Delta\theta_{LPA}\ \Delta\omega_{LPB}\ \Delta\theta_{LPB}\ \Delta\omega\ \Delta\delta\ \Delta\omega_{EXC}\ \Delta\theta_{EXC}\ \Delta T_H\ \Delta T_i\ \Delta T_A\ \Delta a\ \Delta g\ \Delta e_{cd}\ \Delta e_{cq}\ \Delta i_d\ \Delta i_q\ \Delta i_F\ \Delta i_D\ \Delta i_Q\ \Delta i_S\ \Delta V_R\ \Delta E_{ED} \Delta i_{sd}, \Delta i_{sq}, \Delta m, \Delta\psi, \Delta V_{dc}]$$

$$\Delta i_{sd}, \Delta i_{sq}, \Delta m, \Delta\psi, \Delta V_{dc}] \tag{5.27}$$

$$[\Delta y_{sys}] = \begin{bmatrix} \Delta v_{td} \\ \Delta v_{tq} \end{bmatrix} \tag{5.28}$$

The parameters used in the FBM and can be found in [72] and in the Chapter '3' while the parameters used in FRC-WTs can be found in [10] and as follows:

Induction generator (p.u.)
Rating of each unit : 2MVA
Line-to-line voltage: 966V
DC Link Parameters
Reference DC link voltage V_{DC}= 1000V
Capacitor *C*: 10mF

5.5 SSR Damping Controller Design

Linear Quadratic Regulator method (LQR) is used as an optimal control through the grid side converter of the FRC-WTs to damp SSR. To implement the LQR method, all the state variables of the system are assumed to be available for feedback. However, most of the state variables in practise are not available because they cannot be measured easily. Therefore, full order observer is designed based on [79-80] to estimate the unmeasurable state variables and use the observed state variables for feedback.

LQR method and full order observer were designed separately and combined together to form the output feedback control system as shown in Figure 5.8 [80-81]. The feedback gain matrix (k) is generated by the LQR in such a way that the system satisfy the performance requirements in damping SSR. The full order observer was designed so that the observer response is much faster than the system response. The design procedure involves two steps. The first step is mainly to determine the feedback gain vector by using LQR method. In the second step of the design, the target is to estimate the unmeasured state variables by using full order observer.

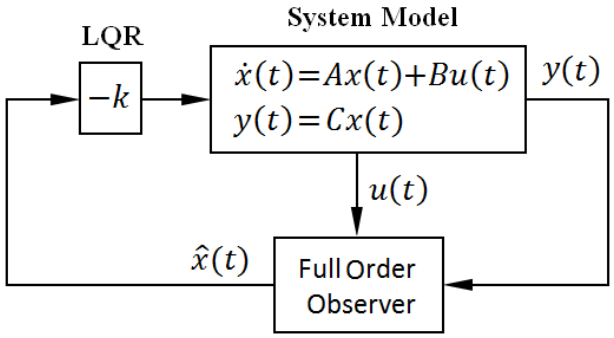

Fig. 5.8 Block diagram showing the plant, the observer and the LQR controller [76].

5.5.1 Linear quadratic regulator

LQR is an optimal control method and has been extensively studied for decades [80-83]. The objective of LQR is to determine the feedback gain matrix (k) for minimizing the performance index to achieve the optimal exchange between the use of control effort, the magnitude and the speed of the response [80]. In addition, this method guarantees a stable control system [80-81]. The system under study expressed in state-space as follows:

$$\dot{x}(t) = Ax(t) + Bu(t)$$
$$y(t) = Cx(t) \quad (5.26)$$

where $x(t)$ is the state vector, $u(t)$ is the system input and $y(t)$ is the system output. A, B and C are constant matrices.

the performance index J is given as:

$$J = \int_0^\infty [x^T Q x + u^T R u] dt \quad (5.27)$$

where Q is the symmetric positive semi-definite weighting matrix on the states and R is the symmetric positive definite weighting matrix on the control input [80].

The weighting matrices Q and R determine the relative importance of the error and the expenditure of this energy. For simplicity the weighting matrices Q and R are chosen as diagonal matrices. The weighting matrix R is set as an identity matrix [80]. The selection of the Q and R is related to the system performance. A certain amount of trial and error is required to reach to a satisfactory design results. To speed the process of selection the elements of Q, participation factor calculations are used. The elements of the off-diagonal of Q are initially chosen regarding to the participation factor of the state variables in the torsional modes. Then these elements of Q are increased until the system reaches the desired results.

Table 5.1 presents the normalized values of the participation factor of the state variables in the torsional modes and mode zero. The eighth column shows the value of the off-diagonal elements of Q. The state variables which represent the speed and the angular position of the rotating masses have high contribution in the torsional modes comparing with the rest of the state variables. As a result, their weighting values in Q should be increased to achieve a better damping of SSR. The last column shows the transpose of the feedback gain matrix k.

Table 5.1 Participation factors related to the torsional modes and the off-diagonal of the Q matrix.

State Variables	M5	M4	M3	M2	M1	M0	Off-Diagonal of Q matrix	k'
$\Delta\omega_H$	0.37	0.078	1	0.036	0.034	0.46	1000	128.58, -379.82
$\Delta\theta_H$	0.37	0.078	1	0.036	0.034	0.46	1000	45.309 , 37.44
$\Delta\omega_I$	1	3E-04	0.195	0.007	0.02	0.432	1000	-292.52, -299.4
$\Delta\theta_I$	1	3E-04	0.195	0.007	0.02	0.432	1000	13.801, -112.02
$\Delta\omega_{LPA}$	0.071	0.245	0.494	0.023	0.006	0.807	1000	-1165.9, -1327.8
$\Delta\theta_{LPA}$	0.071	0.245	0.494	0.023	0.006	0.807	1000	-293.25, -100.56
$\Delta\omega_{LPB}$	0.003	1	0.083	0.008	0.042	0.098	1000	-879.49, -2349.4
$\Delta\theta_{LPB}$	0.003	1	0.083	0.008	0.042	0.098	1000	-101.92 , -97.155
$\Delta\omega$	1E-04	0.379	0.262	0.015	0.037	1	1000	-35.382 , -4050.7
$\Delta\delta$	1E-04	0.379	0.262	0.015	0.037	1	1000	299.73 , -146.8
$\Delta\omega_{EXC}$	2E-07	0.005	0.024	0.001	1	0.293	1000	-74.049 , -114.5
$\Delta\theta_{EXC}$	2E-07	0.005	0.024	0.001	1	0.293	1000	2.5065 , -21.634
ΔT_H	6E-10	7E-08	6E-07	2E-08	1E-07	5E-06	0. 1	-17.071, -60.65
ΔT_I	3E-13	2E-12	1E-10	6E-12	6E-11	5E-09	0. 1	-9.7968 , -58.353
ΔT_{PLA}	4E-16	5E-13	4E-12	2E-13	7E-13	8E-11	0. 1	-26.825, -73.744
Δa	6E-10	7E-08	6E-07	2E-08	1E-07	5E-06	0. 1	0.2379, -0.1126
Δg	6E-10	7E-08	6E-07	2E-08	1E-07	5E-06	0. 1	-0.054, -1.7873
Δe_{cd}	8E-08	0.003	0.068	0.62	4E-04	0.004	1	-5.7122, 10.552
Δe_{cq}	9E-08	0.003	0.065	0.626	4E-04	0.004	1	4.9215 , 0.7783
Δi_d	4E-06	0.005	0.128	1	0.004	0.113	250	54.027 , -169.35
Δi_q	2E-06	7E-04	0.094	0.789	0.002	0.044	250	-61.871, 28.967
Δi_F	6E-07	0.002	0.036	0.172	0.003	0.078	0.1	-57.91 , 206.41
Δi_D	4E-06	0.007	0.066	0.569	0.001	0.033	0.1	-50.035 , 156.45
Δi_Q	1E-06	5E-04	0.043	0.363	0.001	0.026	0.1	62.961, -13.193
Δi_S	6E-07	2E-04	0.02	0.169	5E-04	0.012	0.1	62.545, -13.534
ΔV_R	6E-10	2E-05	2E-04	3E-04	1E-05	3E-04	0. 1	-1.4071, -0.9596
ΔE_{ED}	3E-10	9E-06	7E-05	1E-04	4E-06	7E-05	0. 1	-0.2995, 0.3658
Δi_{sd}	5E-07	0.003	0.038	0.341	2E-04	0.001	0.1	-0.872, 2.3822
Δi_{sq}	4E-07	0.002	0.041	0.365	2E-04	0.002	0.1	4.222, 0.08218
Δm	5E-09	3E-05	3E-04	0.003	8E-07	2E-05	250	12.693, -1.5551
$\Delta\psi$	7E-10	6E-06	6E-05	4E-04	1E-06	5E-05	0.1	-1.555, 17.26
ΔV_{dc}	8E-10	3E-06	8E-05	6E-04	1E-06	4E-05	0.1	9.907, -5.141

$R = [1]$

The optimal control law is given by [80-81] as:

$u(t) = -kx(t)$

where

$k = R^{-1}B^{T}P$ (5.28)

where P is the solution of algebraic Riccati equation as [81]:

$A^{T}P + PA - PBR^{-1}B^{T}P + Q = 0$ (5.29)

The values of the gain matrix k that yield optimal control are obtained by numerical methods for determining the solutions to the algebraic Riccati equation. MATLAB code was used to find the state feedback gain matrix k using the above procedure. MATLAB command "LQR" is used to determine the gain matrix (k) which accepts four parts: A, B and the weighting matrices R and Q.Table 5.2 introduces the procedure to obtain the state feedback gain matrix.

By determining the feedback gain matrix k using all the state variables, it is used as auxiliary input control signal to regulate the reactive power generating by FRC-WTs to damp SSR at the steam turbine.

Table 5.2 The procedure of LQR method [82]

Statement of the problem	
Given the system plant in state space as: $\dot{x}(t) = Ax(t) + Bu(t)$ the performance index as: $J = \int_0^{\infty}[x^{T}Qx + u^{T}Ru]dt$ the conditions are as: $x(t_0) = x_0$; $x(\infty) = 0$	
Find the feedback gain matrix and minimizing the index	
step	**Solution of the problem**
1	Choose the elements of the weighing matrices Q and R
2	Solve the algebraic Riccati equation $A^{T}P + PA - PBR^{-1}B^{T}P + Q = 0$
3	Obtain the feedback gain matrix k as: $k = R^{-1}B^{T}P$
4	Solve the optimal state from $\dot{x}(t) = (A - kB)x(t)$

5.5.2 Full order observer output

A state observer estimates the state variables based on the measurements of the output and control variables of the plant [80]. Then, the actual state variables in ($u = -kx$) are replaced with the estimated states ($\hat{x}$), making the optimal control law be ($u = -k\hat{x}$). The observer is called full order as the order of observer is the same as that of the plant.

Regarding Figure 5.9, the state equations are:

$$\dot{x} = Ax + Bu\ , \qquad y = Cx \tag{5.29}$$

$$\dot{\hat{x}} = A\hat{x} + Bu + L(y - \hat{y})\ , \qquad \hat{y} = C\hat{x} \tag{5.30}$$

$$u = -k\hat{x} \tag{5.31}$$

$$y - \hat{y} = C(x - \hat{x}) = Ce$$

$$\dot{e} = \dot{x} - \dot{\hat{x}} = Ax + Bu - (A\hat{x} + Bu - LC)$$

$$= (A - LC)e \tag{5.32}$$

where k and L are the LQR feedback gain matrix and the observer gain, e represents the error between the actual states and the estimated states, $\hat{y}$ indicates the estimated plant output. The observer design equation $[A - LC]$ decides the dynamic response of the observer relating to that of the plant.

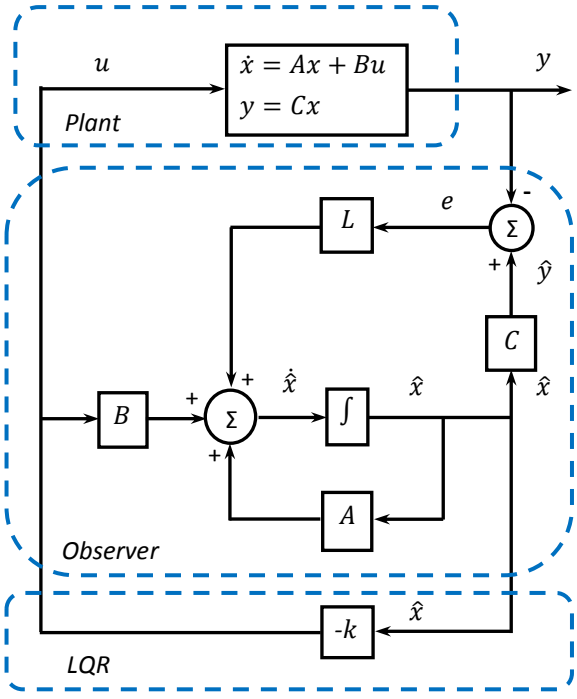

Fig. 5.9 Full-order observer in a state variable feedback control scheme [81]

$$\begin{bmatrix} \dot{x} \\ \dot{e} \end{bmatrix} = \begin{bmatrix} A - Bk & Bk \\ 0 & A - LC \end{bmatrix} \begin{bmatrix} x \\ e \end{bmatrix} \tag{5.33}$$

The goal for the observer is to reduce the error to zero by choosing gain L which makes all the eigenvalues of observer function equation $(A - LC)$ be negative. The characteristic equation for the observed-state feedback controlled system is:

$$\begin{vmatrix} A - Bk & Bk \\ 0 & A - LC \end{vmatrix} = 0 \tag{5.34}$$

$$|SI - A + Bk||SI - A + LC| = 0 \tag{5.35}$$

Regarding equation (5.26), the closed loop poles of the observed-state feedback control system consists of poles due LQR design alone and the poles due to the observer design alone. The optimal control represented by LQR control and full order observer are designed separately and combined to form the observed-state feedback control system.

The poles of the observer are chosen so that the observer response is much faster than the system. The gain matrix of the full order observer is easily computed using the MATLAB command "$PLACE$" which accepts three parts: A, B and vector "P" which represents the desired closed loop system poles. L is selected such that the response of the observer is faster by two to ten times than that of the system to reduce the error to zero so the estimated states quick converge to the actual states. That means the eigenvalues of the observer design equation $[A - LC]$ should be more negative than that of the plant [79-81]. Regarding the limitation of the maximum response speed of the observer, the observer response is chosen to be five times faster than that of the system.

5.6 Simulation Results

The complete state space mode described in section 5.4 is used to study the effect of the FRC-WTs with and without using LQR on SSR through eigenvalue analysis and time domain simulations. The eigenvalue analysis and time domain simulations were performed over a wide range of series compensation. 175 FRC-WT units with a power rating of 350 MW are connected with the FBM.

5.6.1 Eigenvalue analysis

The linearized system was utilised to obtain the eigenvalues of the system defined by equation (5.25) at different series compensation percentages. The eigenvalues of the torsional modes in addition to electrical mode are given in table 5.2. Table 5.3 shows the eigenvalues of the system with and without LQR control at 20%, 30% and 50 % series compensation.

From table 5-3 with 20% series compensation, the negative signs of the eigenvalues real part indicate that the system was stable with and without using any control. However, the torsional modes became more stable by implementing LQR. When the percent of series compensation is increased to 30%, mode 4 turned into oscillating state. This can be explained as the frequency of electric mode is close to the frequency of mode 4. On the other hand, by using LQR method, mode 4 was damped as shown in table 5-3. At 50% series compensation, the positive signs of real part of modes 4 and 3 specify that the system was unstable. Conversely, when LQR was implemented, the system becomes stable and modes 3 and 4 are damped.

Table 5.3. Comparison between eigenvalues at different series compensation levels.

Modes	20% Series Compensation		30% series compensation	
	Without LQR	With LQR	Without LQR	With LQR
5	-0.1817±j298.18	-0.1818±j298.18	-0.1817±j298.18	-0.1818±j298.18
4	-0.2232±j203.14	-0.228±j203.14	+0.494±**j 204.15**	-0.6392±**j204.01**
3	-0.2286±j160.62	-0.2684±j160.63	-0.2547±j160.68	-0.283±j160.68
2	-0.6687±j127.02	-0.672±j127.02	-0.6716±j127.02	-0.6741±j127.03
1	-0.2678±j99.026	-0.4267±j99.052	-0.2907±j99.092	-0.4321±j99.115
zero	-0.2156±j6.6008	-3.1731±j8.8249	-0.3031±j7.0888	-3.1223±j9.0873
SUB	-6.673±j238.17	-6.9766±j237.89	-7.2028±**j205.84**	-7.6768±**j205.63**

Modes	50% Series Compensation	
	Without LQR	With LQR
5	-0.1818±j298.18	-0.1818±j298.18
4	+0.121±j202.75	-0.1486±j202.75
3	**+0.747±j160.77**	-0.829±**j160.70**
2	-0.6823±j127.07	-0.6839±j127.07
1	-0.3617±j99.342	-0.4598±j99.359
zero	-0.4889±j8.2124	-3.0184±j9.7473
SUB	-7.4369±**j157.41**	-8.2819±**j156.86**

5.6.2 Time domain simulation

The time-domain simulation is used to verify the results of the eigenvalue analysis given in Table I, time domain simulation based on the linearized differential equations of the system under study is performed. These linearized equations are solved using Fourth-order Runge-Kutta modified by Gill Routine [84]. The simulation results are obtained when a three-phase fault at bus B, close to the infinite bus, occurs as shown in Figure 5.1. The three-phase fault is initiated at t=1.5 s, with a duration of 4.5 cycles (75 ms). In order to demonstrate the influence of FRC-WTs including LQR control on SSR, two simulation runs were carried out with different series compensation percent. At each simulation, comparison was made between the results to show the contribution of LQR control on SSR.

At 20 % series compensation, the plots of the rotor speed deviation of the synchronous generator, DC voltage deviation as well as the torques between the masses of the turbine-generator model are given in Figure 5.10. The system with and without implementing LQR control is stable and returns to the stability state after the occurrence of fault, indicating that there are no torsional oscillations when series compensation percent is 20%. Moreover, the LQR control substantially enhances the damping of oscillations comparing with the system without it.

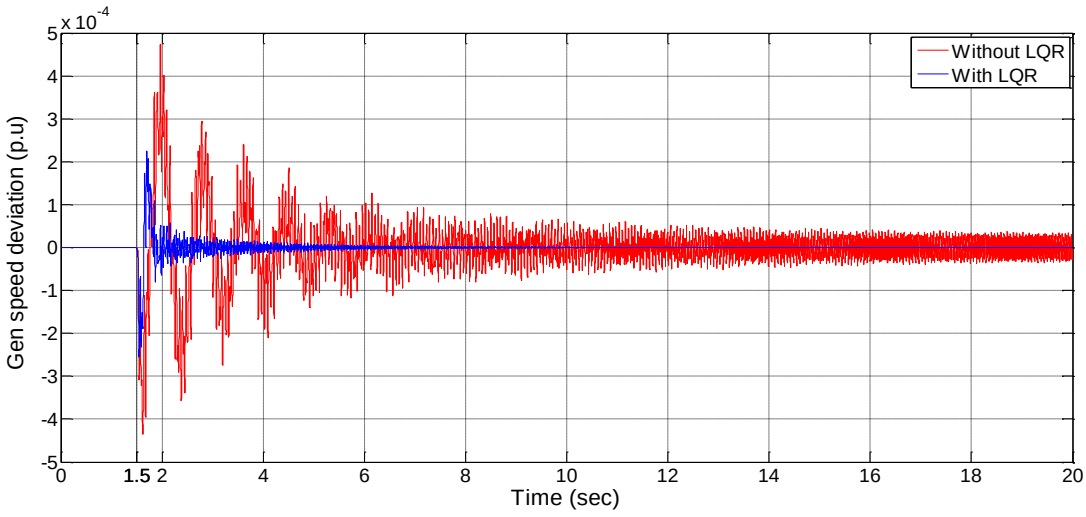

(a)

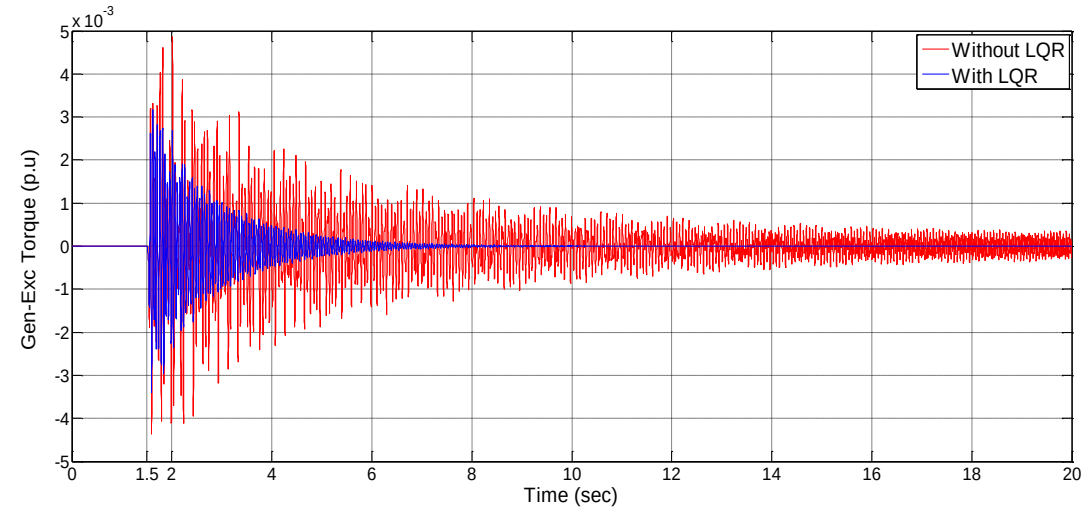

(b)

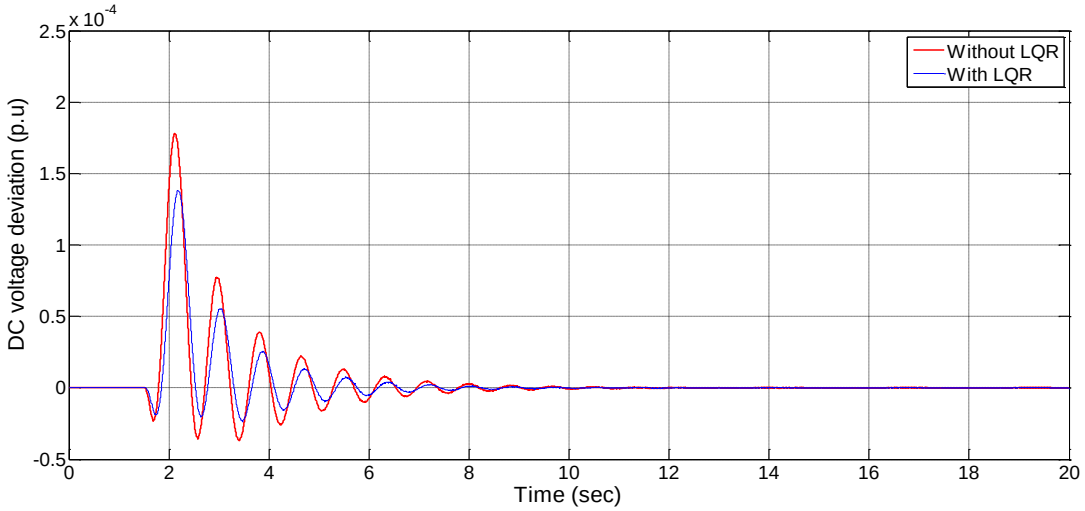

(c)

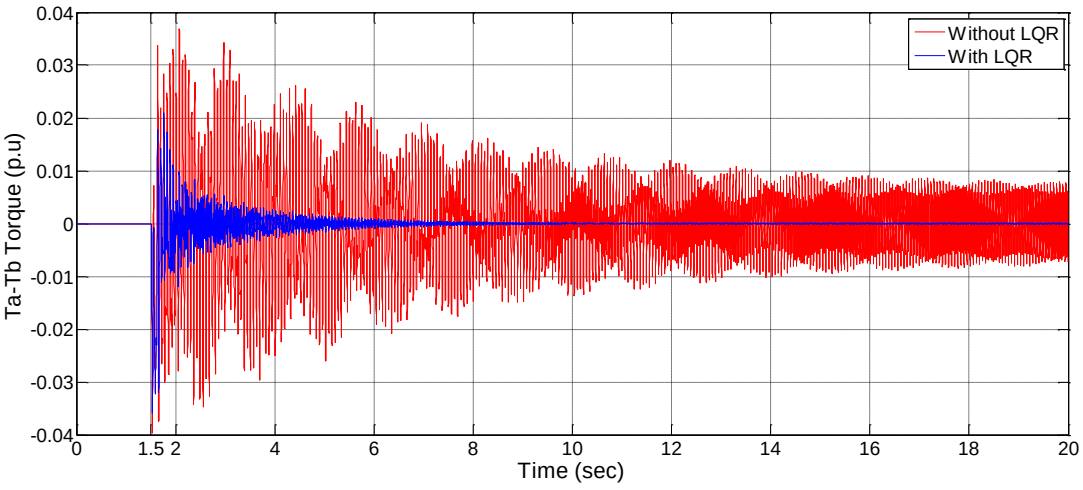

(d)

Fig. 5.10 Simulation results for Modified FBM with and without LQR at 20% series compensation: (a) Rotor speed deviation of the synchronous generator (rad/s), (b) DC voltage deviation, (c) Torque deviation between generator and exciter and (d) Torque deviation between intermediate pressure and low pressure turbines.

Figure 5.11 shows the effect of 50% series compensation on the system via making comparison between results without and with using LQR. It illustrates the instability produced by SSR for the system without implementing LQR to damp SSR. In this simulation results, the dominant frequency of torsional oscillation is 25.58 Hz, which represents the frequency of mode 4 for the Modified FBM without LQR. By applied LQR, the system returns to its stability state after exposing to the fault.

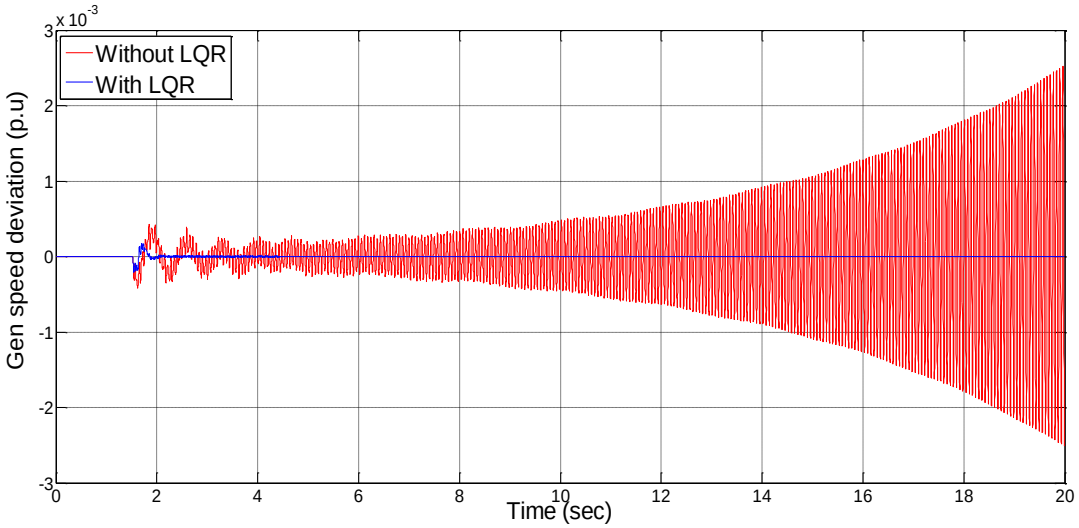

(a)

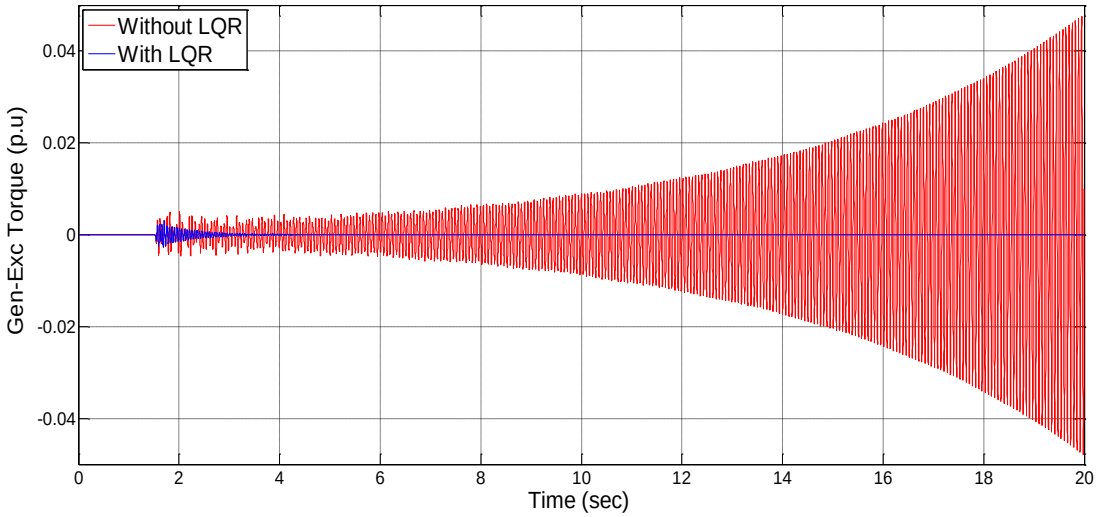

(b)

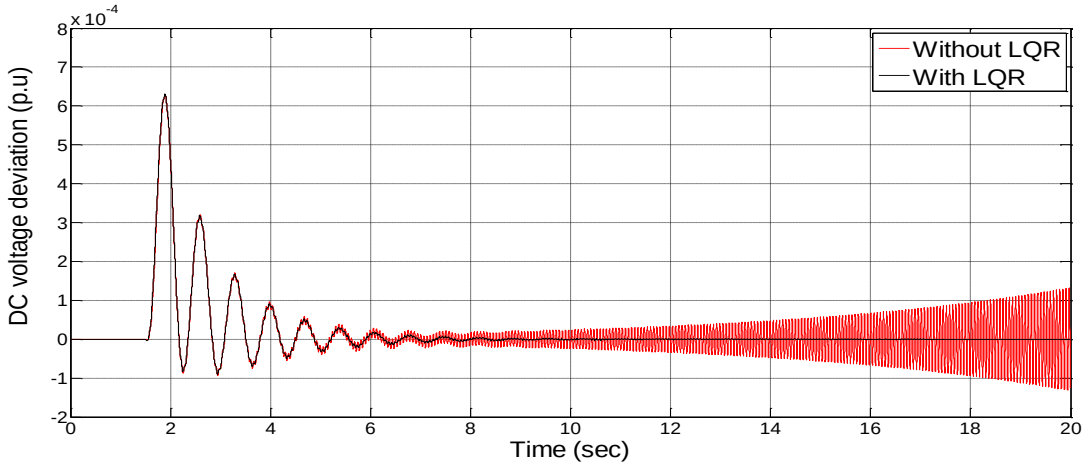

(c)

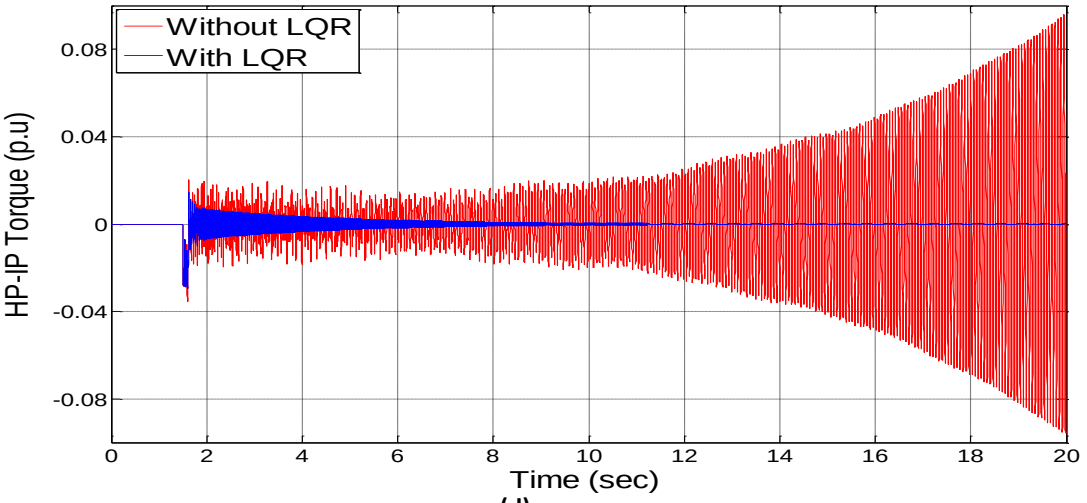

(d)

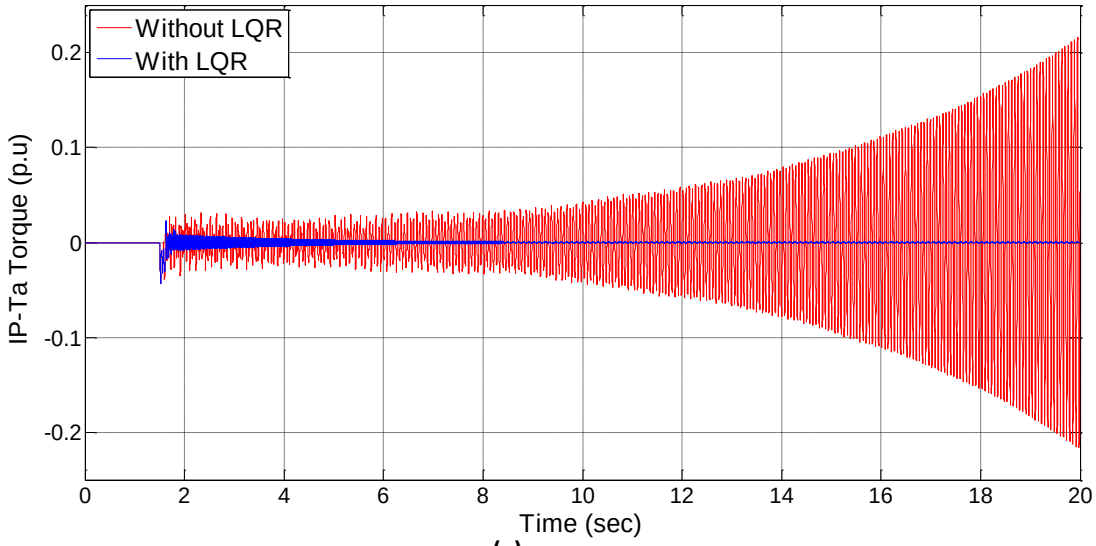

(e)

Fig. 5.11 Simulation results for Modified FBM with and without LQR at 50% series compensation: (a) Rotor speed deviation of the synchronous generator (rad/s), (b) Torque deviation between generator and exciter, (c) DC voltage deviation, (d) and (e) Torque deviation between masses of turbine generator.

5.7 Conclusion

The capability of the grid side converter of FRC-WTs to damp SSR has been investigated. A simulated model of the FRC-WTs connected to FBM was built using MATLAB package.

LQR was designed as auxiliary controller for the grid side converter of FRC-WTs to damp SSR in the steam turbine. Full order observer was designed to estimate the unmeasured state variables needed by LQR to feedback to the system after multiplying with the feedback gain matrix.

The extensive eigenvalue analysis and time domain simulation studies over wide varying levels of series compensation revealed that FRC-WT with LQR controller is able to mitigate the torsional oscillations in the steam turbine caused by SSR. LQR as an auxiliary SSR damping controller within the grid-side ofthe FRC-WTs is an effective controller to damp SSR within the steam turbine shafts if the system is fully visible.

Instead of installing FACT devices only for damping SSR, the grid side converter of the FRC-WTs using auxiliary SSR damping controller can be used.

Chapter 6

Design of Classical SSR Damping Controller For FRC-WTs Using Eigenvalue Sensitivities

6.1 Introduction

Regarding to Chapter ‘5’, the grid side converters of the Fully Rated Converter-Based Wind Turbines (FRC-WTs) can be used for designing a proper auxiliary control to damp SSR in the steam turbine. Choice a suitable control input signal is to damp SSR. The objective of this chapter is to design classical controller within the grid side converters of FRC-WTs for damping SSR within the steam turbine shafts. The applications of eigenvalue sensitivity technique are used to choose the most suitable control input signal to design the SSR damping controller for the grid side converter of FRC-WTs.

In this context, the eigenvalue sensitivity is used to design a supplementary controller for the grid side converter of FRC-WTs to damp the unstable torsional modes of the steam turbine. The most suitable feedback signal is determined by using eigenvalue sensitivities. The controller design comprises two steps: the design of the phase compensation network and the calculation of the controller gain. Digital simulations using a nonlinear system model are performed in order to demonstrate the effectiveness of the proposed supplementary controller to damp SSR.

6.2 System under Study

The single line diagram of the system under investigation is shown in Figure 6.1. FRC-WTs are simulated as a voltage source converter connected to the grid through transmission line (Line II). The primary objective of the grid side converter is to maintain the DC-link voltage and to allow the exchange of the reactive power between the converter and the grid as required by the application specifications [10]. This approach has been used previously in Chapter '5'. The parameters used in the FBM and can be found in [72] and in the Chapter '3' while the parameters used in FRC-WTs can be found in [10] and Chapter '5'.

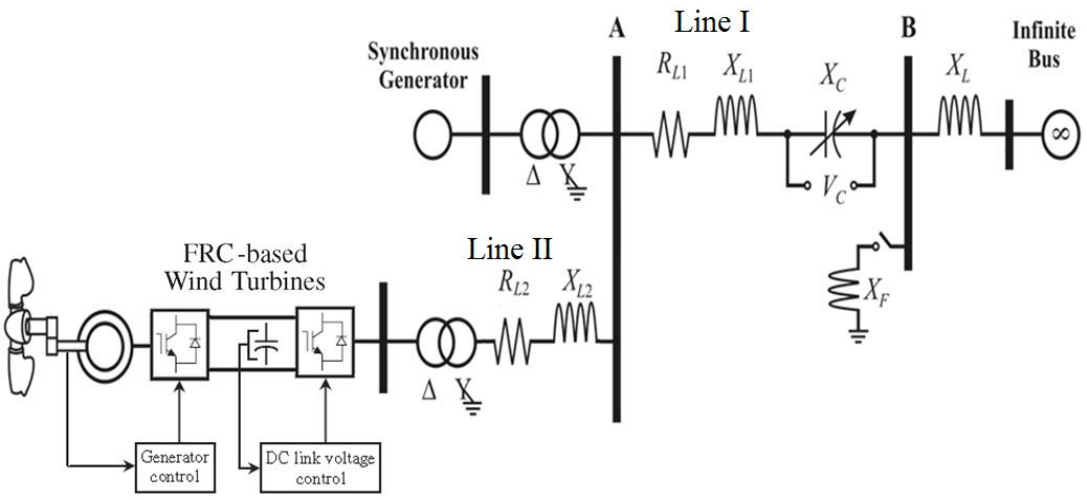

Fig. 6.1 Schematic diagram of Fully Rated Converter-Based Wind Turbines connected to IEEE First Benchmark Model.

6.2.1 Modelling of FRC-WTs

Figure 6.2 shows the control scheme of the grid-side converter of the FRC-WTs. It illustrates the main control of the grid-side converter of the FRC-WTs, where the controllers are designed in the d-q reference frame. The outer control loops provide DC voltage and the reactive power control [10-11].

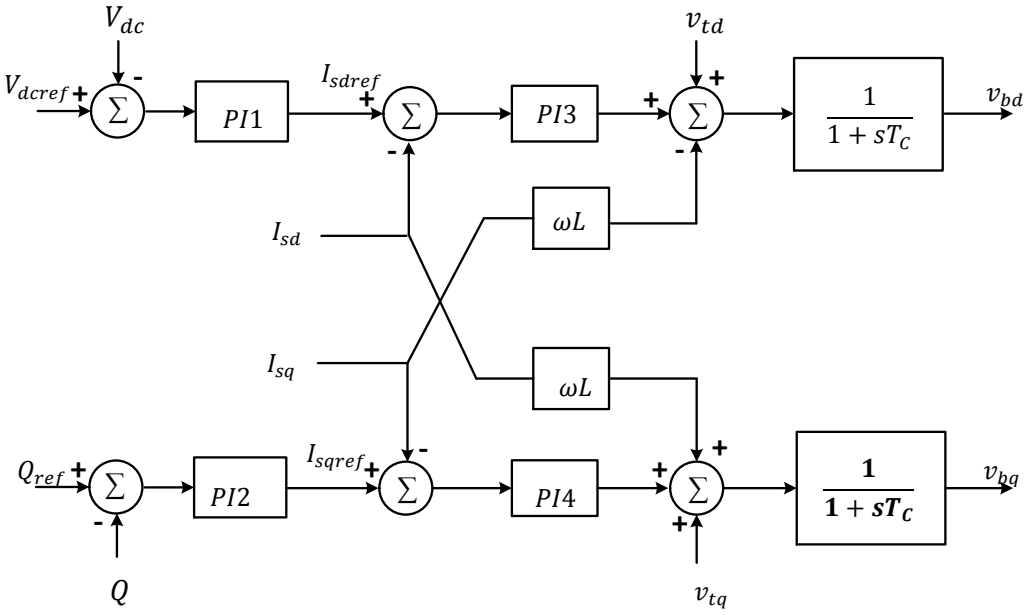

Fig. 6.2 The primary controller for the grid side converter of the FRC-WT

The output of these loops set the references values of the inner current controllers which are fed forward with the SSR damping Reference currents as shown in Figure 6.3. The output of the inner control loops (current loops) form the voltage references for the grid side converter of the FRC-WTs.

The DC voltage is maintained constant by controlling the d-axis current. PI controller PI1 is used to regulate the DC voltage. Therefore, it generates a reference current in the *d*-axis (I_{sdref}). PI controller PI2 is used to regulate the reactive power flow from the FRC-WTs. Therefore, it generates a reference current in the *q*-axis (I_{sqref}).

6.2.2 Hybrid controller for the grid side converter

Eigenvalue sensitivity method is used to select the most suitable feedback signal by using eigenvalue sensitivities for the supplementary control to damp SSR. The Synchronous generator speed deviation ($\Delta\omega$), *d-q* terminal current components of transmission line (line I) and the bus voltage (Δv_t) are selected as system output signals and *q* terminal current component of the transmission line (line II) as input signal (I_{SSR}). The output signal of the supplementary control is added to q current error signal as shown in Figure 6.3. Finally, the d-q components of the terminal voltage at bus "*A"* are added to find the required voltage components at the grid side converter terminals of the FRC-WTs.

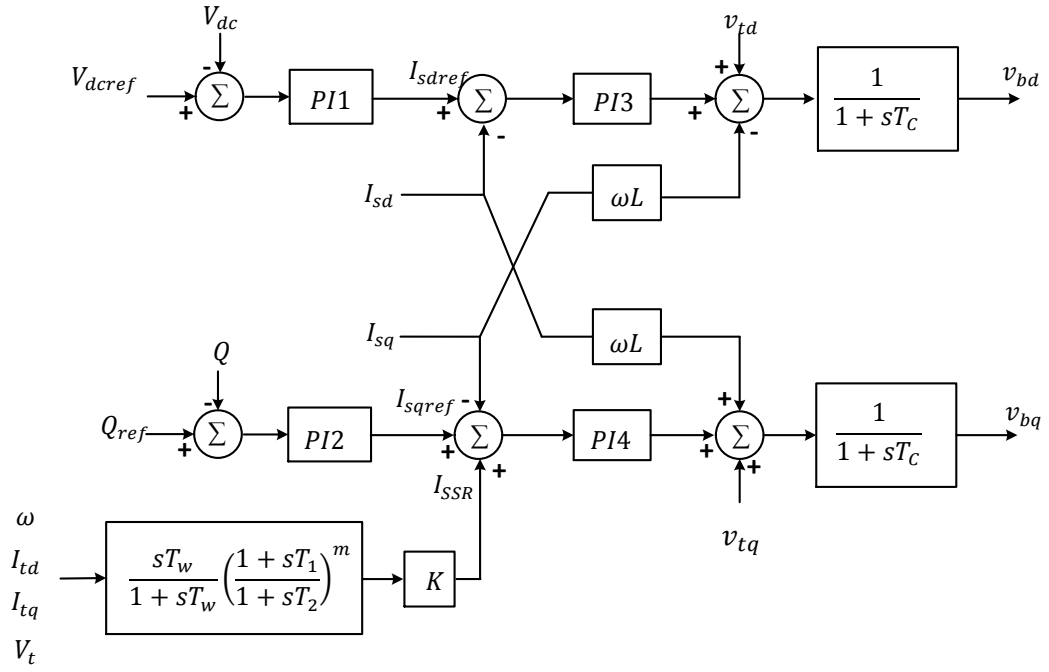

Fig. 6.3 Multiple functional of FRC-WT grid side converter

6.3 Eigenvalue Sensitivity

Eigenvalue sensitivity approach is used to choose the proper local feedback signal and design control to damp the torsional oscillations in the steam turbine shafts because of SSR based. The transfer function of the closed-loop system is expressed as shown in Figure 6.4 as [75]:

$$G(s) = \frac{y(s)}{u(s)}$$
$$= C(sI - A)^{-1}B \quad (6.1)$$

where A is the system matrix, B is the real input matrix and C is the output matrix.

Eigenvalue sensitivity investigates the effect of the input and the output signals on the system performance by calculating the residue associated with the oscillated mode, which is wanted to damp, the i^{th} input and the j^{th} output [81-82]. The transfer function of the i^{th} input and the j^{th} output is expressed in terms of the residue and the system eigenvalue λ_r as:

$$G_{ji}(s) = \sum_{k=1}^{n} \frac{\mathcal{R}_{kji}}{(s-\lambda_k)} = \sum_{k=1}^{n} \frac{C_j v_k \mathcal{W}_k B_i}{(s-\lambda_k)} \quad (6.2)$$

where $\mathcal{R}_{kji}$ is the residue associated with the k^{th} mode, the i^{th} input and the j^{th} output, w_k and v_k are the left and right eigenvectors associated with the eigenvalue λ_k.

$$\mathcal{R}_{kji} = C_j v_k \mathcal{W}_k B_i \quad (6.3)$$

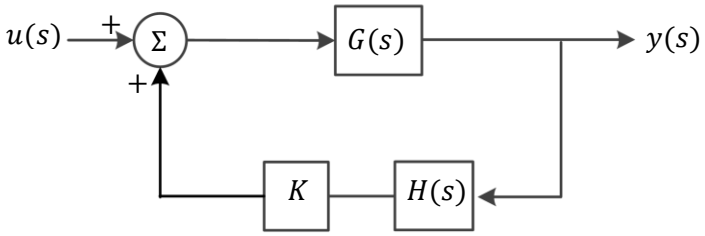

Fig. 6.4 Transfer function of the closed-loop system

In equation (6.3), the term $\mathcal{W}_k B_i$ represents the controllability of k^{th} mode from the i^{th} input ($contr_{ki}$) and $C_r v_j$ represents the observability of the j^{th} by the k^{th} mode ($observ_{kj}$). Therefore, $\mathcal{R}_{kji}$ is expressed in terms of mode controllability and mode observability as [83]:

$$\mathcal{R}_{kji} = contr_{ki} \times observ_{kj} \tag{6.4}$$

Therefore, $\mathcal{R}_{ijr}$ of the oscillation k$^{\text{th}}$ mode provides an idea of how the input u_i affects the oscillating mode λ_k and how visible is from the outputy_j. Therefore, the eigenvalue sensitivity through the residue definition measures the effectiveness of the damping controller and it has been successfully used to select the most suitable feedback signal for the auxiliary SSR damping control. Based on [83], the relation between the residue associated with the eigenvalue λ_k and the feedback transfer function $G(s, K)$ is expressed as:

$$\frac{\partial \lambda_k}{\partial K} = \mathcal{R}_{kji} \frac{\partial G(s,K)}{\partial K} \tag{6.5}$$

where, K is the constant gain of the SSR damping controller, s is Laplace operator and $G(s, K)$ is the feedback transfer function which is expressed regarding to Figure 6.4 as:

$$G(s, K) = KH(s) \tag{6.6}$$

$$\Delta\lambda_k = \lambda_{kdes} - \lambda_k \tag{6.7}$$

where λ_{kdes} represents the desired eigenvalue location for the eigenvalue λ_k.

By substituting equation (6.6) into equation (6.5) and assuming that the gain K is small so ΔK equals K as:

$$\Delta\lambda_k = \mathcal{R}_{kji} K H(s) \tag{6.8}$$

Therefore, the input and output signal to the SSR damping controller of the largest residue is the most suitable signal for the desired mode with the same constant gain value.

6.3.1 Select the control input signal

The system model shown in Figure 6.1 is simulated using MATLAB SIMULINK. By linearizing the system model around the operating condition, the stability of the system can be investigated by using the eigenvalue analysis. Figure 6.5 represents the real parts of the eigenvalues of the FRC-WTs connected to the IEEE First Benchmark Model (FBM) at various series compensation percentage. At 50 % series compensation, mode 3 is unstable as the frequency of subsynchronous mode, SUB mode, is close to the natural frequency of mode 3. The Eigenvalue sensitivity is used to calculate the residue for different control input signals and to design SSR damping controller at 50 % series compensation.

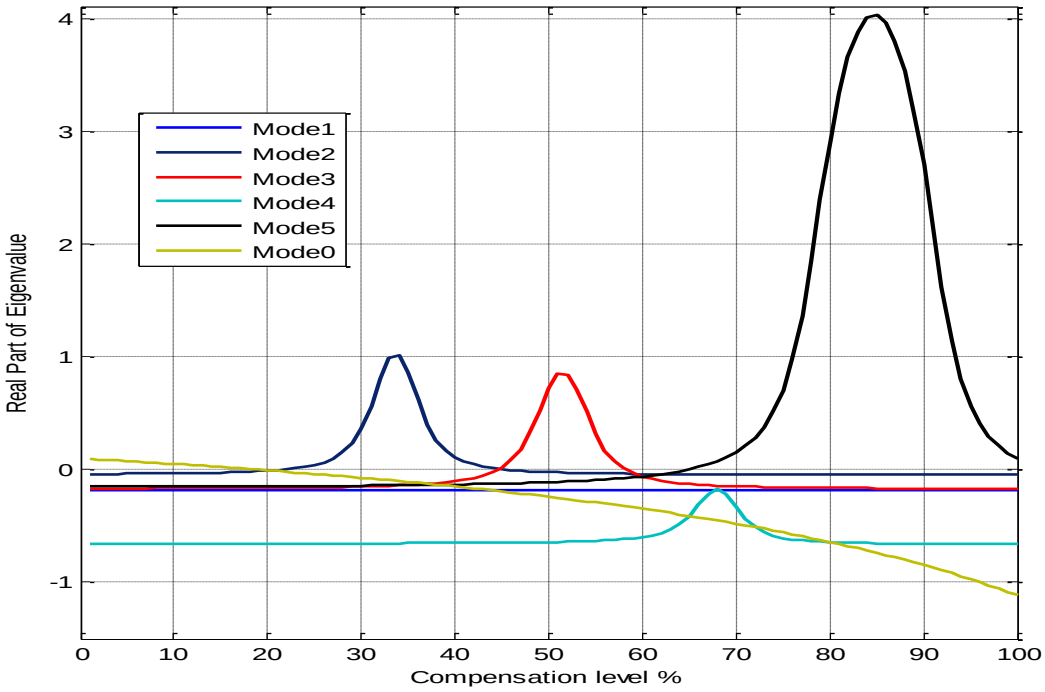

Fig. 6.5 The real part of SSR Mode eigenvalues as a function of the percentage compensation for the FBM featured with FRC-WTs

The input signal to SSR damping controller is chosen between synchronous generator speed deviation, The d-q components of the terminal current in line I and the bus voltage (Δv_t) based on the eigenvalue sensitivity. The magnitudes of the absolute values of the residues are listed in table 6.1. It can be observed that the maximum residue value corresponds to the synchronous generator speed deviation ($\Delta\omega$). This is expected as $\Delta\omega$ is the most suitable control input signal to damp the torsional oscillations within the multi-mass synchronous generator although it is not local signal for the grid side converter of the FRC-WTs to be used. The d-q components of the terminal current in line *I* have quite high residue compared with the bus voltage deviation. The d-q components of the terminal current are the most suitable control input signal as they are easier and more economical to use than synchronous generator speed deviation.

Table 6.1 The residues of the control input signals

	SSR damping control input signals			
	$\Delta\omega$	ΔI_{td}	ΔI_{tq}	ΔV_t
$\lvert\mathcal{R}_{kji}\rvert$	1.4056	1.2047	1.0714	0.0593

6.3.2 SSR Damping control design approach

Based on [3, 6], a lead/lag compensation controller is designed to shift the residue of the unstable mode to the negative axis so that the oscillatory mode will be damped. Figure 6.6 shows the concept of lead/lag compensation using the residue method. The structure of the phase shift compensator is given in [83-84] as:

$$H(s) = \frac{sT_w}{1+sT_w} \times \left(\frac{1+sT_1}{1+sT_2}\right)^m \tag{6.9}$$

where $H(s)$ is the transfer function of the washout function and the lead/lag blocks. The time constant of the washout function, T_w, is taken as 5-10 seconds [84].

The lead-lag parameters are determined as:

$$\Phi_{comp} = 180^\circ - \arg(\mathcal{R}_{kji}) \tag{6.10}$$

$$\alpha_C = \frac{T_1}{T_2} = \frac{1-\sin(\frac{\Phi_{comp}}{m})}{1+\sin(\frac{\Phi_{comp}}{m})} \tag{6.11}$$

$$T_1 = \frac{1}{\omega_i\sqrt{\alpha_C}} \ , \ T_2 = \alpha_C T_1 \tag{6.12}$$

where $\arg(R_{kji})$ is the phase angle of $\mathcal{R}_{kji}$, ω_i is the frequency of the unstable oscillation mode in rad/sec and m is the number of the compensation stages.

Regarding equation (6.8), the gain K is computed as:

$$K = \left|\frac{\lambda_{kdes}-\lambda_k}{\mathcal{R}_{kji}H(\lambda_k)}\right| \tag{6.13}$$

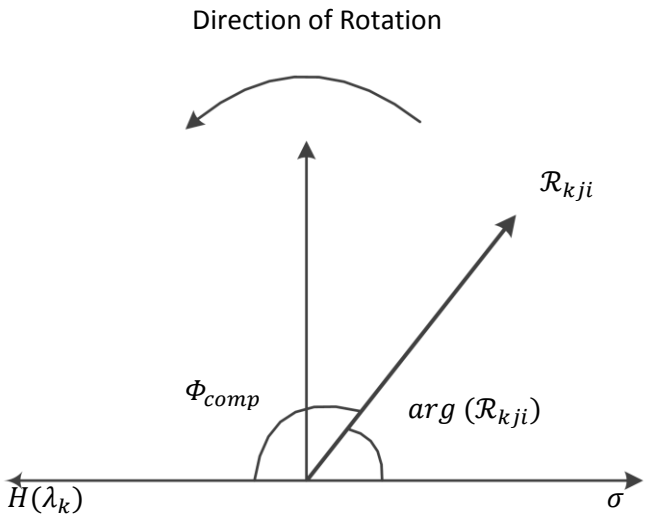

Fig. 6.6 The concept of the lead/lag compensation using residue method [84].

6.4 Simulation Results

The complete state space mode of the FRC-WTs connected to the FBM is used to investigate the effect of using the eigenvalue sensitivity on choosing the control input signal to damp SSR powerful applied to the FRC-WTs through the eigenvalue analysis and the time domain simulations. The eigenvalue analysis and time domain simulations were performed at 50% series compensation. The 175 FRC-WT units with a power rating of 350 MW are connected with the FBM.

6.4.1 Eigenvalue analysis

The linearized system was utilized to obtain the eigenvalues of the system at 50% series compensation. The eigenvalues of the torsional modes in addition to the electrical mode are given in table 6.2. The second column represents the eigenvalues of the system without any SSR damping controller, so the system is unstable as 3^{rd} mode is excited and become oscillating. The other three columns show comparisons between the eigenvalues of the system at different control input signals. According to the comparison between these three output control signals, the synchronous generator speed deviation is the most effective control input signal to damp SSR at the steam turbine. When d-q components of the terminal current are used as control input signals, the oscillatory torsional mode, 3^{th}, is more damped than that when terminal voltage deviation is used as a control input signal. The comparisons between the eigenvalues at different output signals verify the comparisons between the residues of these signals.

Table 6.2 Eigenvalues of modified FBM at different control input signals at 50% series compensation

Modes	Without control	$\Delta\omega$	ΔI_{td}	ΔI_{tq}	ΔV_t
M5	-0.1818±j 298.18	-0.1819±j 298.18	-0.18179 ±j 298.18	-0.18179±j 298.18	-0.18179±j298.18
M4	-0.0325±j 202.75	-0.5417 ±j202.75	-0.13794 ±j 202.74	-0.16441±j 202.76	-0.0911±j 202.76
M3	**+0.2461±j 159.99**	**-0.22367±j159.79**	**-0.14449 ±j 159.99**	**-0.1236±j 159.93**	**-0.1031 ±j 160.09**
M2	-0.624 ±j 127.1	-0.65672±j127.09	-0.62457 ±j 127.1	-0.63159±j 127.11	-0.62129±j127.09
M1	-0.0904 ±j 99.614	-0.4711±j 99.551	-0.16668 ±j 99.56	-0.18848±j 99.64	-0.0918±j99.488
M Zero	-0.2961 ±j 10.36	-0.65195±j10.316	-0.2734±j 10.365	-0.16419±j9.7334	-0.13597 ±j 9.771
Elec. M	-6.2827±j 152.65	-6.2583 ± j 152.9	-6.0592 ±j 151.53	-5.2418 ±j149.68	-2.3618 ±j149.81

6.4.2- Time domain simulation

To support the results of the eigenvalue analysis given in Table II, the time domain simulation based on the linearized differential equations of the system under study is performed. The SSR is triggered by making a small disturbance in the state of the system. In order to demonstrate the influence of the FRC-WTs including the supplementary control on SSR, three simulation runs were carried out at 50% series compensation percent. At each simulation, comparison is made between the results to show the contribution of the supplementary control on damping SSR.

Figure 6.7 shows the time domain simulations of the synchronous generator speed deviation, the terminal voltage of the synchronous generator as well as the torques between the masses of the turbine-generator model at 50 % series compensation without any SSR damping controller. The plots in Figure 6.7 show that the system is unstable because of SSR occurrence.

Figure 6.8 shows the effect of the using supplementary SSR damping controller within the grid side converter of FRC-WTs when the synchronous generator speed deviation is used as a control input signal. The system returns to the stability state after the occurrence of the disturbance. The results reveal that the auxiliary SSR damping controller has a good effective to damp SSR occurrence in the steam turbine shafts.

Figure 6.9 represents the effectiveness of using the d-component of the terminal current as a control input signal for the supplementary control to damp SSR. The auxiliary controller is more effective at damping SSR when the synchronous generator speed deviation is used as opposed to using the d-component of the terminal current as the control input signal.

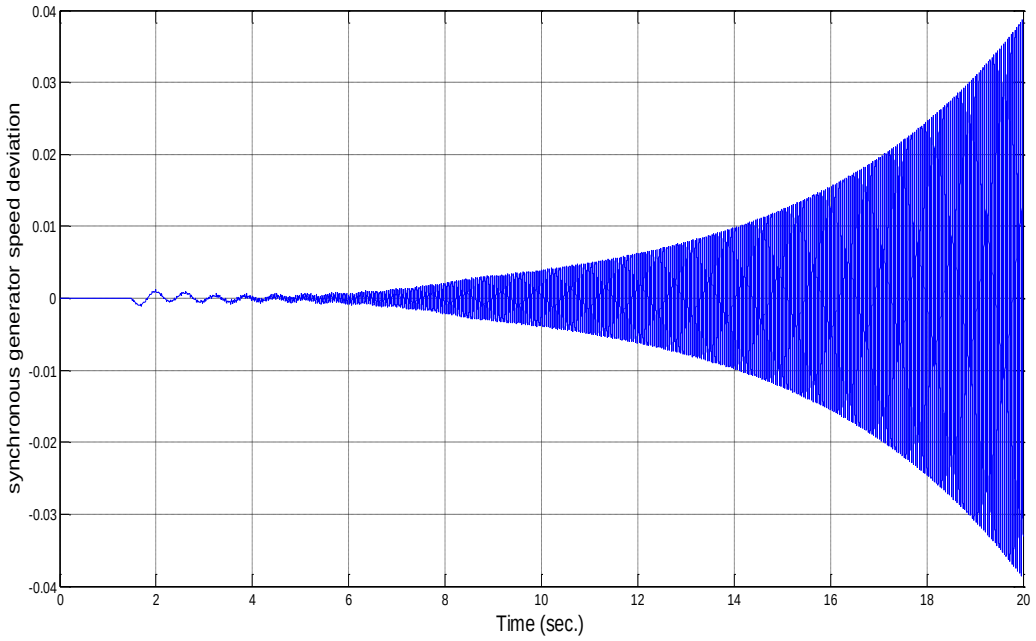
synchronous generator speed deviation
Time (sec.)
0.04
0.03
0.02
0.01
0
-0.01
-0.02
-0.03
-0.04
0
2
4
6
8
10
12
14
16
18
20

(a)

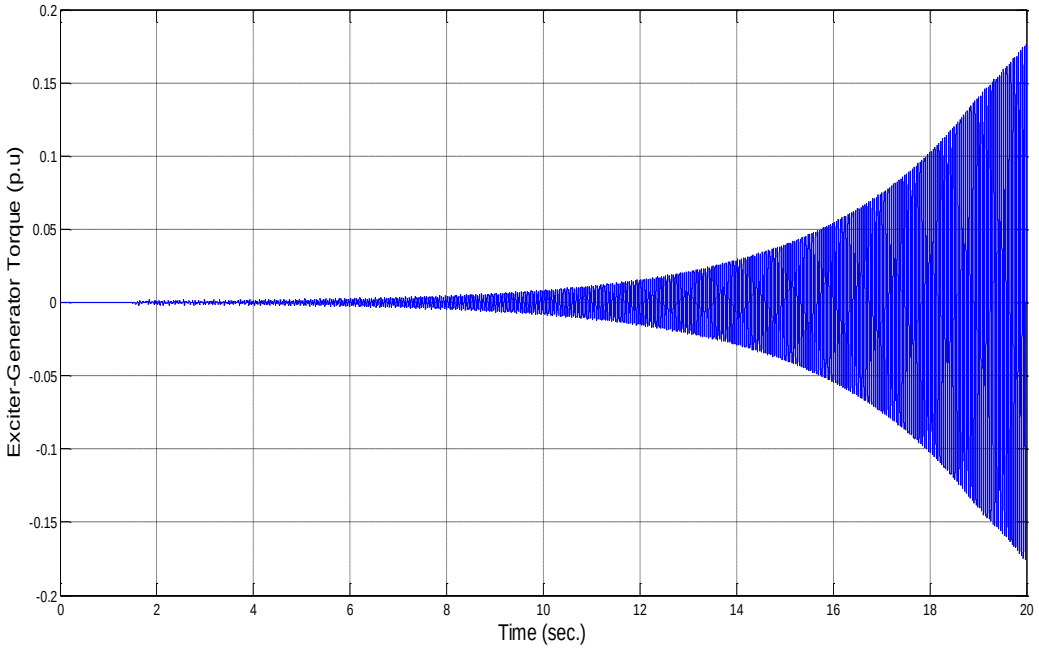
Exciter-Generator Torque (p.u)
Time (sec.)
0.2
0.15
0.1
0.05
0
-0.05
-0.1
-0.15
-0.2
0
2
4
6
8
10
12
14
16
18
20

(b)

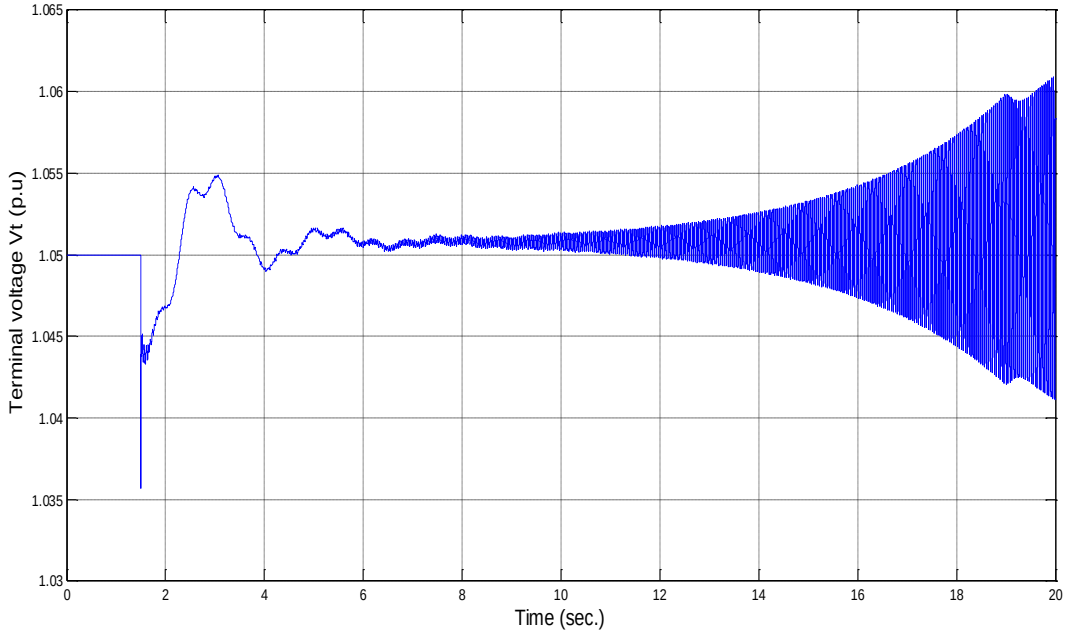

(c)

Fig. 6.7 Simulation results for Modified FBM without any SSR damping controller at 50% series compensation: (a) Synchronous generator speed deviation (p.u), (b) Torque between generator and exciter, and (c) synchronous generator terminal voltage (p.u).

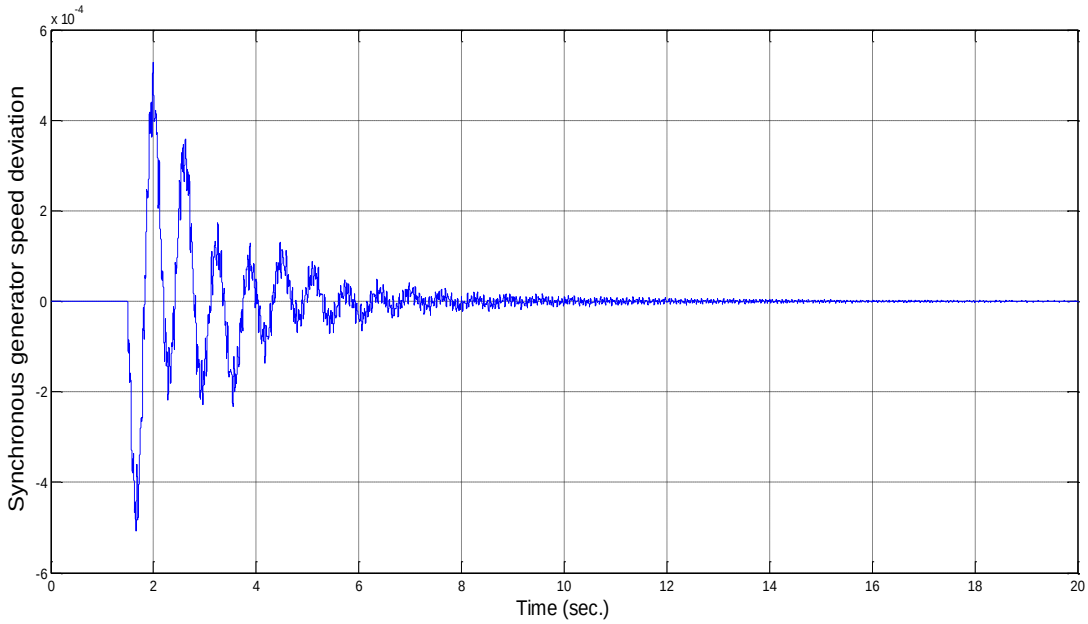

(a)

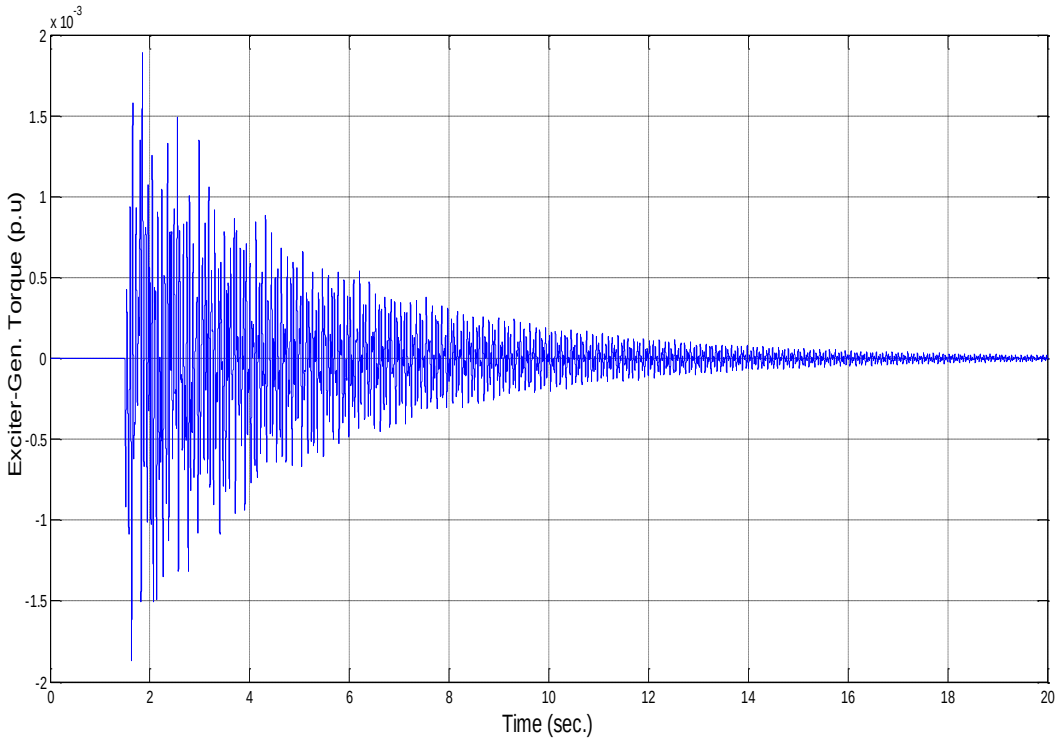

(b)

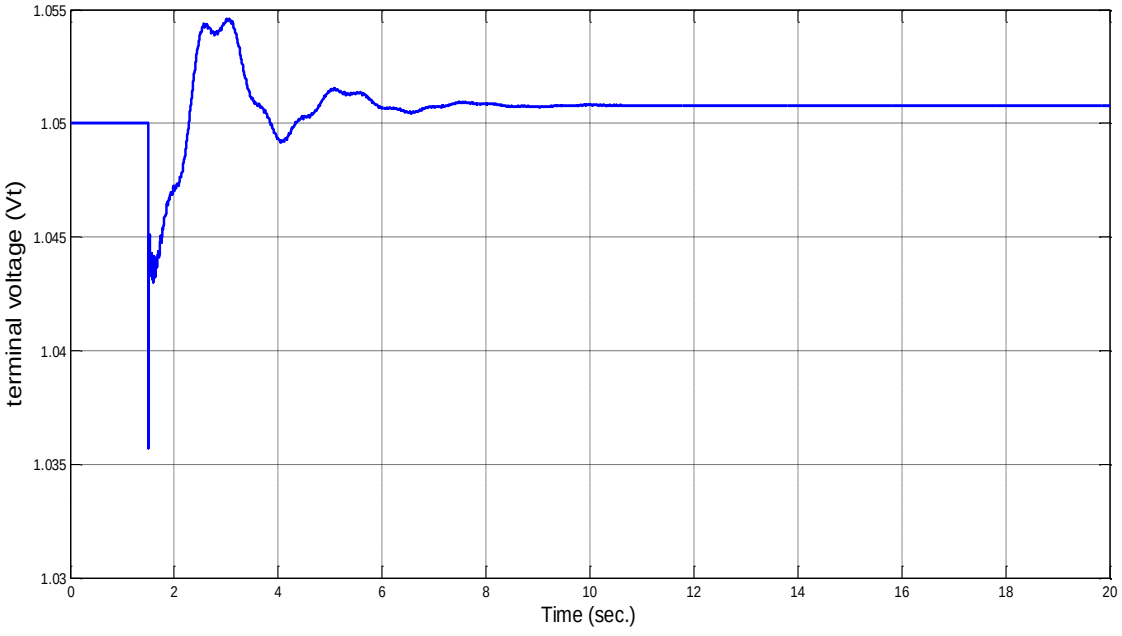

(c)

Fig.6.8 Simulation results for Modified FBM with SSR damping controller at 50% series compensation: (a) Synchronous generator speed deviation (p.u) (b) Torque between generator and exciter, (c) Synchronous generator terminal voltage (p.u).

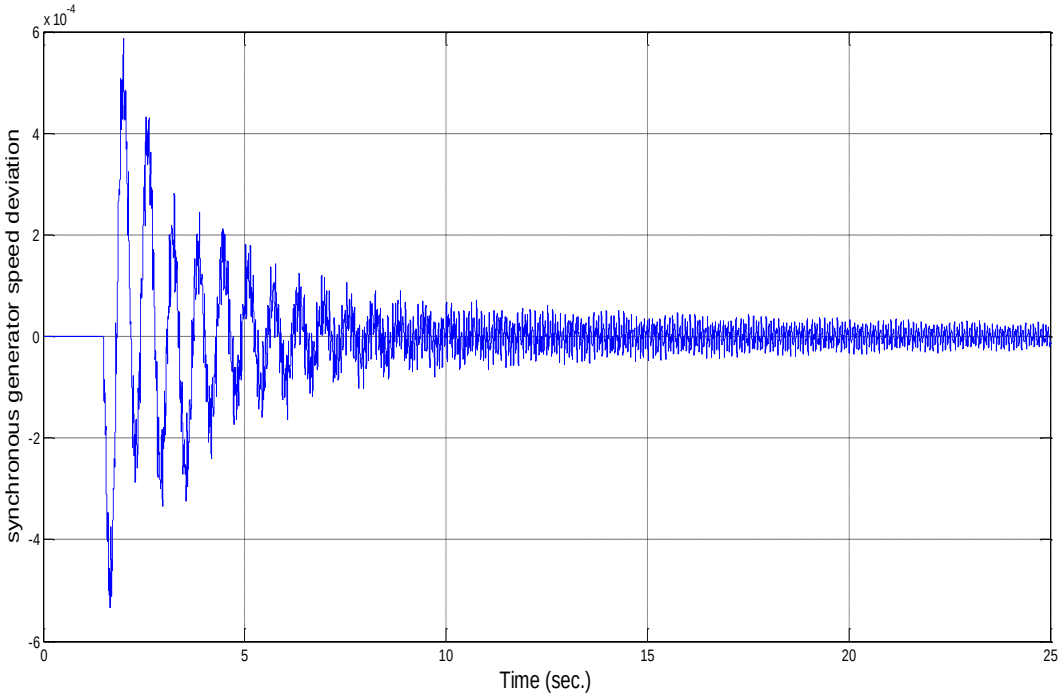
x 10^-4
6
4
2
0
-2
-4
-6
synchronous generator speed deviation
0
5
10
15
20
25
Time (sec.)

(a)

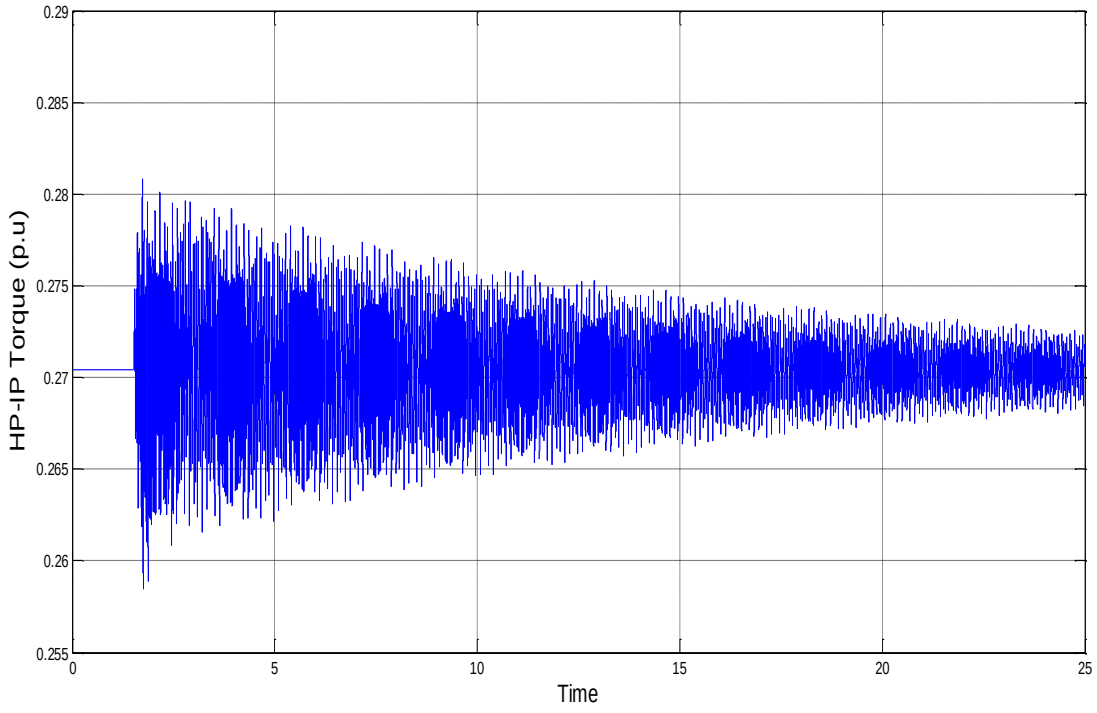
0.29
0.285
0.28
0.275
0.27
0.265
0.26
0.255
HP-IP Torque (p.u)
0
5
10
15
20
25
Time

(b)

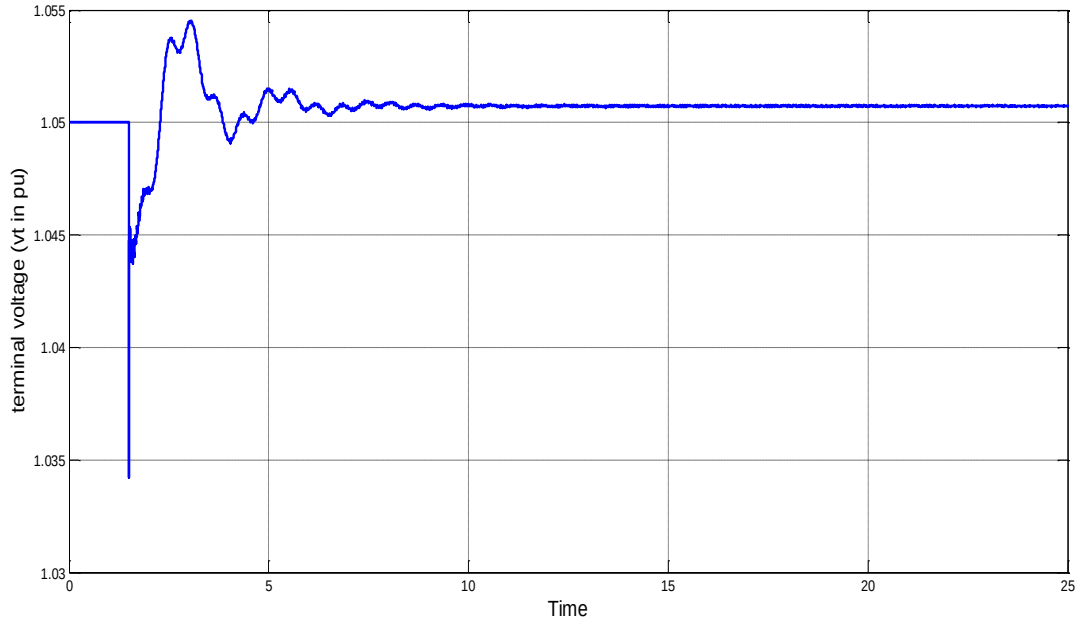

(c)

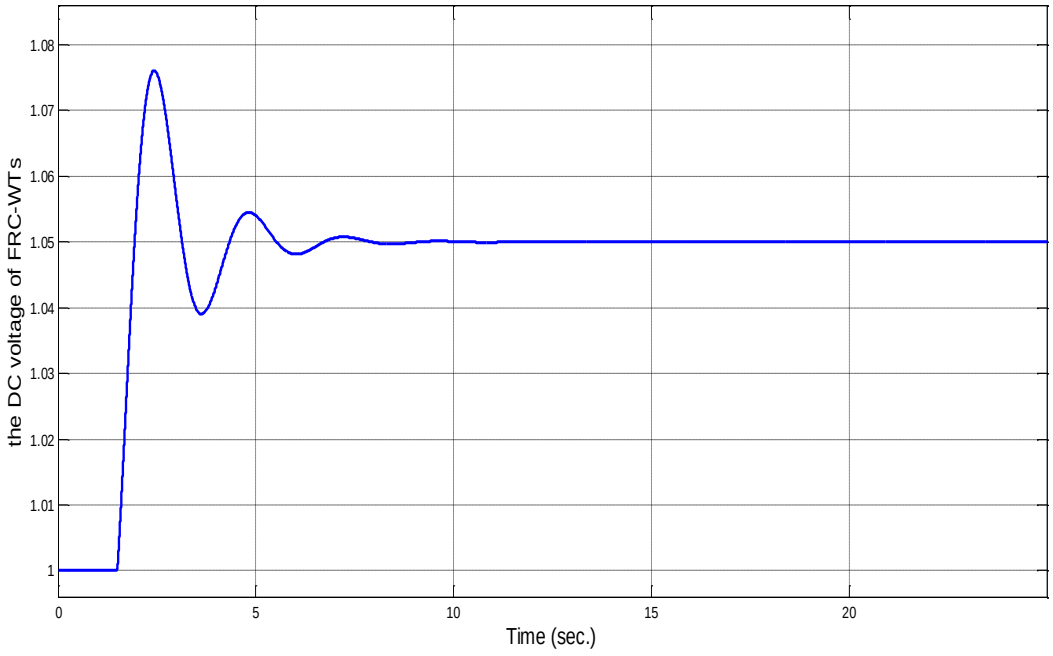

(d)

Fig. 6.9 Simulation results for Modified FBM with SSR damping controller at 50% series compensation: (a) Synchronous generator speed deviation, (b) Torque between HP-IP, and (c) synchronous generator terminal voltage (p.u.) and (d) the Dc Voltage of FRC-WTs (p.u.).

6.5 Conclusion

This chapter has proved the efficiency of classical the damping controller of Fully Rated Converter-Based Wind Turbines to damp SSR occurrence at steam turbine shafts. Eigenvalue sensitivities have been used to choose the most suitable control input signal for the auxiliary control and to design the supplementary controller to damp SSR. The auxiliary controller injects an additional signal into the q-axis component of the FRC-WTs current to regulate the output power of FRC-WTs to damp SSR.

The eigenvalue analysis and time domain simulation for different control input signals revealed that synchronous generator speed deviation is the most suitable control input signal to mitigate the torsional oscillations in the steam turbine caused by SSR and after those d-q components of the terminal current. These results emphasize the results of eigenvalue sensitivities to choose the most suitable output control signal for damping SSR.

Chapter 7-

Conclusions and Further Work

7.1 Conclusions

The proposed reinforcements for the transmission networks for many countries use series compensation to increase the power transfer capability. The effect of the wind farms on the occurrence of Sub-Synchronous Resonance (SSR) in the steam turbine shafts was simulated and investigated to resemble the operation of the mainland networks for many countries such as the UK in 2020.

7.1.1 The effect of FSIG-WTs on SSR

The influence of Fixed Speed Induction Generator-Based Wind Turbines (FSIG-WTs) on SSR in a series compensated transmission line was investigated at a wide range of series compensation levels and different power ratings of FSIG-WTs. Eigenvalue analysis and time domain simulations were carried out using MATLAB and PSCAD.

The results reveal that FSIG-WTs have an adverse effect on SSR occurring at steam turbine shafts. That means connecting FSIG-WTs to the FBM increases the range of series compensation levels at which SSR can occur.

The frequency of the subsynchronous currents over the series compensated transmission line affects FSIG-WTs. Therefore, FSIG-WTs have two slips; subsynchronous slip and the rated slip. The subsynchronous slip changes the

equivalent impedance of the FSIG-WTs which, in turn, causes a reduction of the natural frequency of the series compensated transmission line by changing the value of the equivalent impedance causing it.

7.1.2 Damping SSR using FRC-WTs

The possibility of utilizing the grid side converters of the FRC-WTs to damp SSR was investigated. This investigation was presented by designing an auxiliary SSR damping control within the grid side converters of the FRC-WTs connected to IEEE First Benchmark Model (FBM).

The primary control scheme for the grid side converter of FRC-WTs was designed to control the active and reactive power. An SSR damping controller was designed as an auxiliary controller by using two different types of controller. Eigenvalue analysis and time domain simulations have been carried out using MATLAB to show the capability of FRC-WTs to damp SSR in steam turbine shafts using an auxiliary controller.

a- An optimal controller based on Linear Quadratic Regulator (LQR) was designed as an auxiliary controller within the grid side converter of the FRC-WTs. A full order observer was designed to estimate the unmeasured state variables to enable LQR to feedback all the state variables. The extensive eigenvalue analysis and time domain simulation over wide varying levels of series compensation revealed that the FRC-WT with a LQR controller was able to mitigate the SSR in the steam turbine shafts if the system is fully visible.

b- A classical controller based on the Lead/lag controller to damp SSR in the steam turbine shafts. Eigenvalue sensitivity was studied to choose the most suitable feedback signal and to design an SSR damping controller for the grid side converter of a FRC-WT. The synchronous generator speed deviation was the most suitable control input signal for the Lead/lag

controller to damp SSR in the steam turbine shafts. Eigenvalue results and time domain simulations show that the auxiliary lead/lag controller was able to damp SSR at steam turbine shafts at 50% series compensation.

7.1.3 Contribution of the thesis

The following objectives have been set and achieved:

- To investigate and study FBM using mathematical analysis. FBM was modelled by using MATLAB and PSCAD. The eigenvalue analysis was used to validate the results of the modelled FBM. Furthermore, FBM was modified by integrating different types of wind farms, FSIG-WTs and FRC-WTs, with it.

- To evaluate the effect of the FSIG-WTs on the SSR at steam turbine because of fixed series compensation.

- To design an optimal controller as an auxiliary controller within the grid side converters of FRC-WTs to damp SSR in the steam turbine shafts. The results revealed that if the system is fully visible, LQR controller is an effective controller to damp SSR over a wide range of series compensation.

- To design classical controller as an auxiliary controller within the grid side converters of FRC-WTs to damp SSR in the steam turbine shafts. Synchronous generator speed deviation was the most suitable feedback control signal to damp SSR by using eigenvalue sensitivity method. Lead/lag compensation was designed as an auxiliary controller to damp SSR occurrence at the steam turbine shafts.

7.1.4 Achievements of research

The outcomes of this research were written up in a journal and two conference papers as:

(4) **A. Ewais,** C. Ugalde-Loo, J. Liang, J. Ekanayake, N. Jenkins, "The Influence of the Fixed Speed Induction Generator-Based Wind Turbines on Subsynchronous Resonance," University Power Engineering Conference (*UPEC 2011*), Soest, Germany, Sept. 2011.

(5) **A. Ewais,** C. J. Liang, J. Ekanayake, N. Jenkins, "Influence of the Fully Rated Converter-Based Wind Turbines on SSR," *IEEE PES* Innovative Smart Grid Technologies (ISGT-ASIA 2012), Tianjin, China, May 21-24, 2012.

(6) **A. Ewais,** J. Liang, N. Jenkins, "The Impact of the Fixed Speed Induction Generator-Based Wind Turbines on Power system stability," will be submitted to IET journal.

7.2 Further Work

From this thesis, further avenues of research are available as:

- To investigate the possibility of using Doubly Fed Induction Generator-Based Wind Turbines (DFIG-WTs) to damp SSR in the steam turbine shafts through designing an auxiliary controller.

- To design and build a laboratory based experiment to demonstrate an auxiliary controller within the grid side converters of FRC-WTs and DFIG-WTs to damp SSR occurrence in the steam turbine shafts.

- To implement the two types of the SSR auxiliary damping controller within the FRC-WTs in the G. B. Generic Network to damp SSR caused by installing fixed series compensations in it.

References

[1] United Nations Framework Convention on Climate Change, “Kyoto Protocol to the United Nations Framework Convention on Climate Change,” 1998.

[2] European Commission, “Communication from the commission: Energy efficiency: delivering the 20% target, “, November 2008.

[3] U. S. Energy Information Administration, “International Energy Outlook 2013,” 2013 (online). Available: http://www.eia.gov/forecasts/ieo/.

[4] International Energy Agency, “World Energy Outlook: Executive Summary,” OECD Publishing, April 2014.

[5] Committee on Climate Change, “The Renewable Energy Review Executive Summary,” 2010 (online). Available: http://hmccc.s3.amazonaws.com/Renewables%20Review/Executive%20summary.pdf

[6] B. Fox, D. Flynn, L. Bryans, N. Jenkins, D. Milborrow, M. O'Malley, R. Watson, and O. Anaya-Lara. Wind Power Integration: Connection and System Operational Aspects. The Institution of Engineering and Technology, 2007.

[7] R. Wiser and M. Bolinger, “Wind Technologies Market Report,” Technical Report, U.S. Department of Energy, 2012.

[8] S. Sawyer and K. Rave, “Global Wind Report - Annual Market Update 2012,” Technical Report, Global Wind Energy Council (GWEC), 2013.

[9] J. Wilkes and J. Moccia, “Wind in Power: 2012 European Statistics,” Technical Report, EWEA, 2013.

[10] O. Anaya-Lara, N. Jenkins, J. Ekanayake, P. Cartwright, and M. Hughes, Wind Energy Generation: Modelling and Control. John Wiley and Sons, 2009.

[11] G. Ramtharan, Control of Variable Speed Wind Turbine Generators, PhD Thesis, University of Manchester, UK, 2008.

[12] T. Ackerman, Wind Power in Power Systems, Book, John Wiley and Sons, Chichester, UK. Wiley, 2005.

[13] H. Romanowitz, “California Tehachapi Transmission Line,” in Proc. T&D *IEEE/PES*, pp. 1-2, Apr. 2008.

[14] E. W. E. A. European Wind Energy Association, “Power Europe: Wind Energy and the Electricity Grid,” Nov. 2010.

[15] C. Wessels, N. Hoffmann, M. Molinas, and F. Wilhlem Fuchs, “STATCOM Control at Wind Farms with Fixed-Speed Induction Generators under Asymmetrical Grid Faults,” *IEEE Trans*. *Ind. Electron*., vol. 60, no. 7, pp.2864-2873, July 2013.

[16] S. G. Helbing and G. G. Kiuady, “Investigations of an Advanced Form of Series Compensation,” *IEEE Trans. on Power Delivery*, vol. 9, no. 2, 1994.

[17] R. Grünbaum, P. Halvarsson, P. Jones, A. B. B. Ab, and S.- Vasteras, “Series Compensation for Extended Utilization of Power Transmission Systems,” in *ACDC 2010*, 2010.

[18] R. Grünbaum, P. Halvarsson, and P. Jones, “Series Compensation for Increased Power Transmission Capacity,” in Power Electronics, Machines and Drives (PEMD 2010), 2010.

[19] Siemens, “Discover the World of FACTS Technology,” 2011, (online). Available:http://www.energy.siemens.com/ru/pool/hq/power-transmission/FACTS/FACTS_Technology_.pdf

[20] ABB, “Series Compensation Boosting Transmission Capacity,” 2010, (online). Available:

http://www02.abb.com/global/gad/gad02181.nsf/0/fba60f0238fcfd2ec1257a620031049f/$file/Series+Compensation+-+Boosting+transmission+capacity.pdf

[21] I. K. Kiran and A. J Laxmi, “Shunt Versus Series Compensation in the Improvement of Power system Performance” *International Journal of Applied Engineering Research, DIndigul*, vol. 2, no. 1, 2011.

[22] SIEMENS, “Series Compensation (SC),” 2014 (online). Available: http://www.energy.siemens.com/hq/en/power-transmission/facts/series-compensation/, 13/06/2014.

[23] ABB, “Fixed Series Compensation,” 2014 (online). Available: http://new.abb.com/facts/fixed-series-compensation, 13/06/2014.

[24] M. Matele, “Enhancing of Transmission Capability of Power Corridors by Means of Series Compensation”, PowerTech Conference, Mumbai, India, October 1999.

[25] Electricity Networks Strategy Group, “Our Electricity Transmission Network: a Vision for 2020,” 2012(online). Available: https://www.gov.uk/government/uploads/system/uploads/attachment_data/file/48274/4263-ensgFull.pdf

[26] P. Kundur, *Power System Stability and Control*. McGraw-Hill, 1994.

[27] P. M. Anderson, B. L. Agrawal, and J. E. Van Ness, *Subsynchronous Resonance in power systems*. IEEE Press, 1989.

[28] K. R. Padiyar, Analysis Of Subsynchronous Resonance in Power Systems. Kluwer, 1999.

[29] D. J. McDonald, J. Urbabek and B. L. Damsky, “Modeling and Testing Of a Thyristor for Thyristor Controlled Series Compensation (TCSC)”, IEEE Trans. Power Delivery, PAS vol. 9, No. 1, pp 352-359, Jan. 1994.

[30] L. Kirschner, J. Bohn and K Sadek, “Thristor Protected Series Capacitor: Design Aspects”, AC-DC Power Transmission, 2001. Seventh International Conference on (Conf. Publ. No. 485), pp 138-144, Mumbai, India, October 1999.

[31] J. G. Slootweg, Wind Power: Modelling and Impact on Power System Dynamics, PhD Thesis, Delft University of Technology, 2003.

[32] A. K. Moharana, Subsynchronous Resonance in Wind Farm, Ph.D. Thesis, University of Western Ontario, London, Ontario, Canada. 2012.

[33] M. Bongiorno, A. Petersson and E. Agneholm, " The Impact of Wind Farms on Subsynchronous Resonance in Power Systems", Elforsk rapport 11:29, April 2011. available (online):

http://www.elforsk.se/Global/Vindforsk/Rapporter%20VFIII/11_29_report.pdf, June 2014.

[34] IEEE Subsynchronous Resonance Working Group, "Terms, Definitions and Symbols for Subsynchronous Oscillations," *IEEE Trans. on Power Apparatus and Systems*, vol. PAS-104, no. 6, pp. 1326–1334, 1985.

[35] IEEE Committee Report, "Proposed Terms and Definitions for Subsynchronous Oscillations," *IEEE Trans. on Power Apparatus and Systems,* vol. PAS-99, no. 2, pp. 506-511, Mar.1980.

[36] G. Tang, Damping Subsynchronous Resonance Oscillations Using a VSC HVDC Back-To-Back System, MSC Thesis, University of Saskatchewan, Canada, 2006.

[37] S. C. Sun, S. Salowe, E. R. Taylor, and C. R. Mummert, "A Subsynchronous Oscillations Relay-Type SSO," *IEEE Trans. on Power Apparatus and Systems, PAS-100,* pp. 3580-3589, July 1981.

[38] C. E. Bowler, J. A. Demcko, L. Menkoft, W. C. Kotheimer, and D. Cordray, "The Navajo SMF Type Subsynchronous Resonance Relay," *IEEE Trans. on Power Apparatus and Systems, PAS-97(5),* pp. 1489-1495, Sept. 1978.

[39] L. L. Grigsby, The Electric power Engineering Handbook: Power system Stability and Control. Third Edition, CRC Press, 20012.

[40] R. G. Farmer, L. A. Schwalb, and E. Katz, "Navajo Project Report on the Subsynchronous Analysis and Solution," *IEEE Trans. on Power Apparatus and Systems, PAS-96(4),* pp. 1226-1232, July/August 1978.

[41] N. G. Hingorani, and L. Gyugyi, "Understanding FACTS: Concepts and Technology of Flexible AC Transmission System, IEEE Press, 1999.

[42] D. Rai, S. O. Faried, G. Ramakrishna, and A. Edris, “Hybrid Series Compensation Scheme Capable of Damping Subsynchronous Resonance,” *IET Generation, Transmission & Distribution*, vol. 4 pp. 456-466, 2001

[43] L. A. S. Ilotto, A. Bianco, W. F. Long, and A. A. Edris, “Impact of TCSC Control Methodologies on Subsynchronous Oscillations,” *IEEE Trans. on Power Delivery,* PAS-18(1), pp. 243-252, 2003.

[44] K. V. Patil, J. Senthi, J. Jiang, and R.M. Mathur, “Application of STATCOM for Damping Torsional Oscillations in Series Compensated AC Systems,” *IEEE Trans. Energy Convers*. PAS 13(3), pp. 237–243, 1998

[45] K. R. Padiyar, and N. Prabhu, “Design and Performance Evaluation of Subsynchronous Damping Controller with STATCOM,” *IEEE Trans. on Power Delivery,* PAS-21(3), pp. 1398-1405, 2006.

[46] A. Salemnia, M. Khederzadeh, and A. Ghorbani, “Mitigation of Subsynchronous Oscillations by 48-Pulse VSC STATCOM Using Remote Signal,” *IEEE PowerTech. Conf.*, vol. 1, pp. 1-7, 2009.

[47] F. A. R. A. Owder, and B. T. Ooi, “Series Compensation of Radial Power System yy a Combination of SSSC and Dielectric Capacitors,” *IEEE Trans. on Power Delivery*, PAS-20(1), pp. 458-465, 2005.

[48] R. K. Varma, and S. Auddy, “Mitigation of Subsynchronous Resonance Using PMU-Acquired Remote Generator Speed,” *IEEE Power India Conf.,* pp. 1-8, 2006.

[49] S. Iee, C. C. Liu, “Damping Torsional Oscillations Using a SIMO Static Var Controller,” *IEE Proc. Gener., Transm. Distrib.,* vol. (6), pp. 462-468, 1993

[50] M. Ongiorno, L. Angquist, and J. Svensson, “A Novel Control Strategy for Subsynchronous Resonance Mitigation Using SSSC,” *IEEE Trans. on Power Delivery,* PAS-23(2), pp. 1033-1041, 2005.

[51] R. M. Hamouda, M. R. Iravani,and R. Hackam, “Torsional Oscillations of Series Capacitor Compensated AC/DC Systems,” *IEEE Trans. on Power Systems,* PAS-4(3), pp. 889-896, 1989.

[52] Y. J. Hafiner, H. Duchen, K. Linden, and M. Hyttinen, "Improvement of Subsynchronous Torsional Damping Using VSC HVDC," *Power System Technology PowerCon,* vol. (2), pp.998 – 1003, 2002.

[53] L. Livermore, Integration of Offshore Wind Farms Through High Voltage Direct Current Networks, PhD Thesis, Cardiff University, UK, 2013.

[54] P. Pourbeik, R.J. Koessler, D.L. Dickmander and W. Wong, "Integration of Large Wind Farms into Utility Grids (Part 2 - Performance Issues)", in *Proc. 2003 IEEE PES GM*, pp. 1520-1525.

[55] M. Henderson, D. Bertagnolli and D. Ramey, "Planning HVDC and FACTS in New England," in *Proc. 2009 IEEE/PES PSCE*. pp. 1-3.

[56] "Ercot CREZ Transmission Optimization Study," [Online]. Available:

www.ercot.com.http://transmission.bpa.gov/business/generation_interconnection/documents/STD-N-000001-00-01_071509.pdf

[57] D. J. N. Limebeer and R. G. Harley, "Subsynchronous Resonance of Reep-Bar Induction Motors," *IEE Proc. B Electric Power Applications,* vol. 128, no. 1, pp. 43-51, Jan. 1981

[58] C. E. Bowler and E. Khan, "Wilmarth-Lakefield 345 kV Transmission Series

Capacitor Study: Phase 2 SSR Evaluation Report", Xcel Energy, USA, Job-05-243, Dec. 2005.

[59] A. Tabesh and R. Iravani, "Small-Signal Dynamic Model and Analysis of a Fixed Speed Wind Farm - a Frequency Response Approach," *IEEE Trans. on Power Delivery*, vol. 21, no. 2 , pp. 778- 787, Apr. 2006

[60] R. K. Varma and S. Auddy, "Mitigation of Subsynchronous Oscillations in a Series Compensated Wind Farm with Static Var Compensator," in *Proc. 2006 IEEE Power Engineering Society General Meeting,* pp. 1-7.

[61] R. K. Varma and S. Auddy, "Mitigation of Subsynchronous Resonance by SVC Using Pmu-Acquired Remote Generator Speed," in *Proc. 2006 IEEE Power India Conf.,* pp. 1-8.

[62] R. K. Varma, Y. Semsedini and S. Auddy, "Mitigation of Subsynchronous Oscillations in a Series Compensated Wind Farm with Thyristor Controlled Series Capacitor (TCSC)," in *Proc.* 2007 *Power Systems Conf.: Advanced Metering,Protection, Control, Communication, and Distributed Resources*, pp. 331-337.

[63] R. K. Varma, S. Auddy and Y. Semsedini, "Mitigation of Subsynchronous Resonance in a Series-Compensated Wind Farm Using FACTS Controllers," *IEEE Trans. on Power Delivery,* vol. 23, no. 3, pp. 1645-1654, Jul. 2008.

[64] M.S. El-Moursi, B. Bak-Jensen, M.H. Abdel-Rahman, "Novel STATCOM Controller for Mitigating SSR and Damping Power System Oscillations in a Series Compensated Wind Park," *IEEE Trans. on Power Electronics*, vol. 25, no. 2, pp. 429-441, Feb. 2010

[65] M.S. El-Moursi, "Mitigating Subsynchronous Resonance and Ramping Power System Oscillation in a Series Compensated Wind Park Using a Novel Static Synchronous Series Compensator Control Algorithm," *Wing Engineering,* vol. 15, no. 3, pp. 363-377, Apr. 2012.

[66] A. Ostadi, A. Yazdani, and R. K. Varma, "Modeling and Stability Analysis of a DFIG-Based Wind-Power Generator Interfaced with a Series-Compensated Line," IEEE Trans. on Power Delivery, vol. 24, no. 3, pp. 1504-1514, Jul. 2009.

[67] L. Fan, R. Kvasseri, Z. Lee Miao and C. Zhu, "Modeling of DFIG-Based Wind Farms for SSR Analysis," IEEE Trans. on Power Delivery, vol. 25, no. 4, pp. 2073-2082, Oct. 2010.

[68] L. Fan, C. Zhu, Z. Miao, M. Hu, "Modal Analysis of a DFIG-Based Wind Farm Interfaced With a Series Compensated Network," IEEE Trans. on Energy Conversion, vol. 26, no. 4, pp. 1010-1020, Dec. 2011.

[69] G. D. Irwin, A. K. Jindal, and A. L. Isaacs, "Sub-Synchronous Control Interactions Between Type 3 Wind Turbines And Series Compensated AC Transmission Systems," in Proc. 2011 IEEE PES GM, pp. 1-6.

[70] L. Fan, and Z. Miao, "Mitigating SSR Using DFIG-Based Wind Generation," IEEE Trans. on Sustainable Energy, vol. 3, no. 3, pp. 349-358, Jul. 2012.

[71] C. Zhu, M. Hu, and Z. Wu, "Parameters impact on the performance of A Double-Fed Induction Generator-Based Wind Turbine for Subsynchronous Resonance Control," *IET Renew Power Generation*, vol.6, 2012.

[72] IEEE Subsynchronous Resonance Task Force Of The Dynamic System Performance Working Group Power System Engineering Committee, "First Benchmark Model for Computer Simulation of Subsynchronous Resonance," part 1, IEEE Trans. On Power Apparatus and Systems, PAS-96(5), pp. 1565-1572 Sept. 1977.

[73] R. G. Farmer and A. L. Schwalb, "Navajo Project on Subsynchronous Resonance Analysis and Solutions," IEEE Trans. On Power Apparatus and Systems, PAS-96(4), July/August 1977.

[74] IEEE Committee Report, "Dynamic Models for Steam and Hydro Turbines in Power System Studies", IEEE Trans. On Power Apparatus and Systems, PAS-92, PP. 1904-1915, November/December, 1973.

[75] Wind Power India Website (2010). [Online] available: http://www.windpowerindia.com, June 2014.

[76] M. H. Ali and B. Wu, "Comparison of Stabilization Methods for Fixed-Speed Wind Generator Systems", IEEE Trans. on power delivery, PAS-25(1), pp. 323-331, Jan. 2010.

[77] N. D. Calico, Modelling and Control of a Fully Rated Converter Wind Turbine, PhD thesis, The University of Manchester, UK, 2008.

[78] H. F. Wang, "Applications of Damping Torque Analysis to STATCOM Control," Int. J. Electr. Power Energy Syst., vol. 22, no. 3, pp. 197–204, Mar. 2000.

[79] K. Ogata, Modern Control Engineering. USA: Prentice Hall International, Inc, 1997.

[80] K. Dutton, S. Thompson and B. Barraclough, The Art of Control Engineering, First Edit. Addison-Wesley Longman, 1997.

[81] B. Anderson, J. Moore, Optimal Control: Linear Quadratic Method. Prentice Hall International, INC. , 1989.

[82] G. Shahgholian, S. Eshtehardiha, H. Mahdavi-Nasab, and M. Yousefi, "A Novel Approach in Automatic Control Based on the Genetic Algorithm in STATCOM for Improvement Power System Transient Stability", 4th International IEEE Conference, Intelligent Systems, 2008.

[83] Robert L Williams II and D. A. Lawrence, Linear State-Space Control Systems. Canada: John Wiley & Sons, INC., 2007.

[84] K. E. Atkinson , An Introduction to Numerical Analysis, Second. Canada: John Wiley & Sons (WILEY), INC. 0471624896, 1989.

[85] C-T. Chen. Linear System theory and Design, 3rd Ed. New York, NY, USA; Oxford University PressInc; 1998.

[86] F. L. Pagola, I. J. Perez-Arriaga and G. C. Verghese, "On Sensitivities, Residues and Participations: Applications to Oscillatory Stability Analysis and Control," IEEE Trans. Power Systems, PAS vol. 4, No. 1, pp 278-285, February 1989.

[86] N. Magaji, I. S. Madugu, A. U. Lawan, A. Dan-Isa and M. W. Mustafa, "HVDC Controller for Power System Oscillations," Adaptive Science & Technology (ICAST), 2012 IEEE 4th International Conference on, pp 132-136, 25-27 Oct. 2012, Kumasi.

[87] M. E. Aboul-Ela, A. A. Sallam, J. D. McCalley and A. A. Fouad, "Damping Controller Design for Power System Oscillations Using Global Signals," IEEE Trans. Power Systems, PAS vol. 11, No. 2, pp 767-773, May 1989.

[88] N. Yang, Q Liu and J. D. MCCalley, "TCSC Controller Design for Damping Interarea Oscillations," IEEE Trans. Power Systems, PAS vol. 13, No. 4, pp 1304-1310, Nov. 1998.